Fluorescence Detection of DNA Amplification in Porous Media for Point-of-Care Diagnostics

C. Mallory Monahan

A thesis submitted in partial fulfillment of the requirements for the degree of

Master of Science in Bioengineering

University of Washington

2015

Committee:

Dr. Paul Yager

Dr. Barry Lutz

Program Authorized to Offer Degree: Bioengineering

ABSTRACT

Fluorescence Detection of DNA Amplification in Porous Media for Point-of-Care Diagnostics

C. Mallory Monahan

Chair of the Supervisory Committee:

Dr. Paul Yager, Professor

Department of Bioengineering

The translation of sophisticated, laboratory-developed methods for disease diagnosis into devices appropriate for locations with limited infrastructure—whether that is a military setting, resource-poor country, or a home—requires the development of rapid, inexpensive, robust, and semi-autonomous assays. One common diagnostic testing format that addresses these requirements is the lateral flow test (LFT). These tests use modified porous substrates to automate the delivery of samples *via* wicking, which enables low-cost and equipment-free analysis. These tests also utilize the rehydration of reagents from dry storage in the substrate, which enables multi-step and intervention-free assays. Typically, dry reagents in LFTs are stored with sugars that preserve reagent functionality. However, the formation of concentrated sugar solutions in porous media during drying can lead to non-uniform rehydration of reagents stored by this method. Additionally, in many diagnostic assays, the uniform mixing of targets with multiple reagents at precise concentrations is critical to performance. This is especially true for LFT-based isothermal nucleic acid amplification tests (iNAATs), for which the non-uniform rehydration of reagents causes a drastic reduction in assay performance. Since iNAATs produce

results more rapidly and with increased sensitivity than traditional culture-based methods, their use in the LFT format represents an ideal diagnostic test for use in low-resource settings (LRS). Therefore, further study and development of iNAAT reagent rehydration in porous media is needed to enable improved LFT-based iNAATs for disease diagnosis in LRS.

To this end, we have developed a novel, quantitative, fluorescence-based method for the observation and analysis of isothermal DNA amplification from dry reagents in porous media. Here, we describe this method and accompanying analytical tools to assess variations in reagent composition, imbibition time and target input levels with direct utility for performance quantification of a real LFT-based iNAAT.

TABLE OF CONTENTS

Chapter 1. Introduction 8
1.1 Background & Motivation 8
1.1.1 POC Diagnostics & Lateral Flow Tests. 8
1.1.2 Isothermal Nucleic Acid Amplification Tests 9
1.1.3 Dry Reagent Storage. 12
1.2 MADNAAT Project 13
1.3 Problem Description 13
1.4 Approach & Challenges 16

Chapter 2. Detailed Materials and Methods 19
2.1 Materials and reagents 19
2.2 Device construction 19
2.3 Isothermal strand displacement amplification 19
2.3.1 Quantification of iSDA 19
2.3.2 Reaction. 20
2.3.3 Dry reagent pad preparation 21
2.4.1 In-tube. 21
2.4.2 In-porous media. 21

Chapter 3. Development of a quantitative fluorescence technique method for determining amplicon production in porous media 24
3.1 Motivation & Approach 24
3.1.1 Porous Substrates. 24
3.1.2 Fluorescent Probes 25
3.1.3 Quantification. 29
3.2 Characterization of the background fluorescence on porous substrates 29
3.2.1 Nitrocellulose Substrates. 30
3.2.2 Investigation of other substrates. 34
3.3 Characterization of SBR of fluorescent probes 35
3.4 Behavior of fluorescent probes in the presence of target 38
3.4.1 Compatibility with DNA Amplification. 38
3.4.2 Development of a standard curve 40

Chapter 4. Visualization and quantification of DNA amplification in porous media 45
4.1 Motivation & Approach 45
4.2 Quantification of iSDA in-paper from fresh reagents. 46
4.2.1 Amplification heated in-tube 46
4.2.2 Amplification heated in-paper 49
4.3 Quantification of amplification from dry reagents 51

Chapter 5. Development of analytical tools to assess amplification performance in the MAD NAAT Device 52
5.1 Motivation & Approach 55
5.2 Local Analysis Tools 56

5.2.1 Device design. *56*
5.2.2 Surface Plot Analysis. *57*
5.2.3 Histogram Analysis. *58*
5.3 Application of these tools *59*
5.3.1 Dry Storage Optimization *59*
5.3.2 Variation of imbibition time. *61*
5.3.3 Reagent Composition *65*
5.3.4 Improved temperature control. *68*
5.4 LOD Analysis *70*
Chapter 6. Conclusions and Future Directions ***74***
Acknowldgements ***77***
References ***78***
Appendix I. Properties of Nitrocellulose ..... ***LXXXIII***
Appendix II. Behavior of Fluorescent Probes in the Presence of Target ..... ***LXXXVI***
Appendix III. Real-time amplification in-paper with additional fluorescent probes ..... ***XCI***
Appendix IV. iSDA Mechanism ..... ***XCV***
Appendix V. Correction factor for measurements in-paper ..... ***XCVII***

TABLE OF FIGURES

Figure 1. Gel electrophoresis output of an iSDA reaction. *11*
Figure 2. Non-uniform rehydration of dried sugars in porous media *14*
Figure 3. iSDA efficiency dependence on reagent concentration. *15*
Figure 4. High background fluorescence of nitrocellulose--a common POC substrate *17*
Figure 5. Icons for various heating and measurement combinations. *22*
Figure 6. Mechanisms by which three fluorescent nucleic acid probes function *25*
Figure 7. Quenching mechanism for a target-specific nucleic acid hybridization probe *27*
Figure 8. Examples of three target-specific nucleic acid probes with addition moieties chosen to improve SBR. *28*
Figure 9. Experimental set-up for visualizing fluorescence of porous media on the Zeiss Axiovert25 inverted fluorescence microscope. *30*
Figure 10. Background fluorescence of commercially available nitrocellulose substrates *31*
Figure 11. Fluorescence of components of FF80 backed NC *32*
Figure 12. Background fluorescence of selected porous substrates. *35*
Figure 14. Schematic of STAmp and target amplicon *36*
Figure 15. SBR of target-specific nucleic acid hybridization fluorescent probes. *37*
Figure 16. SBR of P(TxRed) on various porous substrates. *38*
Figure 17. Real-time iSDA in-tube performed in the Qiagen Rotor-Gene 6000 using FAM labeled Pleiades probe. *39*
Figure 18. Fluorescence of Texas Red Pleiades probe in response to 0-2000 nM STAmp acquired in-tube. *41*
Figure 19. 4-Day P(TxRed)-STAmp standard curve in-tube at a gain of 8 ..... *42*
Figure 20. 4-Day P(TxRed)-STAmp standard curve in-paper at a gain of 1 ..... *43*
Figure 21. The effect of heating mechanism on the P(TxRed)-STAmp standard curve on fluorescence measurement in-paper. *44*
Figure 22. Quantification of iSDA output in-tube down to 20 input copies. *46*
Figure 23. Calculated amplicon output from in-tube iSDA reactions at various input copy number and 2 reaction volumes *47*

Figure 24. iSDA reaction performed in-tube and measured both in-tube and in-paper without additives. 48
Figure 25. Real-time amplification from fresh reagents 50
Figure 26. Real-time amplification curves and output for reactions performed from both fresh and dry reagents in-tube and in-paper. 52
Figure 27. Amplification from dry reagents. Schematic of the 2-dimensional paper-network 53
Figure 28. Stitched image of Standard-17 glass fiber post-amplification from dry reagents at 20,000 input copies. 54
Figure 29. Experimental set-up for visualizing real-time amplification from dry reagents on the microscope. 56
Figure 30. Surface plot analysis of amplification from dry reagents 57
Figure 31. Histogram analysis for amplification in-paper..... 58
Figure 32. Effect of drying method on amplicon generation at 20,000 input copies. 60
Figure 33. Reagent compaction after rehydration in Standard-17 using fluorescent dNTPs 61
Figure 34. Percent amplification performance as compared to fresh in-tube for 20,000 input copy amplification reactions heated and measured in-paper from dry reagents at varying rehydration times. 62
Figure 35. Fluorescence signal decrease upon rehydration of FITC-PEG dried in Standard-17 at an imbibition time of 20s..... 63
Figure 36. Rehydration and heating of iSDA reagent pad with STAmp..... 64
Figure 37. Effect of the addition of PEG on amplification performance at 20,000 input copies. 66
Figure 38. Amplification performance at various concentrations of iSDA reagents with primer set "D"..... 68
Figure 39. Amplification in-paper with improved heating control at 20,000 input copies. 69
Figure 40. Images of reagent pads pre- and post-amplification for various input copy numbers 70
Figure 41. iSDA in-tube and in-paper at low copy number. 71
Figure 42. Histograms for 20, 200 and 20,000 input copy amplification from dry reagents. 73
Figure 43. Summary of improvements made to amplification in-paper from dry-reagents at 20,000 input copies.. 74
Figure 44. Schematic for design of a fluorescence-based MAD NAAT as compared to the standard MAD NAAT...... 76

Chapter 1. Introduction

1.1 Background & Motivation

1.1.1 POC Diagnostics & Lateral Flow Tests.

Much of healthcare spending is ineffective and inefficient. This inefficiency is estimated to account for 20-40% of total health care spending—wasting over $1 trillion dollars globally each year and doing little to improve people's health [1]. A large portion of improving health outcomes and expenditures globally is the enhanced detection, treatment and control of disease; but ineffective or undeliverable diagnostics remain an important contributing factor to the loss of monetary resources and human lives. Gold standard diagnostic methods require expensive laboratory equipment and trained personnel for operation [2]. The applicability of such diagnostics is limited because they are not suitable for a variety of settings, including LRSs that bear a large disease burden. Fewer than half of all patients treated in low- and middle-income countries receive care according to clinical guidelines for common diseases in primary care [1]. These areas possess a lack of infrastructure and shortages of trained personnel making execution of these tests difficult [3], yet point-of-care (POC) testing in the developing world and resource-limited settings can be valuable [4][5]. POC testing is advantageous when a rapid answer is required [6] and has the ability to expand healthcare globally by improving the delivery of healthcare, reducing the cost of care and improving patient outcomes [7][8].

POC testing is also of growing importance in the developed world for use in at-home testing [9][10], but is exceedingly important in the developing world for increasing access to diagnosis for infectious diseases including HIV, malaria, tuberculosis and sexually transmitted

infections [11][12]. One group estimated that a rapid, sensitive, specific and widely-available diagnostic for tuberculosis could save 400,000 lives annually [13]. Due to the health risk of these infectious diseases, the ability to diagnose them outside the laboratory could greatly mitigate disease progression and spread. The past few decades have brought a burgeoning of research, particularly in the field of microfluidics, dedicated to reducing the size, cost and user-involvement of diagnostics to make them appropriate for the POC [2] .

One popular format for POC-appropriate diagnostic assay is the lateral flow test (LFT), the most well-known example of which is the rapid pregnancy test [14]. LFTs utilize porous substrates (most traditionally cellulose and nitrocellulose), which are inexpensive, easy to use, rapid, disposable and reduce the need for external pumping equipment due to the properties of the material itself [2]. The use of porous substrates for microfluidic diagnostics began to receive more attention in 2007 with the demonstration of an assay in cellulose to simultaneously detect glucose and protein in urine samples [15]. LFTs have been used in a broad range of applications to detect a wide variety of analytes including proteins, pathogens, drugs, hormones and metabolites for monitoring public health and security [4][20-25]. More in-depth reviews of advances in paper-based diagnostics for POC settings have been published recently by Yetisen *et al.*[16] and by Fu *et al.* [2].

1.1.2 Isothermal Nucleic Acid Amplification Tests

The gold standard of microbial identification is culture and phenotypic differentiation of the pathogen, which requires trained personnel and 1-5 days for diagnosis [17]. This delays treatment time and increases morbidity and mortality of infectious disease. Advances in molecular diagnostics have been developed that use the information encoded in nucleic acids for

disease identification. In addition to being more rapid than culturing methods, using nucleic acids can be advantageous over immunological methods, which are the typical assay used in LFT. These methods increase sensitivity and specificity, providing accurate diagnosis in early stages of disease. Achieving this sensitivity requires amplification of the target to maximize the down-stream signal read-out because the target is often present in low concentrations in the sample [12][17-[18]20].

The earliest demonstrated nucleic acid amplification method is the quantitative polymerase chain reaction [20] (qPCR), which requires cycling between three different temperatures for annealing, hybridization and extension steps. qPCR produces multiple copies of the target strand onto which reporter probes bind to produce a signal corresponding to product concentration. The quantification relies on the timing at which a signal crosses a certain threshold. However, this precise temperature cycling can be difficult to implement at the POC due to the absence of sophisticated laboratory equipment. Isothermal methods have since been developed which fit the requirements for POC diagnostics much better than PCR and are more easily implemented. Some of these isothermal nucleic acid amplification tests (iNAATs) include loop mediated isothermal amplification (LAMP[21]), rolling circle amplification (RCA [61]) and isothermal strand displacement amplification (iSDA[22]).

iSDA is rapid (~10-30 minutes) as compared to other isothermal methods like loop mediated isothermal amplification (60 minutes), can yield a large (~10^{10} fold) amplification and is truly isothermal—without the need for a high temperature initiation step. In iSDA, a nicking enzyme cuts the target strand, thereby allowing the polymerase to extend for the 3’ side of the nicking site, displacing a single-stranded DNA template onto which one of four primers can anneal. Further extension, nicking and primer annealing result in an exponential amplification of

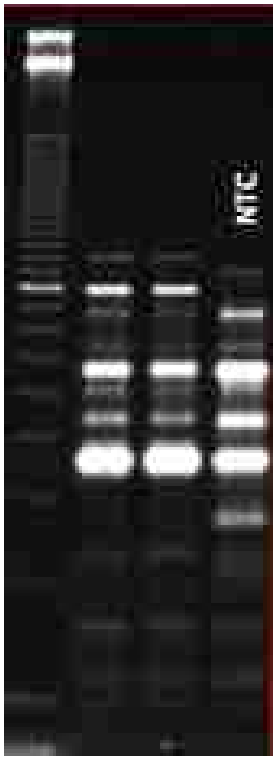

Figure 1. Gel electrophoresis output of an iSDA reaction. Lanes (left to right): 10bp ladder, 1000 input copy (duplicate), NTC. Red arrows indicate location of desired target bands.

the target gene of interest. One of the added complexities that arise using this and other nucleic acid amplification mechanisms is the formation of non-specific background products in additional to the desired product of interest. This can be due to non-target DNA present in the sample or primer mischief. One type of primer mischief can result from even a single 3' base-pair overlap in the nucleic acid components of the system. Such undesired overlaps can then be extended to produce multiple side products that detract from target amplification by depleting deoxynucleotide triphosphates (dNTPs) meant for target amplicon production. In low target input conditions, the extension of primer-dimer products is capable of utilizing more dNTPs and even more background products are created, resulting in an end-point output of the correct amplicons that varies with input copy number.

The number of products produced during an iSDA reaction in the presence of target can be seen in lanes 2 and 3 of the gel in Figure 1 Additionally, examples of the many non-specific products produced during an iSDA in the absence of any target can be seen in lane 4. Due to these non-specific products in this reaction, the use of target-specific probes is necessary for detection. The complexity of such systems creates additional challenges for the implementation of iNAATs into LFTs.

1.1.3 Dry Reagent Storage.

POC iNAATs have the potential to expand access to needed diagnostic methods in low-resource, high disease-burden areas [23]. Although these assays are generally sensitive and specific, in order to be useful in all settings they must also be portable, easy-to-use, robust to uncontrolled environmental conditions, and store on-board stable, ready-to-use reagents [12][23]. Storage of dry reagents on-board a device provides many benefits including 1) reducing the amount of user-steps required to operate the device, 2) removing the need for a cold chain, 3) allowing for device automation, and 4) improving device shelf life and robustness. Indeed, dry reagents are shown to be more resistant to extreme environmental conditions—as encountered in many LRS—particularly when sugar preservatives are added[11][24][25]. Trehalose is one such sugar that has been demonstrated to preserve reagents [26].

Members of the Yager group have demonstrated the use of conjugate pads to store reagents using both traditional microfluidics in 2008 [27] and the lateral flow format in 2012 [28][29]. This technique provides limited control and adds additional parts and device complexity to the assay. Storing the reagents in the primary paper network itself —and not auxiliary conjugate pads—alleviates these drawbacks. Many groups have demonstrated these techniques including the storage of liquid reagents on-chip for DNA extraction [30], storage of freeze-dried reagents in polymer chips for on-chip PCR amplification [31], paraffin-sealed, dried reagents on-chip for PCR at a later time [32], dried down reagents in chips for duplex LATE-PCR [33], the usage of cavities in channel walls to control the reconstitution of dried proteins [26], and the use of "reagent integrators" to store and release dilutions of reagents in microfluidic devices [34]. Storage of dry reagents on porous materials have also been demonstrated for later

rehydration and use in on-paper assays [24] [25]. However, the reagent distribution profiles after rehydration in a heterogeneous porous network have yet to be fully characterized.

1.2 MAD NAAT Project

Current work in the Yager group has focused on the development of a simple, rapid, inexpensive diagnostic tool requiring only one user step, known as the MAD NAAT Project—**M**ultiplexable **A**utonomous **D**isposable **N**ucleic **A**cid **A**mplification **T**est. This device aims to integrate and automate three complex steps—sample preparation, nucleic acid amplification and lateral flow detection—for the purpose of sample-to-result DNA and RNA target identification at the POC. Automating these steps in a manner appropriate to the POC requires the development of low-complexity sample processing methods, fluid flow controls (both geometrical and temporal), and dry reagent storage solutions. The MAD NAAT project has mostly focused on an automated design which mates a tube-based sample preparation with an NAA and lateral flow detection performed in porous media. Due to the complexity of such a project, it is important to have the ability to assess device performance for all stages of the assay. The work presented in this thesis was developed in the context of this larger project and is intended to enable the analysis, in real-time, of the performance of rehydration and amplification in-device.

1.3 Problem Description

Although sugar preservatives have been developed as a useful tool for long-term storage, the use of these reagents has been shown to affect sample and reagent fluid flow from increased

viscosity [2]. These increases become more impactful when dealing with porous media as the ability for solutions to wick through these substrates changes. Lutz *et al.* have demonstrated the viscous fingering effect caused by rehydrating dry reagents in porous materials [35]. This effect occurs at the interface between two fluids when a less viscous fluid chases a more viscous fluid and these patterns result in a non-uniform distribution of reagents (Figure 2).

A. 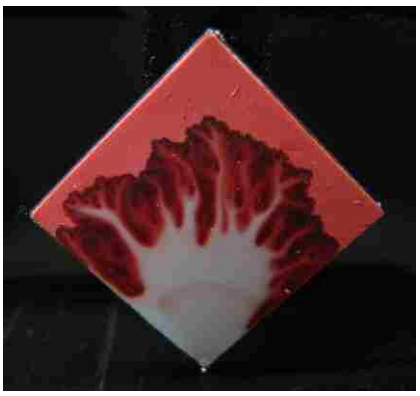 B. 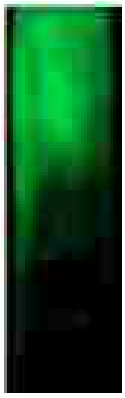

Figure 2. Non-uniform rehydration of dried sugars in porous media. Red food dye dried in the presence of sucrose in nitrocellulose (A) and fluorescently-labeled dNTPs dried in the presence of trehalose and dextran in glass fiber (B). Images by Dr. Barry Lutz and Dr. Melissa Li.

Many chemical processes possess tight concentration tolerances in which performance is highly dependent on reagent concentration. For a nucleic acid-amplification reaction, in which eight or more components may need to be mixed to produce a narrow range of concentrations, this non-uniformity could greatly reduce amplification. We had previously observed this phenomenon in a well-mixed tube environment with the specific amplification mechanism that failed at 0.5x of the nominal iSDA reagent concentration and below as well as 1.75x and above (*Figure 3*). One could imagine that combining a heterogeneous porous substrate, a complex amplification process with a tight concentration tolerance, and a non-uniform reagent rehydration has the potential to possess great detrimental impact on device performance and LOD.

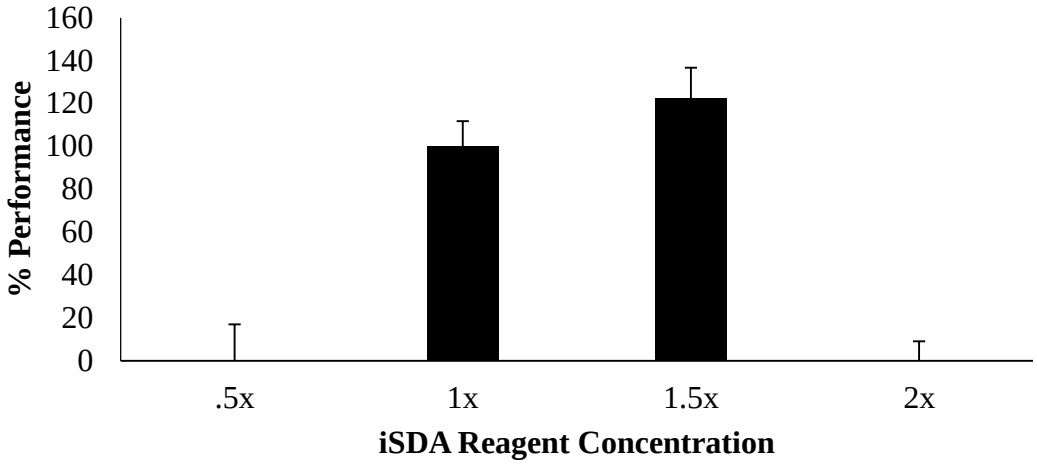

A.

B.

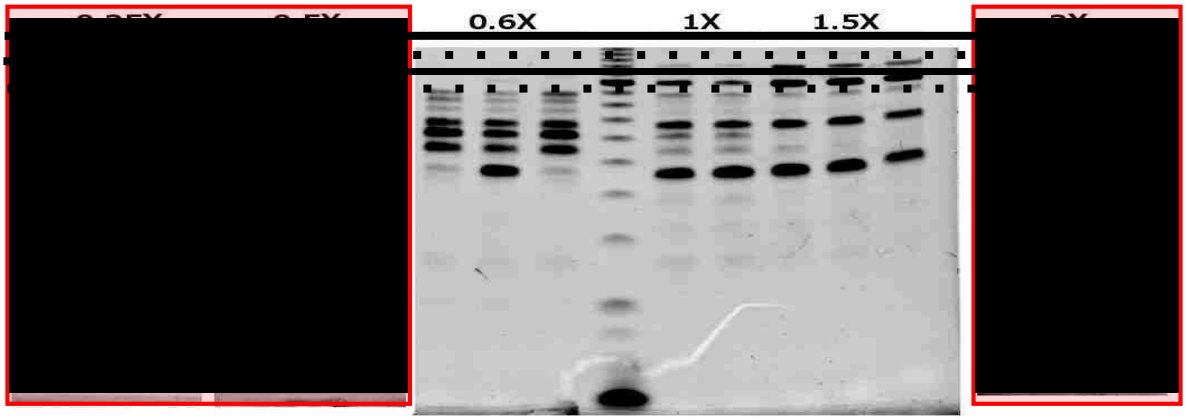

Figure 3. iSDA efficiency dependence on reagent concentration. Amplification performance as compared to initially-determined 1.0x reagent concentration (determined by end-point fluorescence analysis quantified in-tube) (A) and gel electrophoresis analysis by Ryan Gallagher and Enos Kline (B). Dotted lines represent location of desired target bands and red boxes surround gel results from regent concentrations that produced no measurable target amplicons.

1.4 Approach & Challenges

Previously, analysis of amplification performance in-device relied on indirect detection methods that ranged in their usefulness. Gel electrophoresis and lateral flow detection provide information concerning the amplification products, but are slow and must be performed out of the porous substrate of interest. Fluorescence analysis performed in-tube provides rapid, real-time information, yet is performed in-tube and is therefore not applicable to process analysis in the substrate. While these three methods are useful, each technique is unable to convey useful information relevant to device performance. What was needed was a rapid, real-time detection method that would provide information concerning amplification performance in-situ. Therefore, in this thesis I developed an optical method that translates a method for monitoring real-time amplification into a porous medium; allowing the assessment of reagent rehydration and amplification efficiency as it relates to a POC device. We intended the work to also enable optimization of device performance by analyzing the effect of changes such as geometry, composition of additives, or individual reagent concentrations.

To this purpose, the following aims were investigated:

Aim 1. Develop a quantitative method for monitoring DNA amplification in porous media

Aim 2. Validate the ability of this method to visualize and quantify DNA amplification in porous media from fresh and dry reagents

Aim 3. Apply this method to analyze amplification performance in the MAD NAAT device under a variety of conditions

Fluorescence detection has a very low limit of detection—down to one fluorophore with a sufficiently powerful laser and sensitive detector—and adds quantitative capabilities, but because of the need for auxiliary equipment and the high background fluorescence of common POC substrates, this approach has not been explored as vigorously as lateral flow detection methods [16]. Recent advances in inexpensive fluorescence optical methods have lessened this challenge and allow for the use of fluorescence as a detection mechanism for POC diagnostics [36]. Ismagilov, *et al.* have also reported on the use of fluorescence detection for POC diagnostics, and have demonstrated its ability to provide quantitative results over a wide dynamic range *via* digital amplification as an end-point measurement. An additional challenge that arises is that fluorescence visualization can be difficult to perform on porous media due to the high background fluorescence of the porous media themselves. The source of the fluorescence is not clear; it may be additives—depicted in *Figure 4*—and backings as well as scattering of light in the paper substrates [37][38]. Regardless, the ability to use fluorescence for this purpose is valuable, as it allows for the quantification of amplification in the device to assess its performance in real-time.

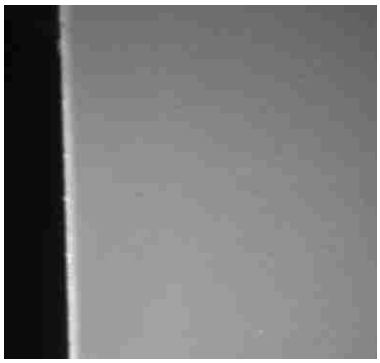

Figure 4. High background fluorescence of nitrocellulose--a common POC substrate. Commercial FF80 backed nitrocellulose taken using a Zeiss Axiovert25 inverted fluorescence microscope (2.5x objective, 500ms exposure, 61 HE FITC filter set with bandpass excitation 474/28nm and bandpass emission 527/54nm).

To take full advantage of the large dynamic range of fluorescence detection, acquiring a substrate with low levels of background

fluorescence is important. Fluorescence has been used for paper-based assays for the sensing of nitroaromatic explosive detection [39], sensing DNA of rolling circle amplification (RCA) products on bioactive paper strips [40], a biomolecule assay using upconversion fluorescence [41] and sensing of non-enzymatic nucleic acid circuits based on strand exchange reactions [42]. These methods also use end-point measurements from reactions performed from fresh reagents, thereby losing important information that exists during the reaction processes in a real-time assay context.

In addition to the ability to quantify how well amplification occurs, fluorescence can be used to assess where it occurs. As discussed previously, rehydration in these heterogeneous materials is non-uniform. Some reasons for this include non-uniform pore distribution as well as viscous instabilities that create a phenomena known as viscous fingering [35]. Using fluorescence, we can monitor both the distribution of reagents upon rehydration and how well local amplification throughout the porous media. A more thorough understanding of the rehydration and subsequent reactions could be used to understand the causes of reduced assay performance in the MAD NAAT device—information that can be used to improve assay functionality.

While this method is useful in the research setting, this technique also has promising applications for a future device. Both performance improvement and a reduction in assay time are extremely important for a successful POC device. A fluorescence-detection system aids as a useful research tool by quantitatively assessing amplification performance. In addition, this system can act as its own detection method, removing the needed for an additional lateral flow detection component and thereby reducing assay time.

Chapter 2. Detailed Materials and Methods

2.1 Materials and reagents

Porous membranes were obtained from Whatman—a GE Healthcare Life Sciences brand (Piscataway, NJ). Those tested include FF80 HP nitrocellulose, AE100 nitrocellulose, Standard-17 glass-fiber, Glass-Fiber F, Fusion 5 glass fiber, QM-A quartz fiber (Q) and 31-ETF cellulose. Other construction materials include Melinex (Fralock, Valencia, CA) and PDMS tape (ARclad 7876, Valley Industrial Tapes, Huntington, NY). Configurations were designed in AutoCAD (Autodesk, San Rafael, CA) and materials were cut on an M-360 laser engraving and cutting system (Universal Laser Systems, Scottsdale, AZ). Amplification reagents were provided by ELITech Molecular Diagnostics (Bothell, WA) and the synthetic amplicon was obtained from Integrated DNA Technologies (IDT, Coralville, IA).

2.2 Device construction

Devices for visualizing fluorescence in-paper were constructed from porous materials encased in outer layers of PDMS tape and inner "spacer" layers of Melinex. The 10 μL reactions were performed on substrates cut to dimensions of 5 x 5 mm and the 35 μL reactions were performed on 5 x 20 mm substrates.

2.3 Isothermal strand displacement amplification

2.3.1 Quantification of iSDA

A standard curve was constructed using a model system for the amplification reaction. The model system consists of a fluorescent probe with a synthetic truncated amplicon (STAmp). The STAmp models the single-stranded product of the asymmetric iSDA reaction, but lacks the primer binding sites of the full amplicon. Solutions comprised of 200 nM probe and varying concentrations of the STAmp were mixed in a buffer of 3.75 mM $MgSO_4$, 42.5 mM K_2HPO_4, and 7.5 mM KH_2PO_4 at pH 7.6 to mimic amplification conditions. Three heating conditions were considered: heat in-tube/measure in-tube; heat in-tube/measure in-paper; heat in-paper/measure in-paper. The fluorescence values obtained using the Rotor-Gene or Axiovert25 microscope were then averaged and the signal-to-background ration (SBR) was calculated for all concentrations. These standard curves were then used to translate fluorescence intensity to amplicon output either in-tube or on-porous media.

2.3.2 Reaction.

Amplification reactions were performed in 35 μL volumes. The amplification master mix consisted of 3.75 mM $MgSO_4$, 42.5 mM K_2HPO_4, and 7.5 mM KH_2PO_4 at pH 7.6; 250 nM forward, 1 μM reverse, and 50 nM bumper primers; 0.2 mM dNTPs; 200 nM Texas Red-labeled Pleiades fluorescent probe, abbreviated P(TxRed), unless otherwise noted; 6.75 U Nt.BbvC1B and 8.0 U WarmStart BST 2.0 DNA polymerase; and 10% trehalose and 2.5% dextran. Some experiments also included 2.5% polyethylene glycol (PEG) in the reaction mix. Reactions were initiated by the addition of methicillin-resistant *Staphylococcus aureus* (MRSA) gDNA to the amplification master mix.

2.3.3 Dry reagent pad preparation.

Two types of dry reagent pads were prepared. The first type, which was designed to determine the general concentration factor of reagents upon rehydration, contained fluorescent PEG (2.5% FITC-PEG) in the presence of 10% trehalose and 2.5% dextran. The second type, which was used to test amplification efficiency, contained the amplification master mix described above. Amplification pads were prepared by blocking with a solution of 1% bovine serum albumin and 0.01% Tween (1%-0.01%), and drying overnight. The blocked pads were then filled with amplification master mix and lyophilized for 2.5 hours.

2.4 Fluorescence visualization

2.4.1 In-tube.

Fluorescence measurements for tube-based assays were taken in a qPCR thermocycler (Rotor-Gene 6000, Corbett Life Science, Sydney, Australia) at 49°C until the fluorescent signal reached steady state. These experiments will be referred to as “in-tube”. Fluorescence measurements were taken in either the green channel (peak excitation and emission wavelengths of 494 nm and 516 nm) or the orange channel (peak excitation and emission wavelengths 585 nm and 610 nm) at a gain of 10.

2.4.2 In-porous media.

Fluorescence measurements on porous media were taken on an Axiovert 25 inverted fluorescence microscope (Carl Zeiss, Jena, Germany) using an infinity-corrected Zeiss 2.5x objective with 0.75 NA. The filter set used for fluorescence visualization was the Zeiss 61 HE

dual FITC/Rhodamine filter set with bandpass excitation values of 474/28 nm and 585/35 nm and bandpass emission values of 527/54 nm and 645/60 nm. These experiments will be referred to throughout this work as "in-paper". Automated image capture was controlled by open source software (μManager, San Francisco, CA) with a Retiga camera (QImaging, British Colombia, Canada) set to 200 ms exposure and at 1 frame per minute.

Due to various heating and measurement combinations used in this thesis, colored icons were developed to clarify which pairing was used (Figure 5).

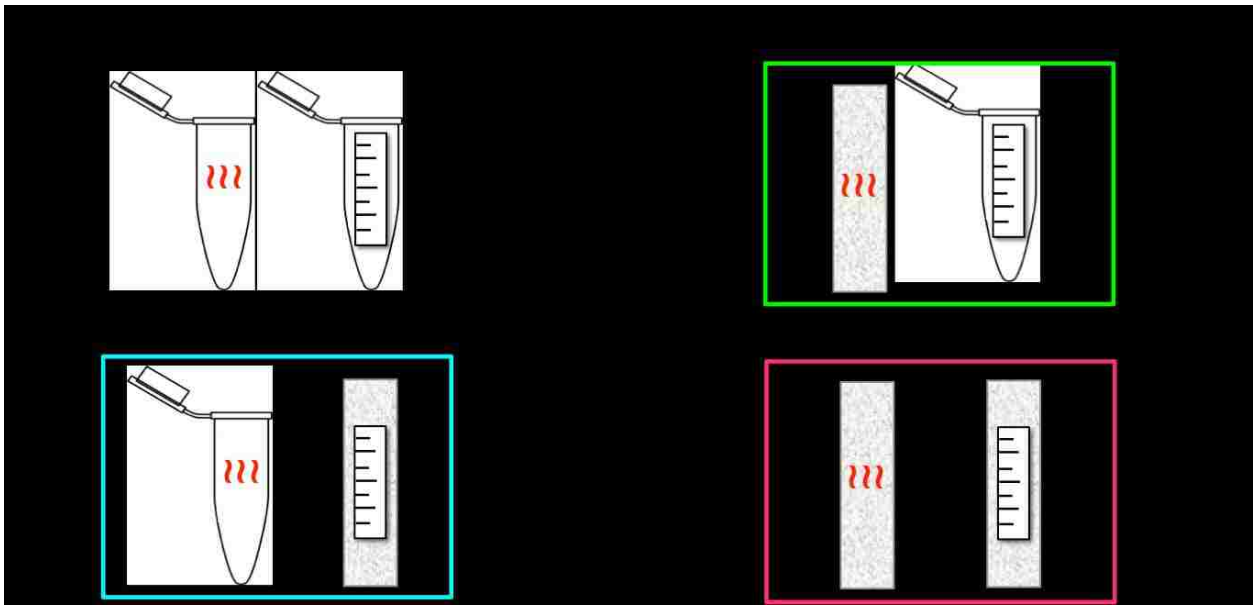

Figure 5. Icons for various heating and measurement combinations.

2.5 Imbibition and rehydration rates

Imbibition was varied using a New Era Syringe Pump Systems Inc., (model NE-1010) syringe pump to obtain rehydration times ranging from 20 seconds to 240 seconds. Rehydration rate was determined by flowing Tris-Edetic Acid (TE) buffer over glass fiber pads dried with

either FITC-PEG or Rhodamine-Dextran and analyzing the time in which the fluorescence signal decreased to 15% of its initial value.

2.6 Image analysis

Analysis of amplification on porous media after rehydration was performed using ImageJ (National Institutes of Health, Bethesda, MD) and Mathematica (Wolfram Research, Champaign, IL). Intensity values were averaged over 25mm^2 sections. STAmp calibrations in-paper were determined by averaging the fluorescence intensity over the entire pad. The performance of amplification reactions in-paper was characterized by averaging the fluorescence intensity within 100 pixels^2 regions of interest (ROIs) or 2500 pixels^2 for the LOD determination experiments. Histograms and surface plots were then generated from these data.

Chapter 3. Development of a quantitative fluorescence technique method for determining amplicon production in porous media

3.1 Motivation & Approach

3.1.1 Porous Substrates.

Most commonly, fluorescence measurements are performed on a transparent or black substrate because these substrates provide an environment with low background levels of fluorescence. This results in very sensitive measurements; for example fluorescence can enable the detection of NAA products from 1 input copy into the amplification reaction [43]. However, for the purpose of the MAD NAAT project, measurements must be performed on porous materials. As mentioned previously, many porous substrates are known to have high levels of background fluorescence caused by manufacturing additives and backing components, as compounded by optical scattering in the substrate. These high levels of background fluorescence shrink the dynamic range of the measurement system. Therefore, we aimed to choose a substrate with the lowest level of background fluorescence to take advantage of the large dynamic range fluorescence detection allows. While having low background fluorescence is vital, the substrate must also be functionally compatible with the chemical processes of interest. For the purpose of this thesis, this process was an iSDA reaction for a gene specific to the bacterium *Staphylococcus aureus*.

3.1.2 Fluorescent Probes.

In this project, the substrate in which the amplification occurs is only one of the components requiring optimization. Another important component is the molecule used to monitor amplification—a fluorescent probe. There are many mechanisms by which fluorescence can be used for nucleic acid detection; obtaining a fluorescent reporter that behaves desirably is of equal importance as choosing an appropriate substrate. Three common fluorescent reporters are used for nucleic acid detection: intercalating dyes, hydrolysis probes, and hybridization probes (Figure 6). The first is a non-target specific probe whereas the latter two are target-specific probes. Intercalating dyes are often aromatic and preferentially bind to double-stranded DNA (dsDNA), but will also bind to single-stranded DNA (ssDNA) at a lower efficiency. Intercalating dyes possess low levels of fluorescence in solution, but are able to insert themselves between the planar bases of DNA. This insertion improves the quantum yield of these molecules, causing the fluorescent signal to increase.

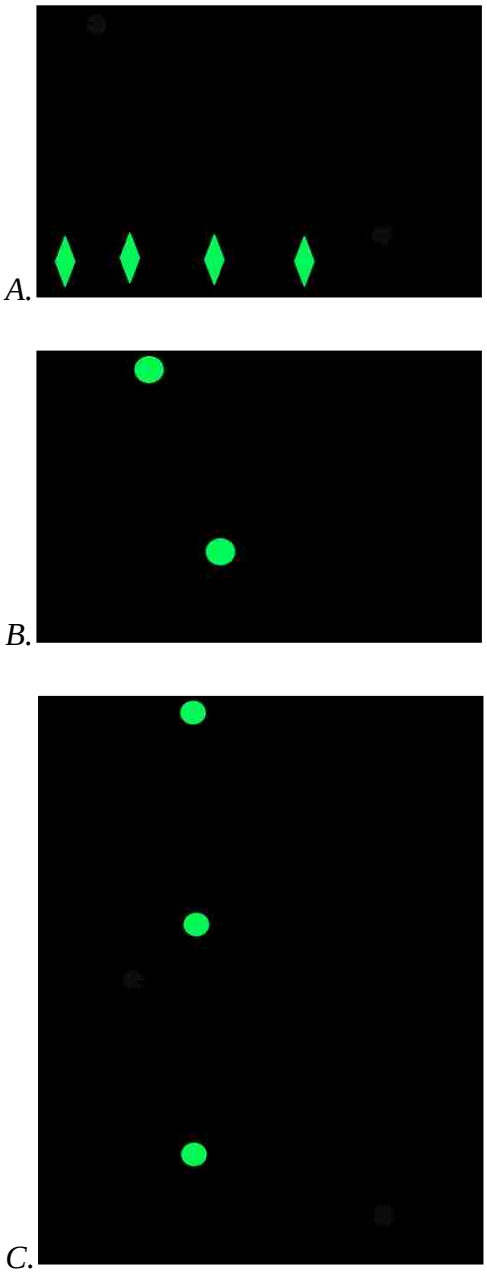

Figure 6. Mechanisms by which three fluorescent nucleic acid probes function. Intercalating dye (A), hybridization probe (B) and hydrolysis probe (C).

As discussed previously, the amplification reaction with which the MAD NAAT project is dealing produces many target and non-target reactions. Therefore, intercalating dyes are not applicable. Signal intensity using target-specific probes is determined by the binding of

the probe to a nucleic acid target. These types of probes utilize two molecules to produce a signal—a fluorophore (donor) and a quencher (acceptor). When these two moieties are in close proximity, the quencher molecule is able to absorb the energy of a fluorophore in a raised energy state, allowing the donor to return to its ground state without the emission of a photon. This quenching can occur through Förster resonance energy transfer (FRET) or contact quenching. The FRET mechanism depends upon the medium between the molecules, the transition dipole orientations of both molecules (rigid or in motion), the overlap between the fluorescence emission spectrum of the donor and the absorption of the acceptor, and the distance between the donor and acceptor. For a suitable pair of chromophores, and a set of the above characteristics, there is a distance at which the energy transfer rapidly- drops to through 50% efficiency—the Förster radius. This characteristic distance is usually 10-100 Ångstroms (roughly, 3-30 nucleotides in a DNA double helix molecule), which can make an effective detector of binding to the target amplicon [44]. In contact quenching, the donor and acceptor molecules interact by proton-coupled electron transfer through the formation of hydrogen bonds[44] . A schematic of this quenching mechanism can be seen in Figure 7.

Hydrolysis probes differ from hybridization probes in that they rely on hydrolytic polymerase enzymes [45]. These probes first bind to the nucleic acid sequence of interest and, as polymerization occurs in the amplification reaction, the 5'-3' exonuclease activity of the polymerase enzyme cleaves the fluorophore from the probe and displaces the complex. However, the enzyme used in the iSDA reaction for this work is non-hydrolytic, so this type of probe is not applicable.

We mainly considered hybridization probes, which can be uni- or dual-labeled. Uni-labeled refers to probes that have the fluorophore and quencher on different nucleic acid strands

while in the case of dual-labeled hybridization probes, both the fluorophore and quencher molecules are located on the same molecule. In the absence of the target, the probe forms a random coil structure that brings the fluorophore and quencher into close proximity. This contact relies on electrostatic forces, which can be weakened in higher temperature environments such as occur in amplification reactions. Therefore, some dual-labeled probes have been manufactured with additional moieties that decrease the distance between fluorophore and quencher pairs to improve FRET or contact quenching and lower background fluorescence in the absence of the target.

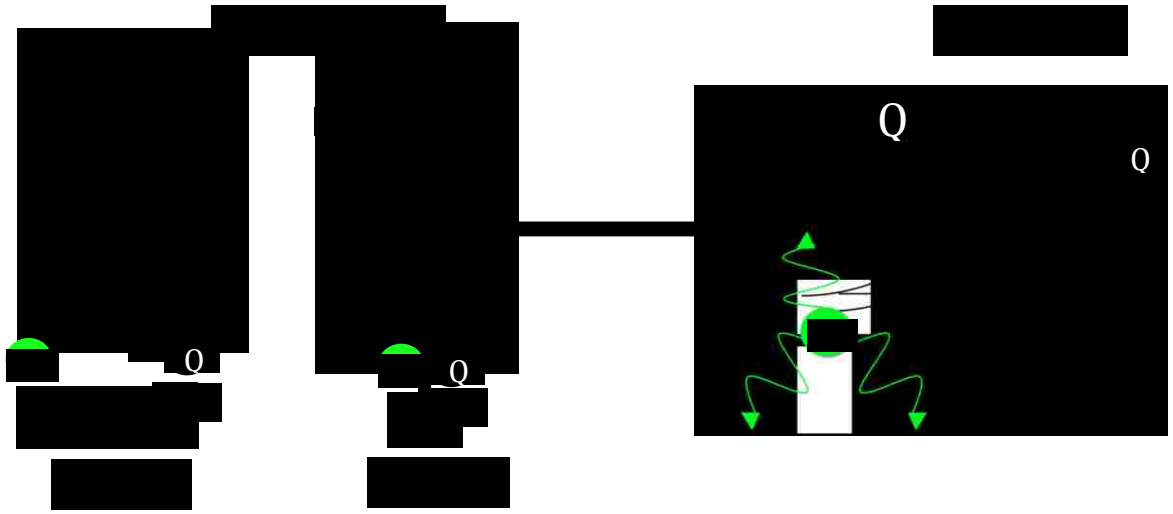

Figure 7. Quenching mechanism for a target-specific nucleic acid hybridization probe

We chose three types of fluorescent probes to characterize in the context of the porous substrates: 1) a Pleiades probe from our collaborating company (ELITech Molecular Diagnostics, Bothell, WA), which has a minor groove binder that increases the melt temperature of the sequence to its compliment and increases specificity to the target as well as brings the fluorophore and quencher in closer contact to decrease background fluorescence [46][47]; 2) a molecular beacon (MB) (Integrated DNA Technologies, Coralville, IA), which has self-

complementary regions on both ends of the probe that anneal to form a stem-loop hairpin structure and co-localize the fluorophore and quencher [48] and 3) a Zen probe (Integrated DNA Technologies, Coralville, IA) as a negative control since it functions *via* a hydrolytic mechanism (Figure 8).

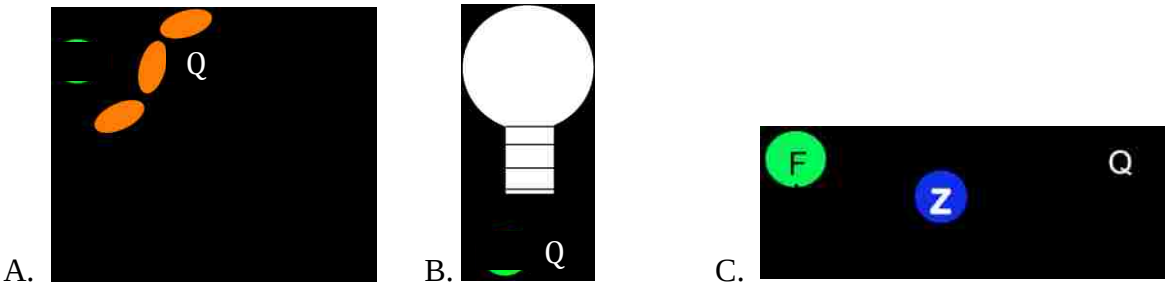

Figure 8. Examples of three target-specific nucleic acid probes with addition moieties chosen to improve SBR. Pleiades (A), Molecular Beacon (B), Zen (C).

The Pleiades and Zen probes utilize FRET quenching while the MB utilizes a combination of FRET and contact quenching. The MB, Zen and one Pleiades probe all possess a FAM fluorophore as their reporter with an absorption maximum at 494 nm and emission maximum of 521 nm. While the other Pleiades probe has a Texas Red fluorophore as its reporter with an absorption maximum at 593 nm and emission maximum of 617 nm. In the literature, these probes reportedly possess low background fluorescence and high signal increases in the presence of target, but these features do not necessarily persist upon interaction with a porous substrate [46]. The interaction of nucleic acids with porous materials is not generally understood, and so the behavior of the probes in the specific design context used must be characterized.

For this application, the optimal probe has a high SBR; specifically a low background level of fluorescence when no target is present and a very high level of fluorescence upon target

hybridization. Additionally, an ideal probe should be resistant to photobleaching on the time scale of the amplification. To achieve the highest SBR, both the substrate and the fluorescent probe must be carefully chosen. Therefore, I aimed to choose a porous substrate and fluorescent probe combination with the following characteristics: (1) Low background fluorescence; (2): Large signal increase in the presence of target; (3): Supports iSDA.

3.1.3 Quantification.

Assessing pathogen load rapidly and quantitatively is important for the diagnosis of many infectious diseases and has powerful prognostic values [17]. Fluorescence detection is useful for its ability to provide rapid and quantitative, real-time information and therefore we desired to create a robust and quantitative analysis technique for the specific amplification reaction. Further development of a quantitative analysis technique to assess amplification performance could provide us with much useful information to inform further engineering designs of the MAD NAAT and future projects.

3.2 Characterization of the background fluorescence on porous substrates

3.2.1 Nitrocellulose Substrates.

To address the first criterion of achieving low background signals, the background fluorescence of different substrates were measured on a fluorescence microscope using a device set-up demonstrated in Figure 9.

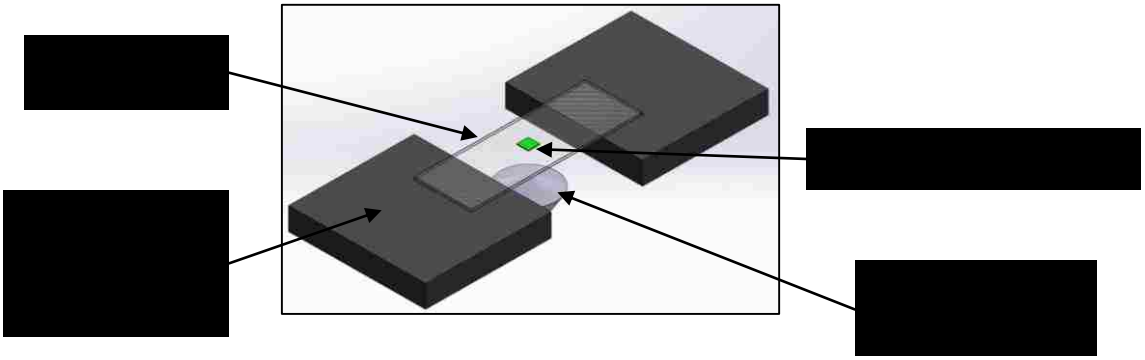

Figure 9. Experimental set-up for visualizing fluorescence of porous media on the Zeiss Axiovert25 inverted fluorescence microscope.

A variety of nitrocellulose samples were analyzed from three manufacturers—GE Healthcare Life Sciences (FF80, FF80PEGMA, FF80PEGDA, FF60, FF60GMA, FF85), Millipore (HF075, HF135, HF180) and Whatman (Prima 60, Prima 85, AE98, AE100). Images of these substrates were captured and the average fluorescence intensity across a $25mm^2$ section of the membrane was calculated Figure 10).

Unbacked nitrocellulose (UBNC)—AE98 and AE100—possessed the lowest background fluorescence, while the FF80 Mylar-backed nitrocellulose (MBNC) series possessed the highest. This data also highlighted the non-uniform illumination issues that were present with the hardware at the initiation of this project. Initially, FF80 MBNC had been targeted in the MAD NAAT project as the best substrate for fluid flow control and to support amplification and lateral flow detection, but would be problematic with fluorescence detection. Therefore, the

cause of this extremely high background was probed more thoroughly. Due to the stark discrepancy between the background fluorescence of UBNC and MBNC, it was hypothesized that the Mylar backing was the source of this fluorescence.

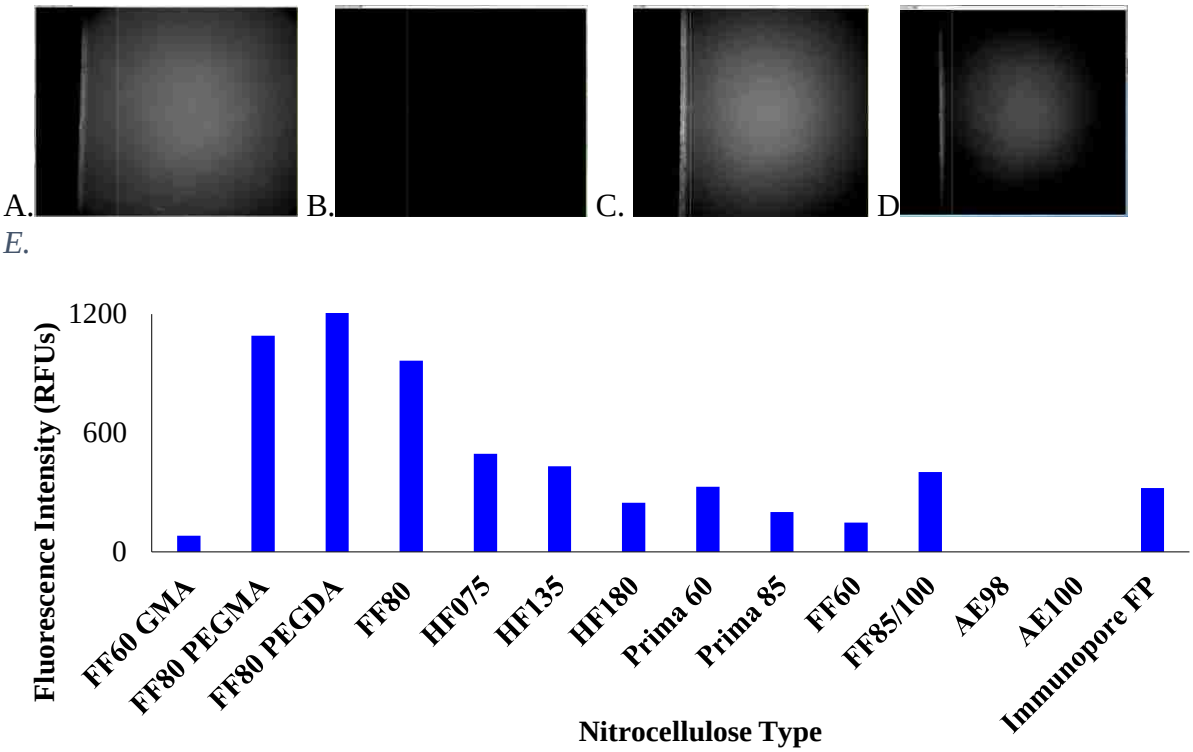

Figure 10. Background fluorescence of commercially available nitrocellulose substrates. Fluorescent images taken using a Zeiss Axiovert25 inverted fluorescent microscope at 5x magnification, gain of 1 and an exposure time of 500ms with Zeiss 61 HE FITC filter set. Selected images (A-D) and fluorescence values for all substrates calculated using ImageJ (E). GE FF80P-PEGMA v1.1 (A), Whatman AE 100 v 1.3 (B). Millipore HF135 v1.2 (C), GE FF60 GMA v1.1 (D).

For a better understanding of the source of fluorescence for this substrate, the emission spectrum was gathered on an Infinite 200 PRO plate reader (Tecan Group, Switzerland) first for FF80 MBNC. Small rectangles of nitrocellulose were cut with scissors and placed in a black 96 well plate. Emission scans were performed at an excitation value of 350 nm with a gain of 100 and an integration time of 100 μs. The fluorescence intensity over ten wells was averaged; the

MBNC exhibited very high fluorescence at 350 nm excitation (Appendix Figure 2**)**.

Next, pieces of FF80 MBNC were crudely, but effectively, separated into the Mylar and nitrocellulose components using a razor blade. Small squares of the Mylar backing or the nitrocellulose substrate manually scraped off the backing were placed in the Tecan plate reader and scanned under the same conditions as the FF80 MBNC. However, neither the nitrocellulose itself, the Mylar backing, nor the summation of the fluorescence data for the two would account for the high background of the FF80 MBNC (Figure 11). These parts were also imaged *via* fluorescence microscopy to determine whether this observed phenomena was an artifact of the plate reader, but fluorescence images confirmed this observation.

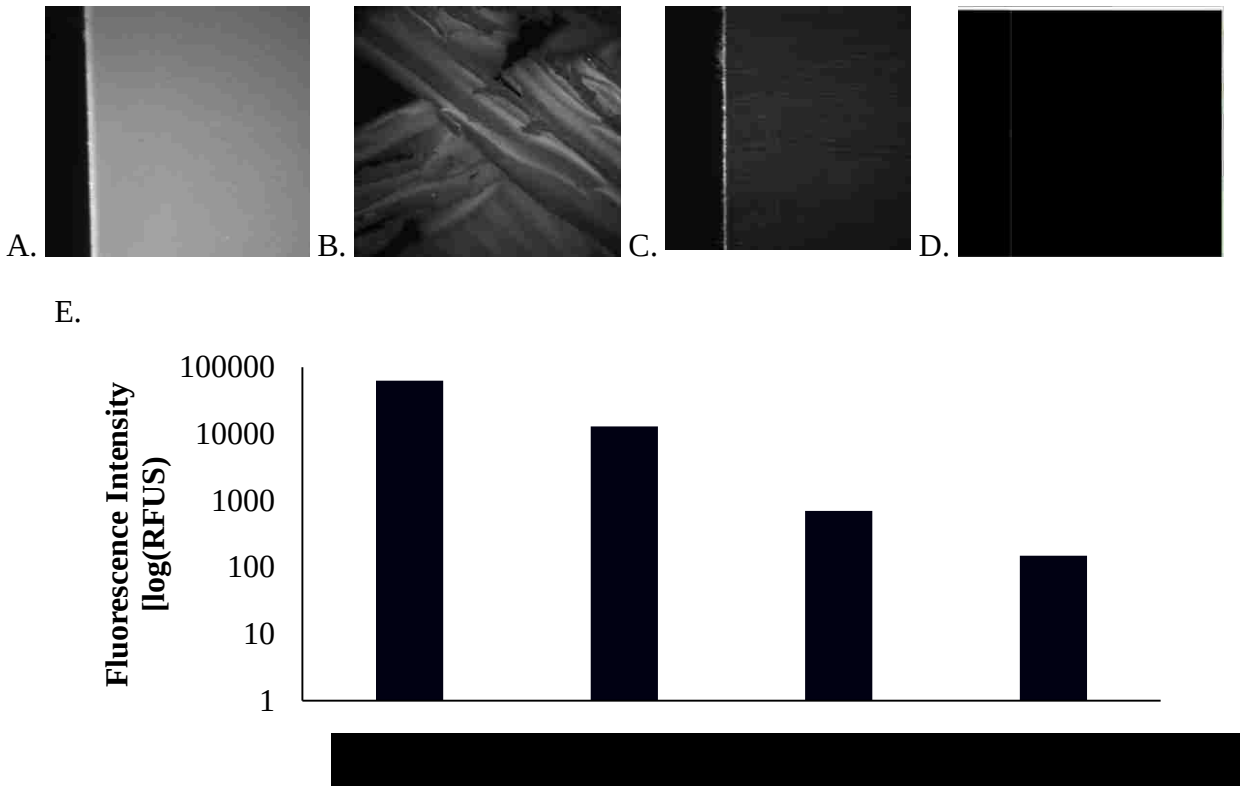

Figure 11. Fluorescence of components of FF80 backed NC. FF80 PEGMA (A), nitrocellulose only (B), Mylar only (C) and AE100 unbacked NC (D). 2.5x magnification (A-D) and 500ms exposure (A,B), 1s exposure (C,D). Peak intensity values at Excitation/Emission 494/517 (E).

An experiment in which the nitrocellulose was also removed layer by layer with a piece of tape was performed to determine where within the depth of the NC the fluorescence was originating (Appendix Figure 3). However, the fluorescence intensity was proportional to the remaining thickness of the material. This suggests that the fluorescence results not from the surface of the material, but is a property that persists through the width of the NC membrane. Some groups have reported high brightness values from porous materials due to light scattering in the medium that could be one source of these high fluorescence intensities, although this hypothesis requires much further investigation [49] . From this data, it was determined that commercially-available MBNC possessed exceedingly high background fluorescence and therefore did not meet the requirements needed for the substrate, but AE100 UBNC could be a potential candidate.

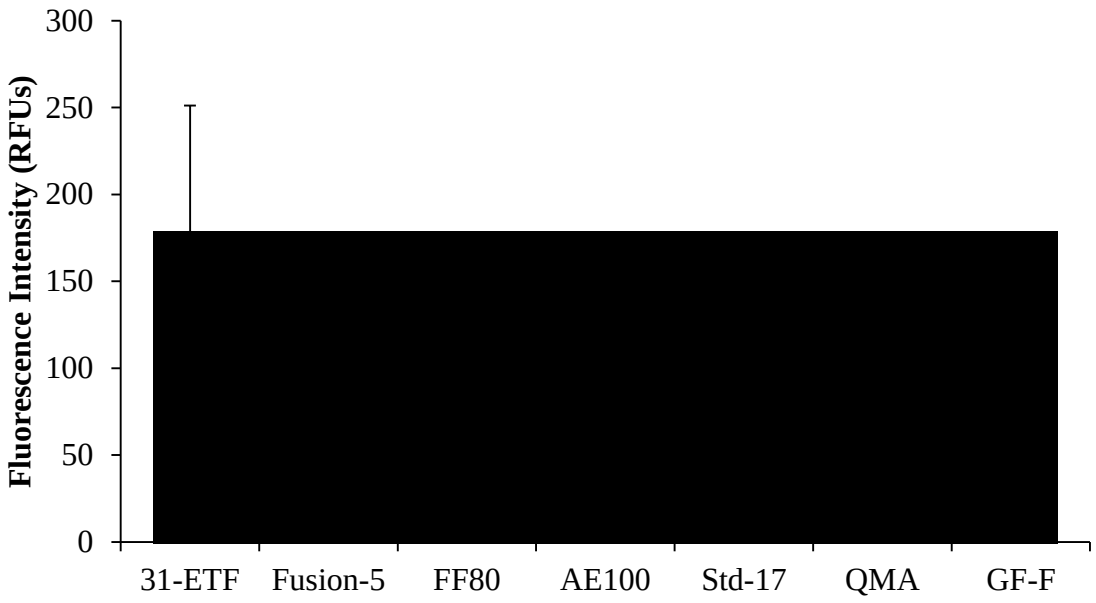

Figure 12. Background fluorescence of selected porous substrates. Intensity values acquired using the Axiovert25 fluorescence microscope with Zeiss 61 HE rhodamine filter set with a 2.5x object at 200 ms exposure.

3.2.2 Investigation of other substrates

One important criterion for these POC diagnostics is the rapidity with which the test can take place. One drawback with using nitrocellulose as the primary fluid network for the MAD NAAT device was the slow wicking rate of the material. To increase the speed of this platform, faster wicking materials were investigated. Fortunately, given the high fluorescence background of MBNC, other substrates could be investigated that might have lower background fluorescence. UBNC and MBNC were compared to three glass fiber materials (Standard-17, Glass Fiber-F, Fusion-5), a quartz fiber membrane (QMA) and a cellulose membrane (31-ETF). When this analysis was expanded to other types of porous substrates, cellulose was determined to have the highest background fluorescence, quartz the lowest, followed by glass fiber (Figure 12).

Others have postulated that the high background fluorescence of these fibrous materials are due to optical whiteners that absorb light in the ultraviolet and violet region of the visible light spectrum and emit light in the blue region [62]. In an attempt to reduce fluorescence contributions from these potential additives, the background fluorescence intensities of these three media were checked with the Zeiss 61 HE dual FITC/Rhodamine filter set with bandpass excitation values of 474/28 nm and 585/35 nm and bandpass emission values of 527/54 nm and 645/60 nm (Appendix Figure 5). The rhodamine filter set did result in a lower background fluorescence for FF80 MBNC, AE100 UBNC and Standard-17, yet this decrease was not substantial, suggesting that the additives are not the main source of the high background fluorescence.

Although there were a few candidates for fluorescence visualization, Standard-17 glass fiber was chosen as primary substrate for the MAD NAAT project because of its fast wicking

properties and compatibility with iSDA. Therefore, Standard-17 was used for all subsequent experiments.

3.3 Characterization of SBR of fluorescent probes

This fluorescent probe was desired to have a high SBR on the porous substrate and quantitatively report the amplicon production. The background fluorescence of the four fluorescent probe candidates was measured first in-tube (Figure 13). The background fluorescence of the probes was measured at 49°C to mimic the environment of an iSDA reaction. Both Pleiades probes had the highest background fluorescence, while the Zen had the lowest.

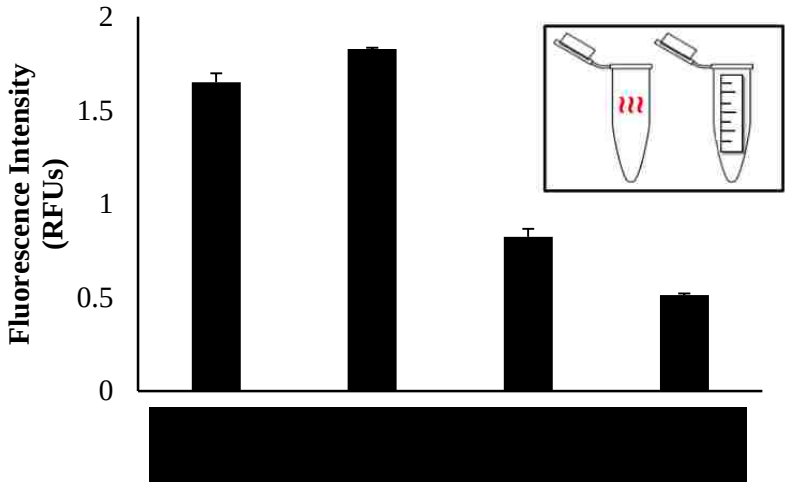

Figure 13. Background fluorescence of probes measured in-tube on the RotorGene 6000 at 49ºC of two Pleiades probes, a MB and Zen probe. Gain=7.7; n=3.

Although the Pleiades probe exhibited the highest level of background fluorescence, the characteristic of importance was the SBR. Therefore, after the background was established, the signal upon hybridization was investigated. To determine signal increase, a model system was designed by Dr. Joshua Bishop that used an oligonucleotide analog to the amplicon that possessed a complimentary sequence to the binding region of the fluorescent probe (Figure 14). The use of a synthetic truncated amplicon (STAmp) allows for the omission of an amplification reaction, thereby reducing complexity and variability. Additionally, the absence of the primer flanking regions helps prevent contamination.

A. 5’-TGA ACC AAA GCA TTG TTG ATG AAT TAG TCA TCA TTG ATT TAG ACA CTG AAA A-3’

B.

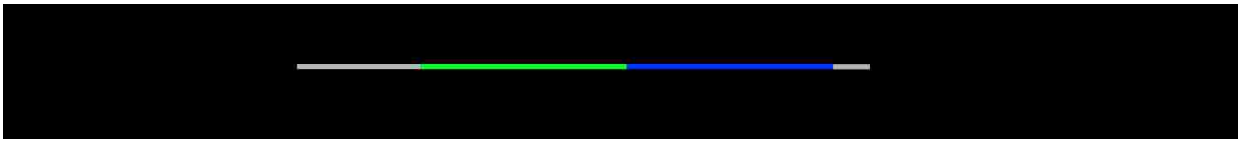

Figure 14. Schematic of STAmp and target amplicon. STAmp sequence (A) and schematic of binding domains of the target amplicon (B). Green binding domain represents the fluorescent probe-binding region and the bracket denotes the STAmp region portion of the amplicon.

The STAmp was mixed in excess with the fluorescent probes and fluorescence was acquired in-tube and in-paper. For in-paper SBR calculations, the measurement of the fluorescence signal produced by each membrane wetted with Tris-EDTA (TE) buffer only was taken first. The next measurement of the fluorescence signal was taken of the membrane with 200 nM probe only and the final measurement was taken of the membrane in the presence of 200 nM probe and an excess of STAmp at 400 nM to ensure all of the probe sites that were available could be occupied. The SBR was calculated for each membrane by dividing the fluorescence signal of the probe-STAmp complex by the summed fluorescence of the wet membrane and the probe in the absence of target (Equation 1). The in-tube SBR was calculated with the same equation, but with F_S=0.

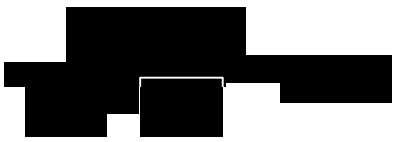

Equation 1. Signal-to-background ratio calculation. Probe (P), target (T), substrate (S).

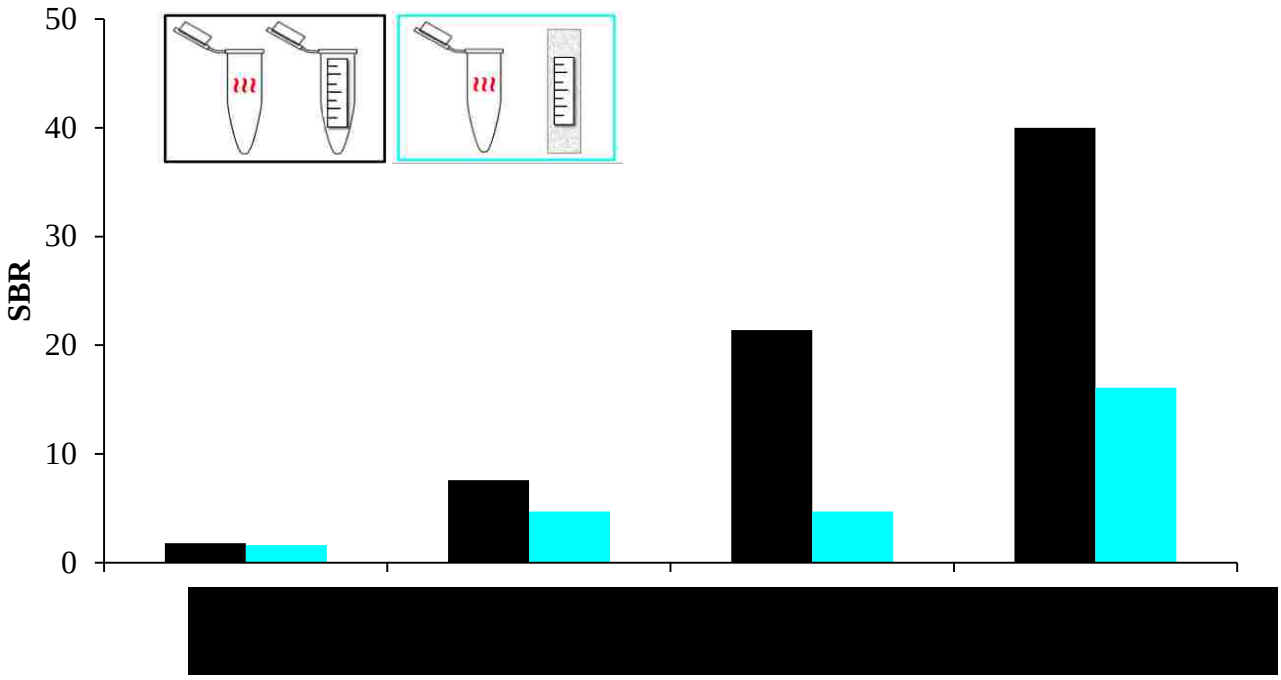

Figure 15. SBR of target-specific nucleic acid hybridization fluorescent probes. SBR of target-specific nucleic acid hybridization fluorescent probes. Heating performed in-tube for both conditions and measurements performed in-tube (black) and in-paper (blue). In-paper measurements obtained on the Axiovert25 inverted fluorescence microscope at 2.5x magnification, 500 ms exposure time.

From these values the SBR was calculated. The Pleiades probes were found to possess the highest SBR in-tube and in-paper (Figure 15). The Texas Red label had the highest SBR in-tube (40) and in-paper (16) and was also found to be much more resistant to photobleaching on porous media than its FAM analog (Appendix IV). Therefore P(TxRed) was chosen as the most desirable probe candidate. Once this probe was chosen, the SBR on different substrates was determined to ensure the best pair was selected. It was determined that the P(TxRed) on Standard-17 had the highest SBR (Figure 16). This membrane also possessed the fastest wicking

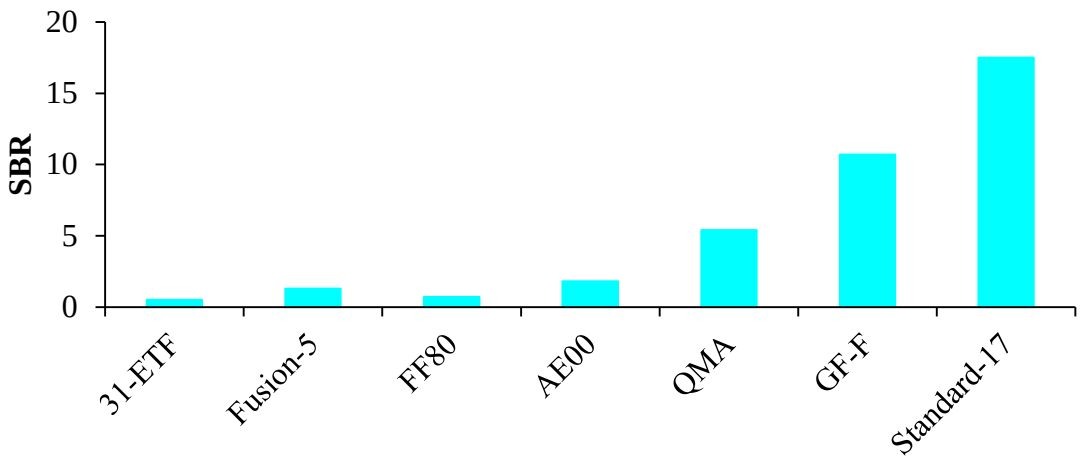

Figure 16. SBR of P(TxRed) on various porous substrates.. SBR for various porous substrates. Numbers above bar graph represent the calculated signal: background ratio. Membrane+TE buffer (black), probe +0 nM target (gray), probe +400 nM target (red).

rate and capillary rise time of the materials tested, which are beneficial to the performance of a rapid diagnostic test. Therefore, Standard-17 was used for the rest of the experiments.

3.4 Behavior of fluorescent probes in the presence of target

3.4.1 Compatibility with DNA Amplification.

The Pleiades probe chosen for its high SBR was used in the iSDA reaction to determine its compatibility in a tube-based assay. The Pleiades probe demonstrated a behavior that was consistent with target production in exponential amplification and could therefore remain the probe of interest (Figure 17).

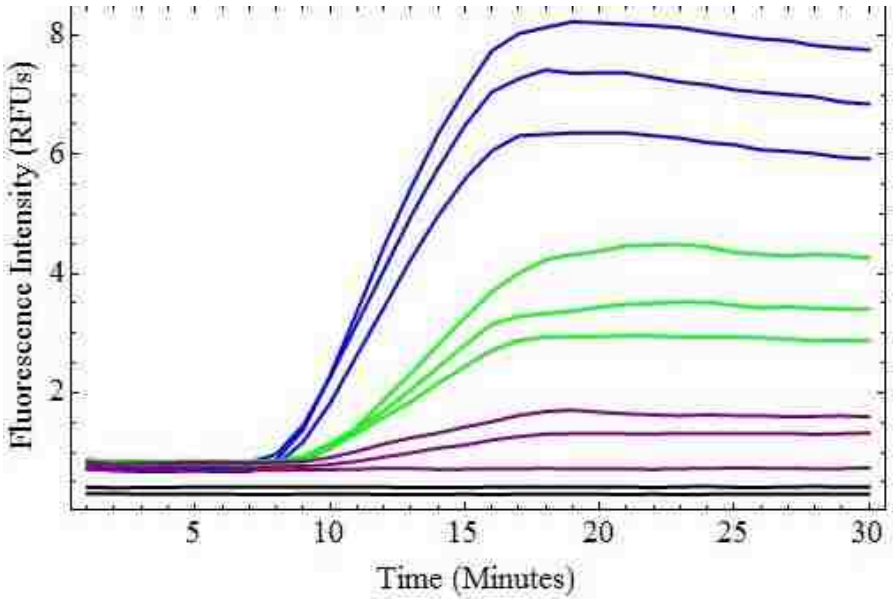

Figure 17. Real-time iSDA in-tube performed in the Qiagen Rotor-Gene 6000 using FAM labeled Pleiades probe. 2000 input copies (blue), 200 input copies (green), 20 input copies (purple) and 0 input copies (black)

Of the other probes, the Zen probe demonstrated existent, but poor amplification compatibility, whereas the MB probe performed very poorly (Appendix Figure 10). The hydrolytic Zen probe was able to produce a low fluorescent signal, but the quantified amplicon generation was very small as compared to results gathered with the Pleiades probe. Although the Bst 2.0 Warm-Start polymerase enzyme is not marketed as hydrolytic and therefore there should be no fluorescent signal, we believe this enzyme does indeed have a small percentage of hydrolytic activity based on the manufacturer's guidelines. This activity could be increased at the elevated temperature in which iSDA is performed and therefore a small amount of fluorescent signal could be generated.

The data acquired concerning the behavior of the MB in response to STAmp as well as in iSDA suggests that the poor performance observed was due to poor probe design by myself and

Dr. Joshua Bishop. The end-point behavior of the MB in response to STAmp when measured at 25°C was closer to the expected behavior than when measured at 49°C, suggesting that elevated temperatures are one cause of the reduced reporting capability of the MB (Appendix Figure 9). Although the probe was designed using NUPACK software (Pasadena, CA) that predicted that at the iSDA temperature (49°C), the probe-target complex would account for >90% of the structures, the MB probe did not function as expected. The robustness of the probe to increased temperatures could potentially be improved by increasing the length of the stem region to 6 nucleotides. Additional data for these probes can be found in Appendix II. Nevertheless, the P(TxRed) probe met the desired requirements was chosen as the most optimal probe among the candidates.

3.4.2 Development of a standard curve

In-tube. To produce a quantitation method for the amplification, it was necessary to confirm the expected fluorescence response of the probe. The initial heating protocol was adapted from ELITech and the temperature profile to construct these standard curves consisted of a 95°C melting step followed by a slow hybridization from 95-49°C at a step of 1°C/minute. According to first principles, a 1:1 binding stoichiometry should be observed between the fluorescent probe and target sequence until the concentration of STAmp exceeds the concentration of probe. Since 200 nM of fluorescent probe was used in most reactions, the fluorescence behavior should be linear with increasing target concentration until the concentration of STAmp exceeds 200 nM [50]. At this point, the fluorescence intensity should

saturate and not vary with increasing STAmp concentrations. The behavior of the probe in response to increasing input concentrations of STAmp was as predicted (Figure 18).

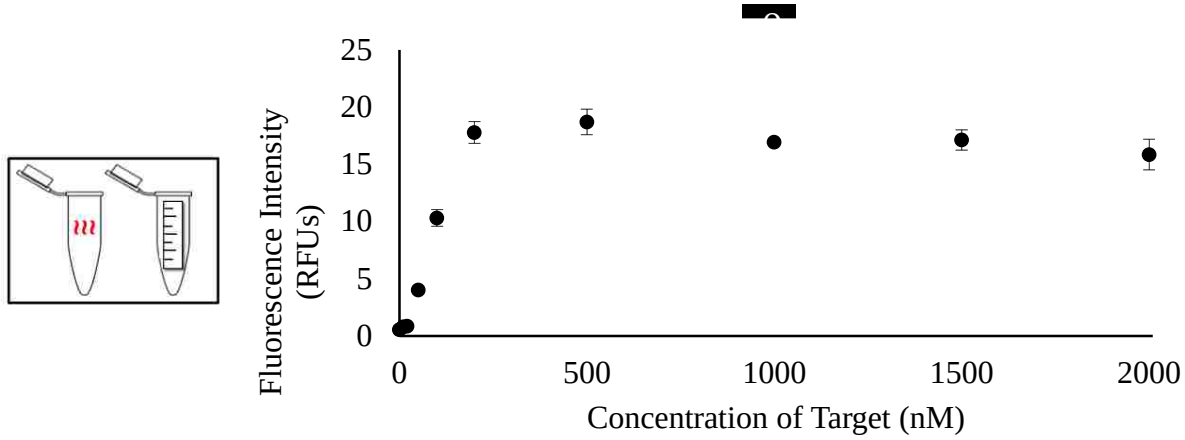

Figure 18. Fluorescence of Texas Red Pleiades probe in response to 0-2000 nM STAmp acquired in-tube.

After this validation, standard curves obtained with and without these denaturing and hybridization steps were compared. After 30 minutes of heating at 49°C, the fluorescence of the complex had reached a steady state value. Binding efficiency was found to be slightly improved upon the addition of this extra heating—R^2 value of 0.99 vs. 0.97. However, due to the additional time needed for this protocol (120 minutes *vs.* 30 minutes), this small improvement was not sufficient to warrant extra heating time. Therefore, subsequent standard curves were constructed by holding the temperature of the reaction at 49°C for 30 minutes and measuring the end-point fluorescence. This technique is more easily adaptable to, and more in line with, the in-paper experiments, as the slow hybridization would be more difficult to implement with the electric heater used.

Reactions were prepared by combining 200 nM of the P(TxRed) fluorescent probe with varying concentrations of the STAmp in the same buffer as is used for iSDA. This solution was

heated and measured in-tube and a standard curve was constructed relating fluorescence units to number of STAmp molecules. I converted the relative fluorescence units (RFUs) into a percentage increase over background (**%F**). This number was beneficial due to the use of the internal reference of the donor fluorescence. This method was adopted from Bidinotsi *et al.* and provided a signal corrected for potential artifacts and day-to-day fluctuations [51]. Standard curves produced on four consecutive days demonstrated the robust quantitative ability of this technique (Figure 19). The maximum fluorescence signal obtained using STAmp and 200 nM probe is a 5x signal increase from the background. The ability to tune this standard curve to achieve a range appropriate for the amplification was also demonstrated (Appendix Figure 7). That is, by doubling the probe concentration, the saturation point occurred at 400 nM STAmp as opposed to 200 nM STAmp and the signal intensity at saturation for the 400 nM probe was twice the signal intensity at the point of saturation for the 200 nM probe.

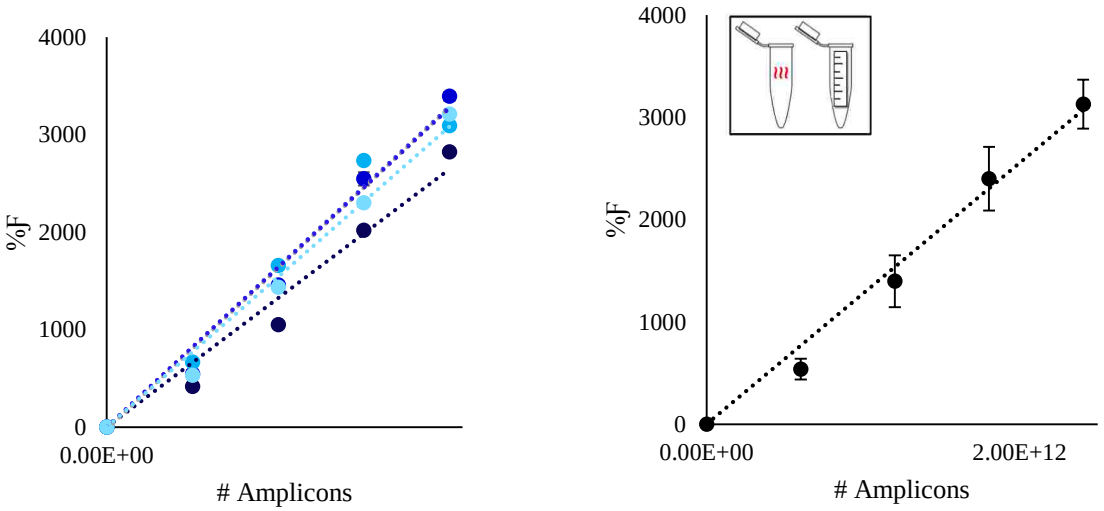

A. B.

Figure 19. 4-Day P(TxRed)-STAmp standard curve in-tube at a gain of 8. Four curves (A) and the average of all four curves (B). For curve B, slope=1.3E-9, R2=0.99.

In-paper. Once the behavior of the P(TxRed) in response to STAmp was verified in-tube, the next step was to translate this quantification method onto Standard-17 glass fiber. The fluorescence behavior of the P(TxRed)-STAmp complex was first visualized by performing all heating in-tube and only measurement in-paper to determine whether the expected behavior could be seen. A standard curve over four days of measurements performed in-paper was obtained with the same robust behavior as observed for the standard curve measured in-tube (Figure 20**).**

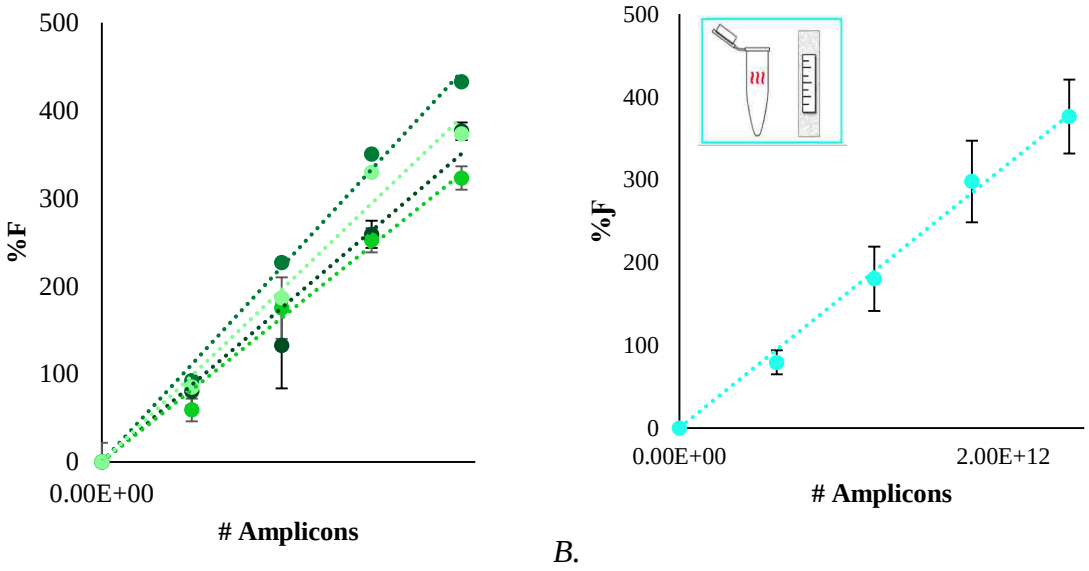

A. *B.*

Figure 20. 4-Day P(TxRed)-STAmp standard curve in-paper at a gain of 1. All four curves (A) and the average of all four curves (B). For curve B, slope=1.6E-10, R2=0.99.

Once this was verified, the binding of the P(TxRed) to the STAmp in-paper was quantified by performing both heating and visualization in the Standard-17 membrane. Any intensity differences between heating performed in-tube and heating performed in-paper were determined to more accurately quantify amplicon production during amplification. A 44% loss in fluorescence intensity was observed when the solutions were heated in-paper as opposed to in-tube (Figure 21).

This knowledge can be used to develop a correction factor for measurement in-tube vs. measurement in-paper. The three tools discovered and developed in this chapter—low background fluorescent substrate, high SBR fluorescent probe, robust quantitative standard curve—could now be combined to visualize and quantify amplification in porous media.

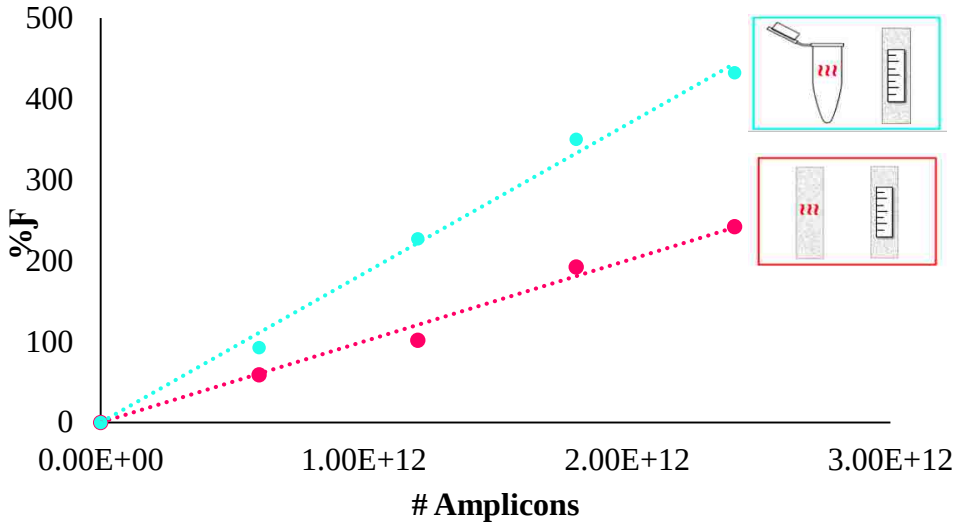

Figure 21. The effect of heating mechanism on the P(TxRed)-STAmp standard curve on fluorescence measurement in-paper. Heated in-tube (blue) and heated in-paper (pink).

Chapter 4. Visualization and quantification of DNA amplification in porous media

4.1 Motivation & Approach

As mentioned previously, the goal of the MAD NAAT project is the development of a robust, rapid, sensitive and easy-to-use diagnostic device. Invariably, when transferring these well-developed laboratory assays into a new substrate, which must store and support these processes under non-optimal conditions, there will be performance losses. The quantitative fluorescence optical method developed in Chapter 2 allows for the visualization and assessment of the impact these processes have on device performance. With the appropriate substrate, probe and quantitative standard in place, these component parts could be implemented in the system to visualize and quantify amplification in-paper from first fresh reagents and then dry reagents. This data will provide us with a validation of this optical method in porous media.

In addition to providing the ability to determine the heterogeneity of rehydration and amplification performance from dry reagents in the device, this tool could be implemented as a detection method in lieu of lateral flow detection. Currently, the lateral flow detection system used for this device must be performed on nitrocellulose because its pore structure and wicking rate make this material preferable for binding capture probes. However, as this material is a slow-flowing substrate, this detection method adds 10-15 minutes to the total device run time. The goal is to make this MAD NAAT device as rapid as possible in order to meet the requirements at the POC, and this step adds valuable time. This fluorescence method allows for detection in-situ, thereby improving the speed of the device. Although lateral flow detection is often used in POC diagnostics, because of its simple read-out and lack of auxiliary equipment,

many groups have developed inexpensive and simplified fluorescence detection systems that could be implemented in LRS, making this detection method feasible [52].

4.2 Quantification of iSDA in-paper from fresh reagents.

4.2.1 Amplification heated in-tube

Using the calibration curve obtained from the fluorescence of the P(TxRed)-STAmp complex, the amplicon output of the iSDA reaction was determined for different DNA copy inputs. With this technique, I was able to visualize and quantify amplification down to *20 input copies* in-tube (Figure 22). According to our collaborator Dr. Jan Englund at Seattle Children's Hospital, the current clinical range for detection of MRSA is 10^2-10^7 input copies and therefore this detection method enables detection below the clinical range

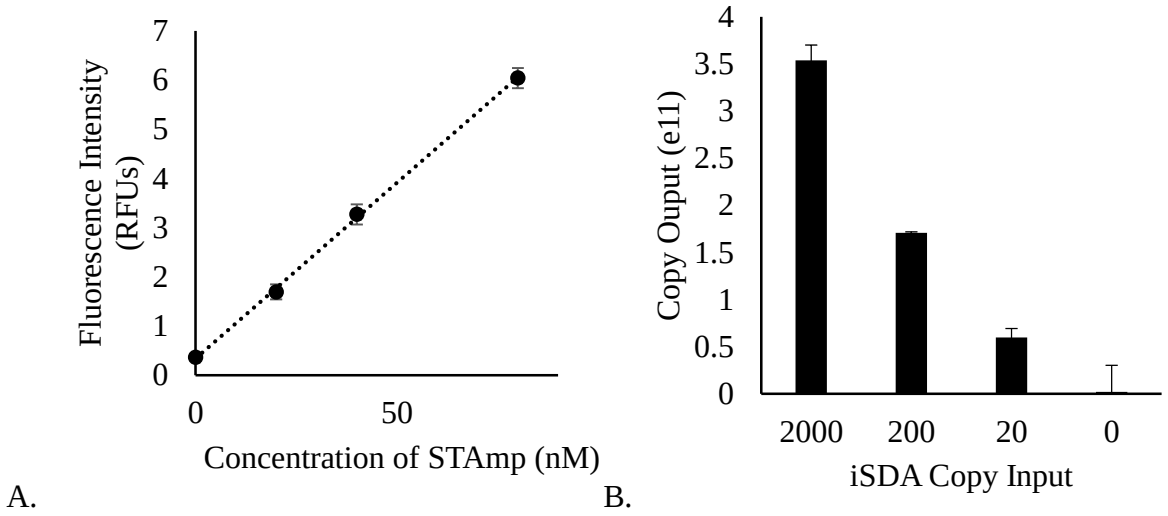

Figure 22. Quantification of iSDA output in-tube down to 20 input copies. STAmp standard curve (A), R^2=0.99933 used for the quantification of a tube based iSDA reaction (B).

With this capability, the next step was to determine whether the amplification performance is dependent on DNA concentration and reaction volume. The two main volumes of interest were 10 μL and 35 μL. 10 μL was the maximum volume that can be visualized with Standard-17 with the current microscope set-up, whereas 35 μL was the reaction volume used in the MAD NAAT device. It was of interest to determine whether the two volumes would result in distinctly different amplification outputs. Amplification reactions were prepared and run in-tube with the same nominal DNA copy input of 20,000 for a 35 μL or 10 μL amplification reaction with a DNA concentration of approximately 500 copies/μL or 2,000 copies/μL, respectively (Figure 23). The 10 μl reaction first appeared to produce less amplicons using the STAmp calibration curve. However, it should be noted that previous calibrations using the Rotor-Gene 6000 qPCR machine showed that the fluorescence signal for reactions volumes below 20 μL exhibited a 20% lower fluorescent signal for an equivalent STAmp concentration as reactions volumes larger than 20 μL (Appendix Figure 18). Therefore, it likely that a percentage of this

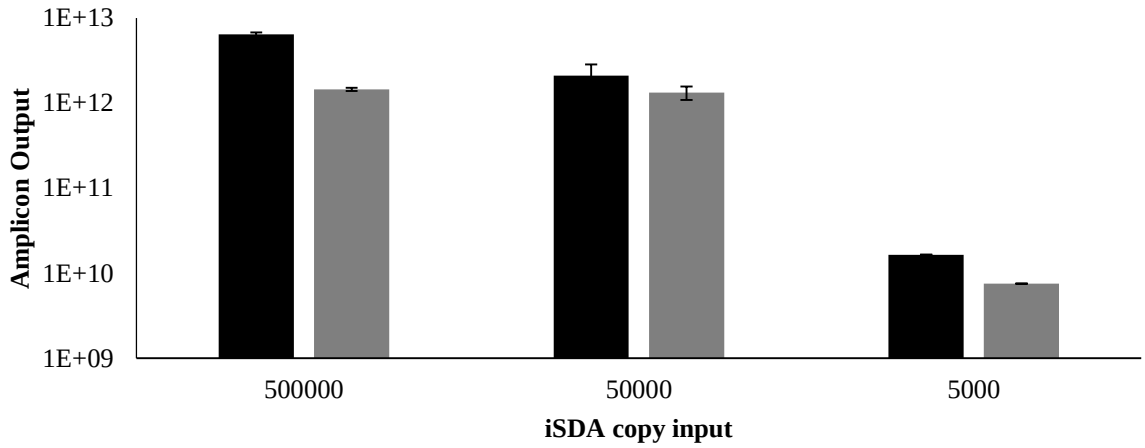

Figure 23. Calculated amplicon output from in-tube iSDA reactions at various input copy number and 2 reaction volumes: 35 μL reactions (black) and 10 μL reactions (grey).

signal loss is due to measurement error rather than reduced amplicon production. Regardless, the amplification performance is very similar between the two reaction volumes.

Once DNA concentration was not found to have a large impact on amplicon production, iSDA output could be quantified using the STAmp calibration curves in-tube and in-paper. iSDA reactions were mixed, heated and measured in-tube. Post-amplification, the same reactions were transferred onto Standard-17 membranes and fluorescence intensity was measured in-paper. Fluorescence measurements acquired in-tube and in-paper were quantified using their respective STAmp calibration curves in the absence of any additives (Figure 24).

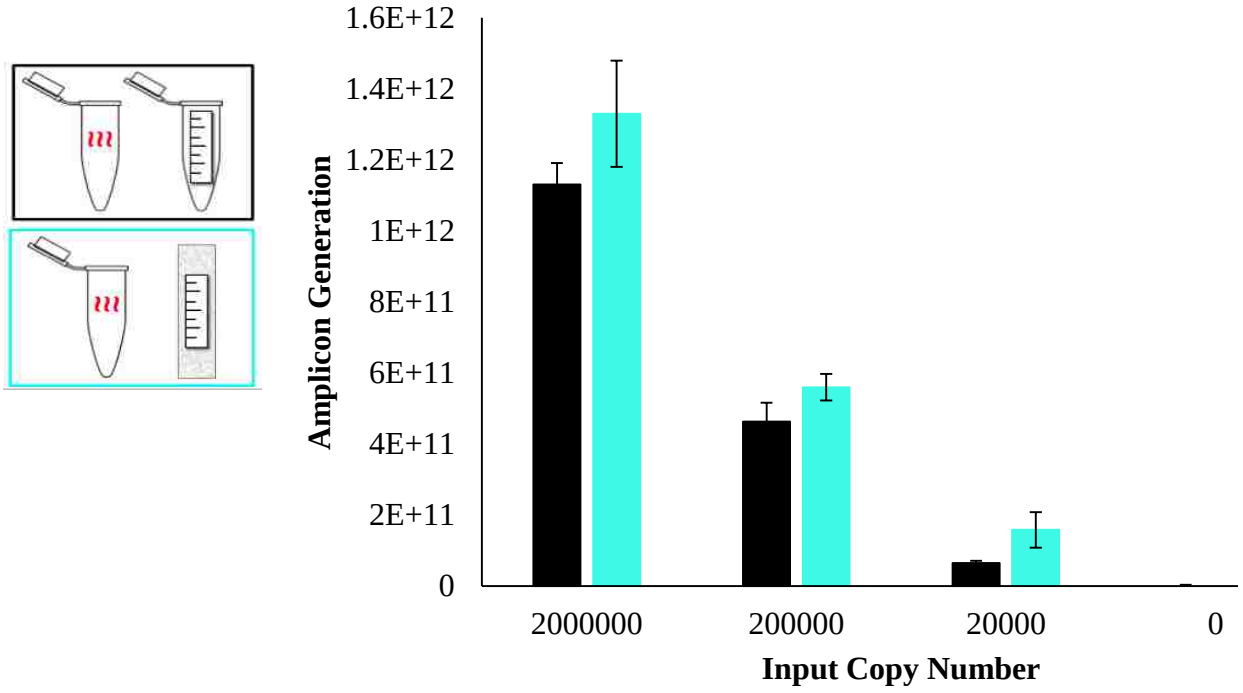

Figure 24. iSDA reaction performed in-tube and measured both in-tube and in-paper without additives. End-point quantification for reactions heated in-tube but measured in-tube (black) and measured in-paper (blue). n=3

4.2.2 Amplification heated in-paper

After proving that the amplification products in-paper could be quantified, the next step was to observe real-time amplification in-paper. Amplification reagents with a reaction volume of 10 μL were mixed in-tube and applied to a 5 x 5 mm glass fiber pad in a device chamber. Images were captured every minute and the fluorescence output was measured and quantified by averaging the pixel intensity over the 25mm^2 area of the pad (Figure 25). In conjunction, a reaction was heated and measured in-tube as the control. Although the same fluorescence behavior was observed in-paper as is observed in-tube, when compared to in-tube amplification there was a delay in the time at which fluorescent signal was observed to surpass the background fluorescence and also a decrease in total amplicon generation. Initial hypotheses suggested that the lift-off time for the amplification reaction in the glass fiber was slower than for the tube assay, possibly due to reduced heating efficiency, although data presented later in this work will prove otherwise. However, even with this slight delay, the amplification is complete in less than 20 minutes, which is faster than many other isothermal amplification methods.

We believe that this method represents the first visualization of real-time DNA amplification in porous media and is a technique that provides useful information that improves the understanding of the process occurring in the substrate. With this validation, we could move on toward more device-like systems by visualizing amplification from dry reagents.

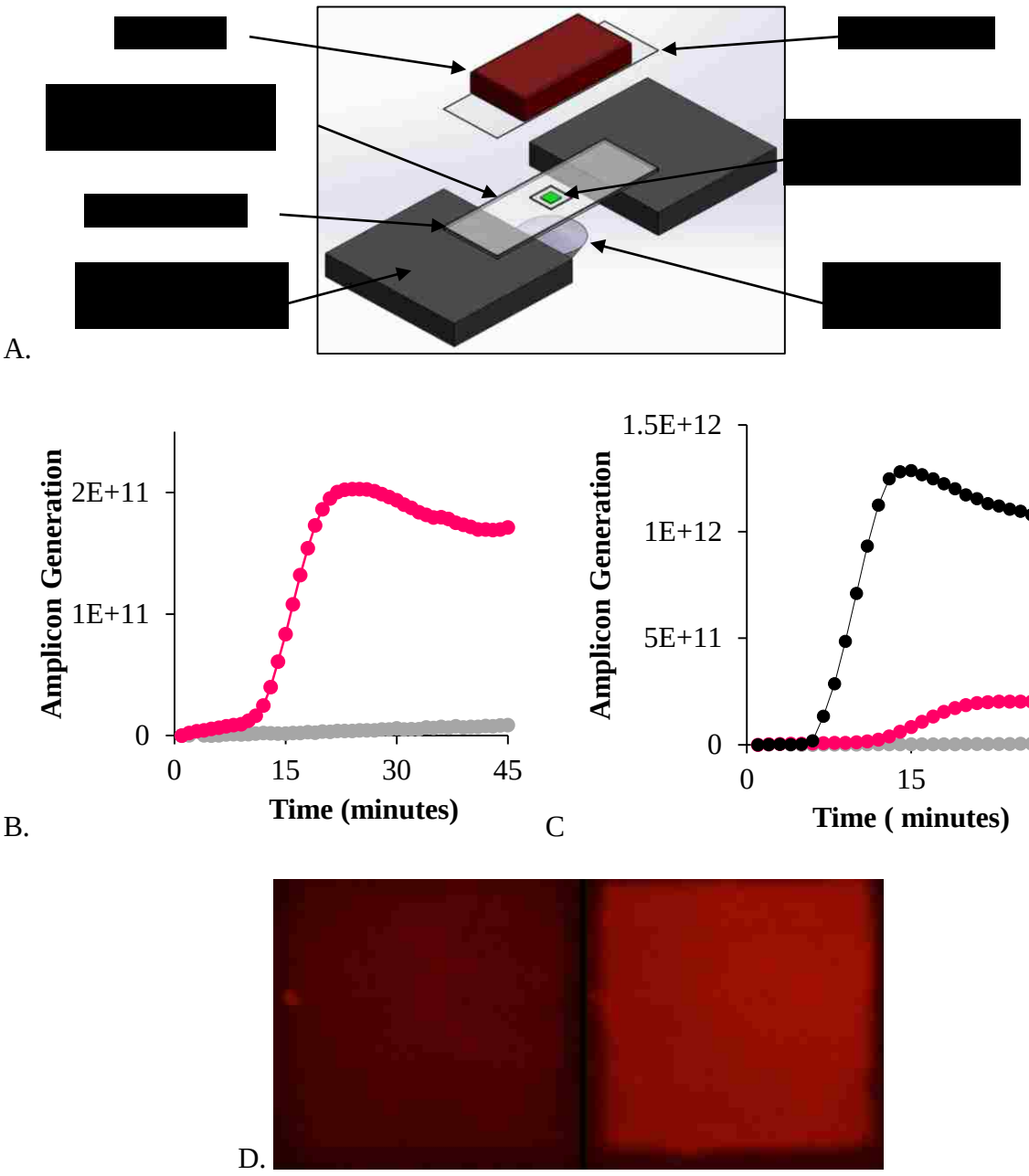

Figure 25. Real-time amplification from fresh reagents. Experimental set-up for amplification reactions performed in-paper (A). Amplification heated and measured in-paper (B) at 20,000 input copies (pink) and 0 input copies (grey). Results from B compared to amplification heated and measured in-tube (black)(C). Images of glass fiber substrate at t=0 (left) and t=30 minutes (right) for the 20,000 input copy reaction (D).

4.3 Quantification of amplification from dry reagents

With the standard curves and correction factors quantified, movement toward amplification in-paper from dry reagents was continued. To set a baseline for these experiments, iSDA was performed at 20,000 input copies of MRSA DNA since the output for the specific iSDA assay used was easily visible in-tube and in-paper. This reaction was performed in-tube from fresh reagents, in-paper from fresh reagents and in-paper from dry reagents (Figure 26). In this case, dry down was performed only using 10% trehalose and 2.5% dextran as the starting case. A further description of the method for storing dry reagents in porous materials can be found in section 4.3.1.

From this data, an amplicon production that is four times less in-paper using fresh reagents as compared to in-tube. Amplicon production is further reduced by four times when amplification is performed from dry reagents in-paper as compared to fresh reagents in-paper. The resulting 6% performance observed from amplification performed from dry reagents in-paper as compared to amplification from fresh reagents in-tube illuminates the losses experienced in this system. Due to these loses, we desired to investigate possible ways to improve amplification from dry reagents in porous media.

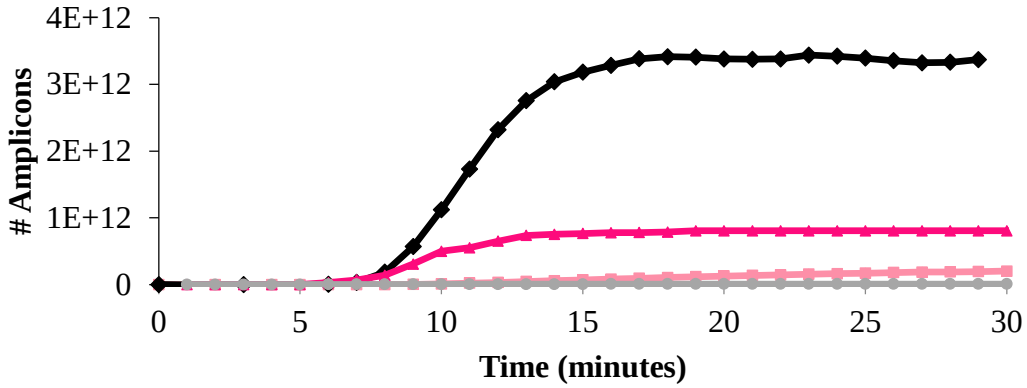

A.

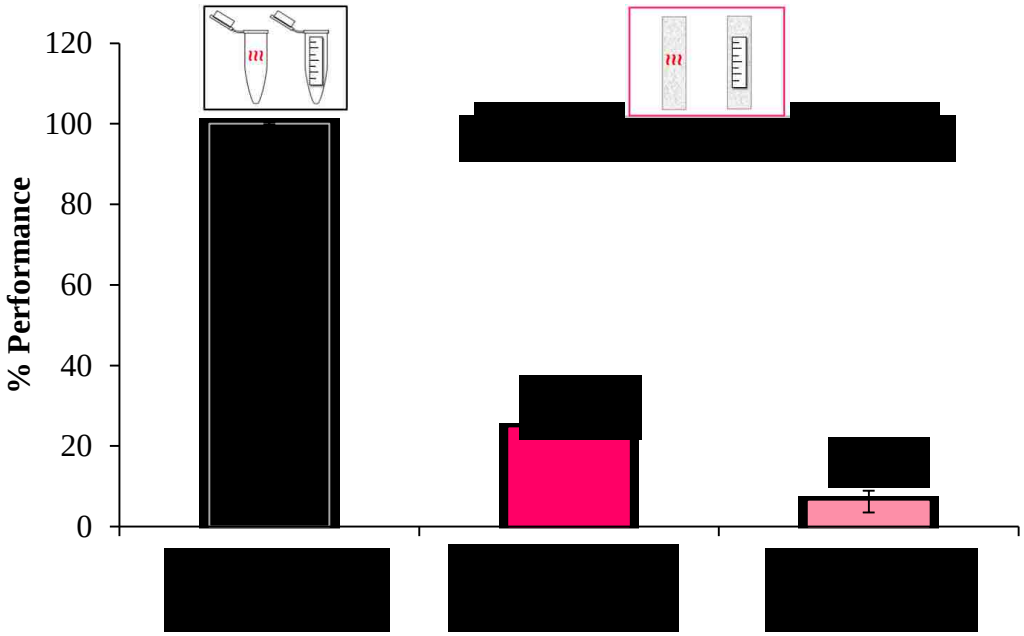

B.

Figure 26. Real-time amplification curves and output for reactions performed from both fresh and dry reagents in-tube and in-paper. Real-time amplification curves from 20,000 input copies of genomic MRSA DNA in-tube (black), in-paper from fresh reagents (dark pink), in-paper from dry reagents (light pink) and a fresh, in-paper NTC (shown in gray) (A). Percent performance of amplification as compared to fresh, in-tube reactions at 20,000 input copies (B).

A.

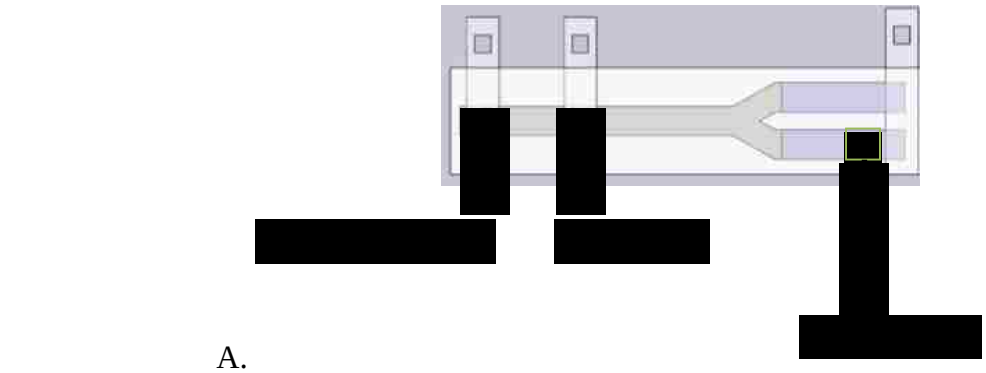

B.

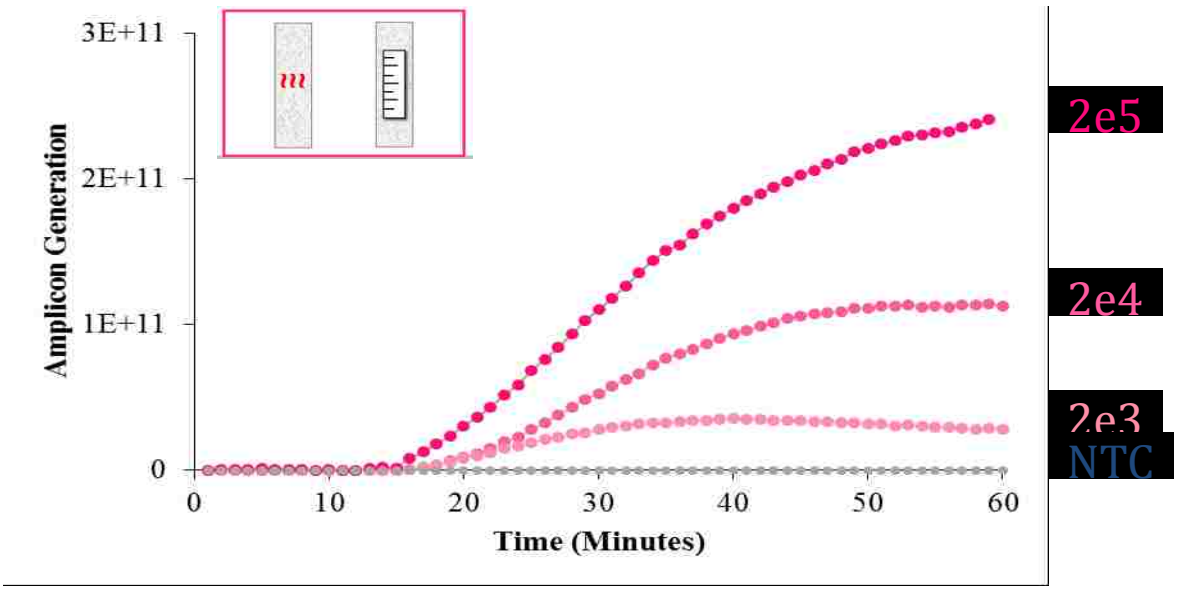

C.

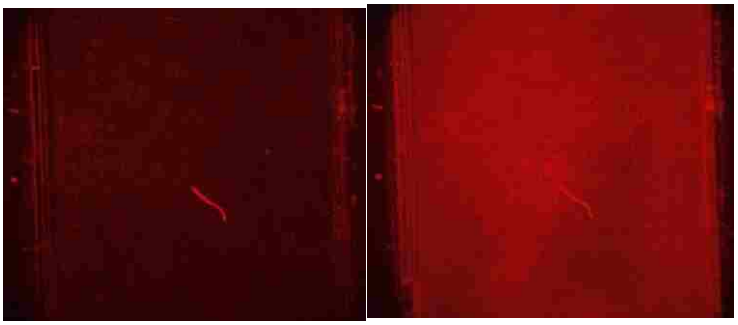

Figure 27. Amplification from dry reagents. Schematic of the 2-dimensional paper-network (A); real-time curves (B) for input copies of 200,000 (dark pink), 20,000 (pink), 2,000 (light pink) and 0 (grey); images at t=0 (left) and t=30 minutes (right) for the 20,000 input copy (C).

Once the ability to visualize and quantify amplification from dry reagents was determined, we moved toward visualization in a real device to determine whether amplicon production was lower in this context. The devices analyzed were one of the versions used in the MAD NAAT device, with the omission of the nitrocellulose lateral flow strips after the amplification zone. 80µL of DNA was added to the glass fiber sample port of the device followed by 120 µL TE chase buffer. The amplification zone was heated at 49°C for 30 minutes and fluorescence was visualized using fluorescence microscopy. This device was assessed at 2e5, 2e4 and 2e3 input copies (Figure 27). Amplification lift-off times were observed to be much later than in-tube (12-18 minutes in-paper vs. 7 minutes in-tube). The amplicon production at 20,000 input copies for this data resulted in only 3% performance as compared to fresh in-tube. We believe this could be due to inhibition caused by material choices for the valve used to stop fluid flow past the amplification region. This hypothesis is due to the reduced amplification region observed at the downstream end of the amplification pad that was in contact with the valve (Figure 28). With the knowledge of this baseline performance, we could then assess how changes to the device might affect amplification efficiency and improve amplification in-paper from dry reagents.

Fluid Flow →

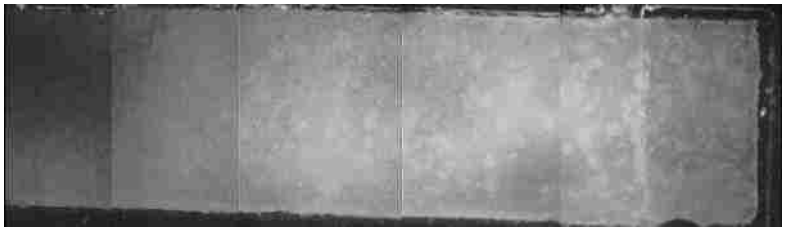

Figure 28. Stitched image of Standard-17 glass fiber post-amplification from dry reagents at 20,000 input copies. 20 mm amplification pad image taken at t=60 minutes using the Zeiss 61 HE rhodamine filter set on the Axiovert25 microscope with 2.5x objective and 200 ms exposure time.

Chapter 5. Development of analytical tools to assess amplification performance in the MAD NAAT Device

4.4 Motivation & Approach

The ability to visualize and quantify amplification in-porous media from dry reagents is a unique and important tool in the development and optimization of POC diagnostics. One of the benefits of this technique is the ability to obtain spatial information over the entire region of the substrate in real-time as opposed to the global, end-point analysis that is often used for these assays. In this chapter, I will describe evaluation tools that allow for enhanced analysis of the data obtained from the optical method previously presented. Furthermore, demonstrations of these tools to analyze and assess changes in the MAD NAAT device will be shown.

This quantitative fluorescence detection tool has unique capabilities to answer questions concerning amplification performance in response to device and assay variations such as reagent composition, method of dry down storage, and rate of rehydration, among others. I will first present the analytical tools to assess these changes then apply the novel optical method and analysis tools to investigate variations caused by these changes. Amplification performance will be determined using two metrics—the time for the fluorescent signal to reach 15% over background and the total amplicons produced. The former is important for POC diagnostics because of its role in total assay time while the latter is important because of its role in device LOD. Finally, the most optimal combination will be used to determine the current LOD of this detection system.

4.5 Local Analysis Tools

4.5.1 Device design.

One of the drawbacks of previous experiments attempting to look at amplification along a 20 mm strip was the 5 mm visualization window of the fluorescence microscope. To observe amplification along the whole strip, a rig was built that allows imaging along the whole length of the 20 mm strips in real-time by moving the slide 5 mm every 15 seconds to maintain the 1-frame/minute capture rate previously used in a real-time experiments (*Figure 29*). With this capability, we could regain the information previously lost by imaging only 25% of the pad in real-time.

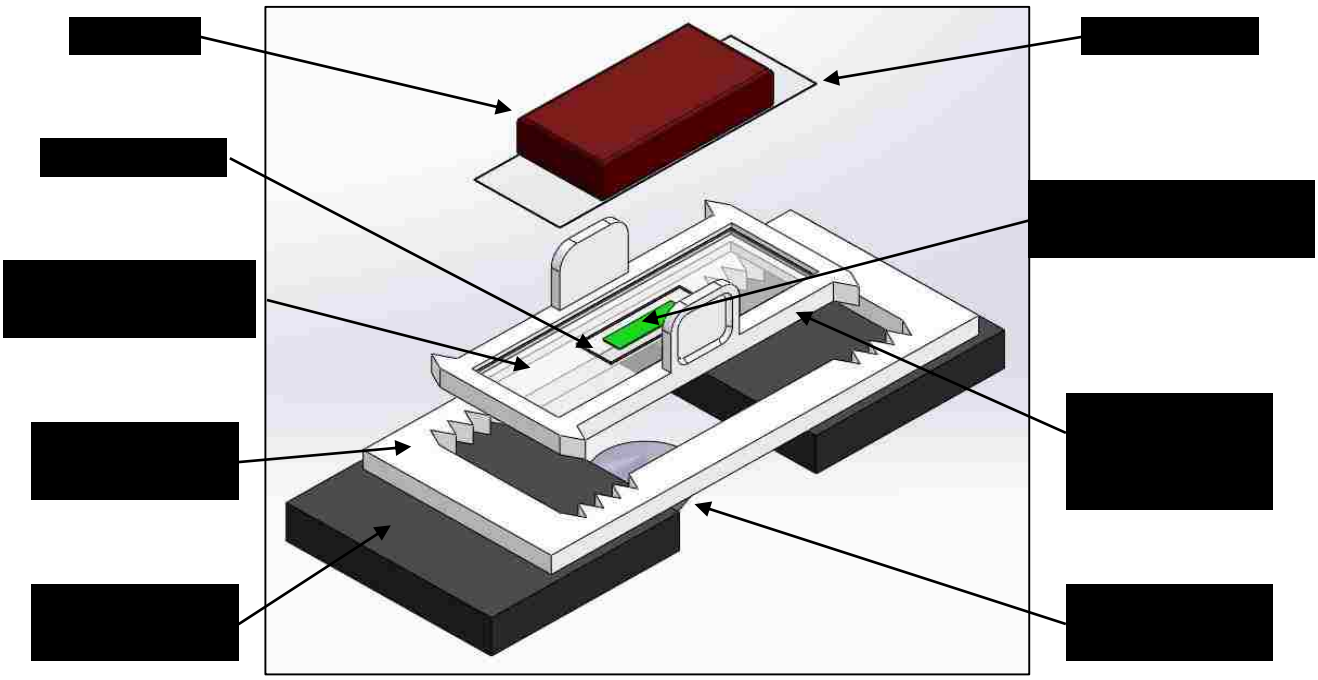

Figure 29. Experimental set-up for visualizing real-time amplification from dry reagents on the microscope.

4.5.1 Surface Plot Analysis.

The real-time images previously shown from amplification from dry reagents in porous media demonstrated a long-expected non-uniformity in amplification. To quantify the extent of this non-uniformity, Dr. Joshua Bishop and I developed a way to analyze and display local amplification information for the entire reagent pad. We imported the data acquired from the first run of amplification from dry reagents at 20,000 input copies into Mathematica. This image was compartmentalized into 100 pixels^2 regions of interest (ROIs), which resulted in over 9000 ROIs. For each of these, the amplification curve was plotted in terms of amplicons produced. Since the

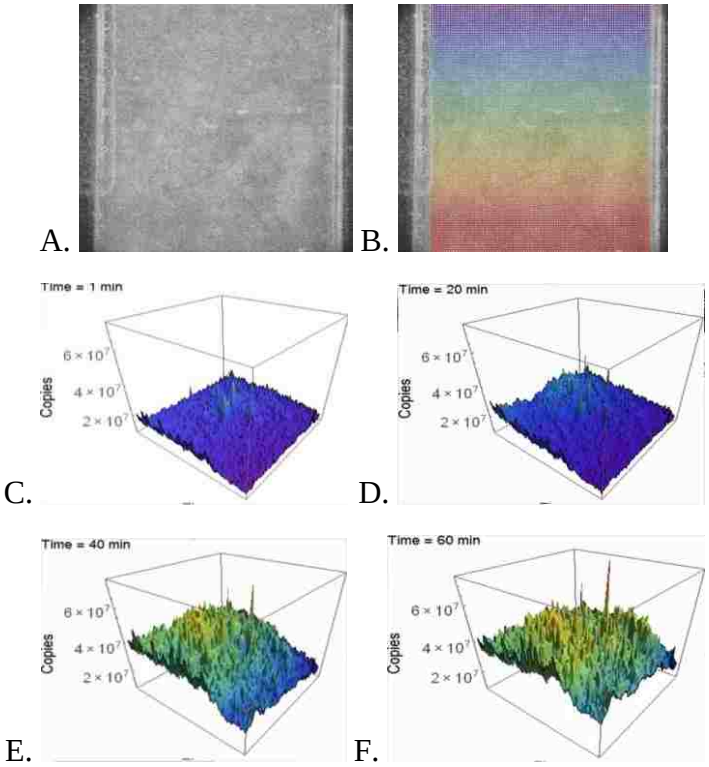

Figure 30. Surface plot analysis of amplification from dry reagents. Image at t=60 minutes of amplification region (A) and with grid overlay (B). Surface plot of real-time amplification video from dry reagents at t=0 minutes (C), 20 minutes (D), 40 minutes (E) and 60 minutes (F).

visualization of the amplification curve for all ROIs is difficult to interpret, a surface plot of these curves was used to display the information more effectively (Figure 30C-F).

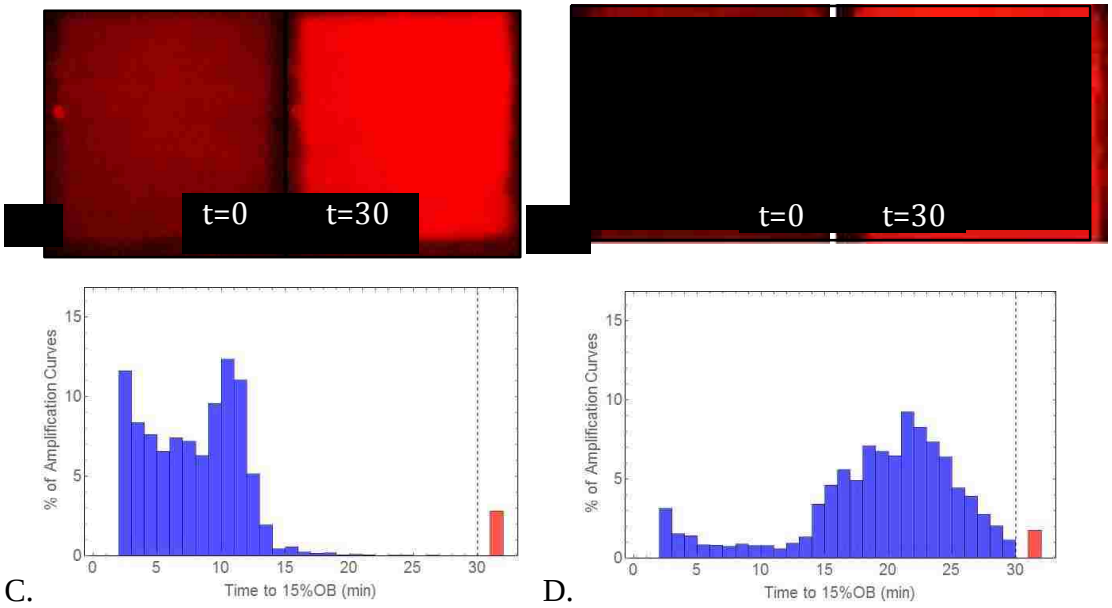

Figure 31. Histogram analysis for amplification in-paper. Real-time amplification from fresh reagents in-paper (left) and dry reagents in-paper (right). False-colored images at t=0 and t=30 minutes (A,B) Histogram of 9373 amplification curves depicting time to reach 15% over background (C,D).

4.5.2 Histogram Analysis.

The other metric chosen to quantify amplification performance was the time for the fluorescent signal to reach 15% over background. This metric could be applied to each of the ROIs created for the surface plot analysis. The histogram for the amplification curves for all ROIs was calculated for both fresh and dry reagents (Figure 31). For amplification from dry

reagents a histogram with a mean of 19 minutes and standard deviation of 6 minute was observed. Analysis for the histogram data for amplification from fresh reagents shows a distribution with a much lower mean—8 minutes—and a standard deviation of 5 minutes.

4.6 Application of these tools

4.6.1 Dry Storage Optimization.

Long-term dry storage of the reagents needed for amplification is extremely important in the development of a POC assay. That is why the efficiencies of the two drying methods available in the lab—vacuum drying and freeze drying (or lyophilization)—were compared. In both cases, the amplification reaction mixture was first applied onto glass fiber pads placed in a 12 well-plate before drying. Vacuum drying was performed using a miVac gene concentrator at 25°C (Barnstead, Ipswich, Suffolk) for 2 hours. Lyophilization was performed by first submerging the plate and amplification pads in liquid nitrogen for 1 minute then transferring them to a FreeZone Freeze Dry System (Labconco, Kansas City, MO) for 2.5 hours. Amplification was performed by heating in-paper from reagent pads dried either by vacuum drying or lyophilization. After thirty minutes of heating at 49°C, the reagent pads were centrifuged in a spin column and the liquid was collected. This liquid was then transferred into a tube and the end-point fluorescence was measured and quantified using the Rotor-Gene (Figure 32).

In this experiment, the amplicon production for the amplification reaction using vacuum dried reagent pads was found to produce 77% less amplicons than amplification in the freeze-dried pad. Although this is only 1 experiment, this result aligns with the knowledge concerning

the benefits of freeze-drying. We believe this is because the structure of the iSDA components—particularly enzymes—is preserved better with the rapid freeze-dried process [53]. There are two main mechanisms by which trehalose is postulated to preserve enzymes [54]. One such is water-replacement theory in which the trehalose molecules are able to replace the water content in the protein, thereby preserving its structure. The dominating theory on why trehalose works is the vitrification theory. This is similar to how a fly is preserved in amber, where the trehalose forms a protecting layer around the protein to maintain its structure and therefore functionality. We believe that through freeze-drying, the trehalose is able to more effectively preserve these proteins because of the rapidity of the process, thereby maintaining amplification performance.

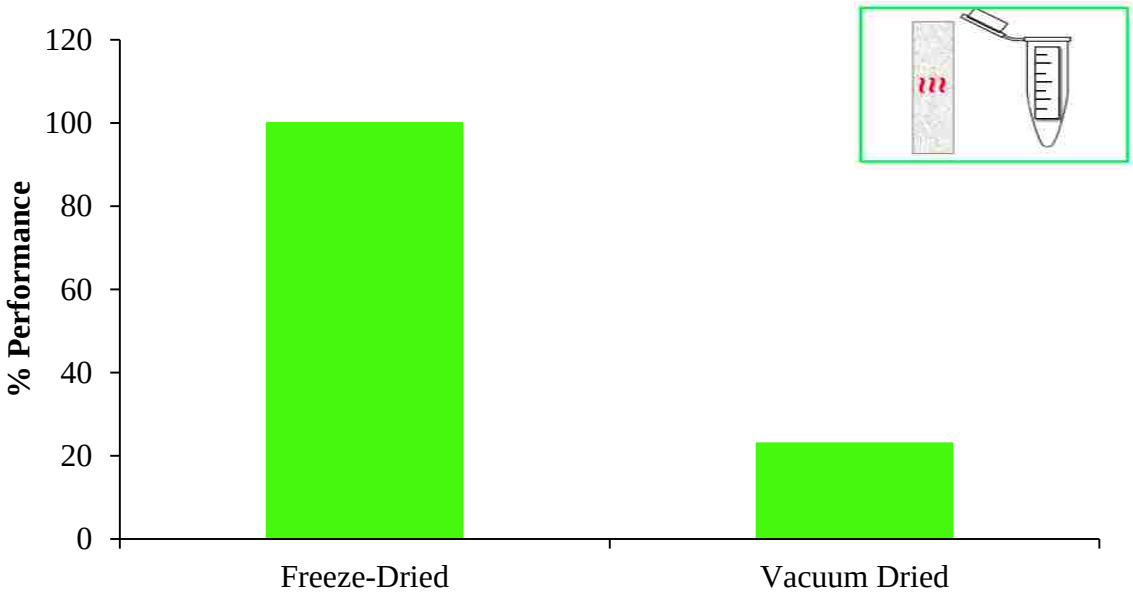

Figure 32. Effect of drying method on amplicon generation at 20,000 input copies. Percent performance compared to freeze-dried. Heating performed in-paper and measurement performed in-tube.

4.6.2 Variation of imbibition time.

Data demonstrating the sensitivity of iSDA performance to reagent concentration was shown in Figure 3. Amplification was either very poor or non-existent at concentrations outside the range from 1.0x-1.5x. In an effort to determine the distribution of reagents throughout the amplification pad after rehydration, reagent pads were made with only fluorescent dNTPs, 10% trehalose and 2.5% dextran, dried *via* lyophilization and rehydrated. The distribution of fluorescent dNTPs was visualized post-rehydration by Dr. Melissa Li. A compaction of reagents at the downstream end of the pad was observed and the fraction of the pad with relative fluorescence intensity outside of the area between 1.0x and 1.5x was high (Figure 33). This data, combined with the in-tube analysis depicting the tight concentration tolerance of iSDA, demonstrated the likelihood of reduced amplification performance when amplification is performed from dry reagents in porous materials.

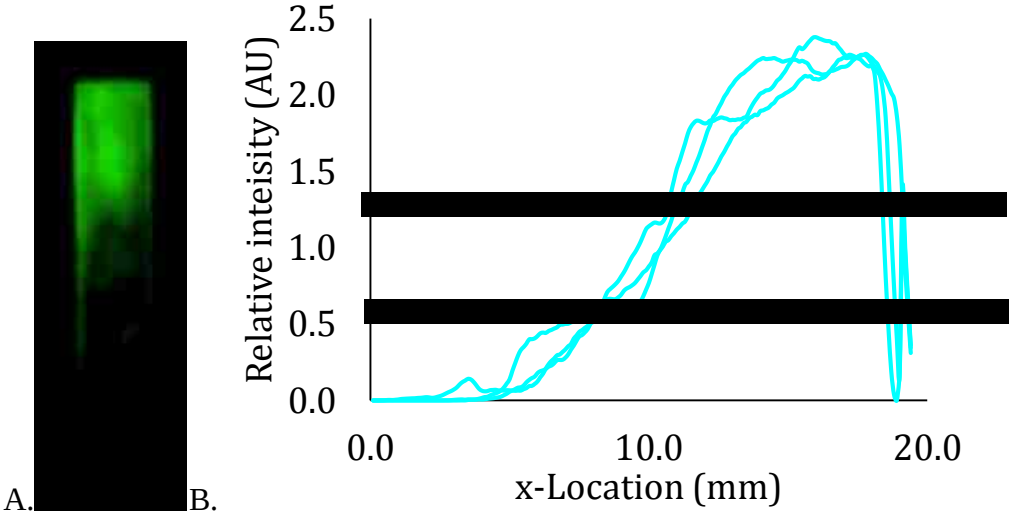

Figure 33. Reagent compaction after rehydration in Standard-17 using fluorescent dNTPs. Image of reagent pads dried with 10% trehalose and 2.5% dextran post rehydration (A). Relative fluorescence intensity along the pad calculated and plotted over 3 reagent pads (B). Dotted lines represent area within which amplification would be expected to occur.

To reduce the compaction of reagents during rehydration, we hypothesized that controlling the imbibition rate could change the rehydration profile. This in turn would alter the amount of reagent compaction and therefore, vary the amplification performance. Increasing the imbibition time was thought to result in an increase in the amount of compaction of reagents, thereby reducing amplification performance. However, when imbibition was controlled using a syringe pump (New Era Syringe Pump Systems Inc., Farmingdale, NY) for fluid delivery into the amplification pads, no significant relationship could be obtained between amplification performance and rehydration time (Figure 34).

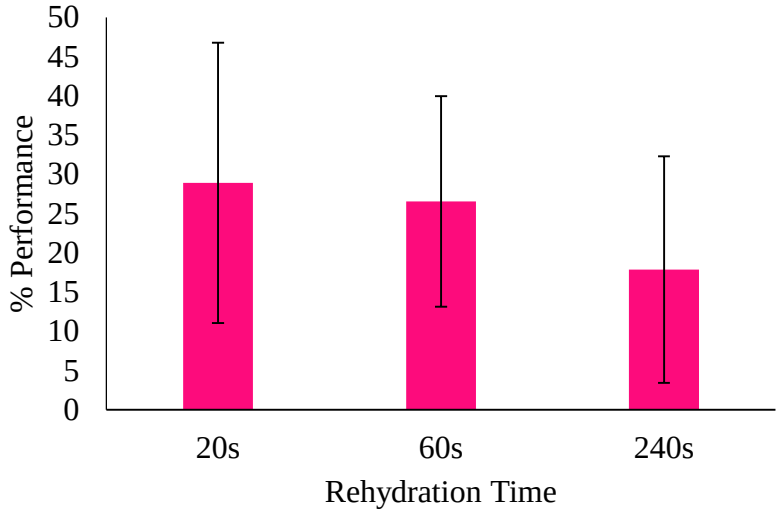

Figure 34. Percent amplification performance as compared to fresh in-tube for 20,000 input copy amplification reactions heated and measured in-paper from dry reagents at varying rehydration times. Reagent pads dried down with 10% trehalose, 2.5% dextran and 2.5% PEG 8000. n=10.

One possible mechanism for the lack of trend in amplification performance in response to varying imbibition rate was the rapid speed of rehydration. When rehydrating pads dried with fluorescently-labeled sugars at an imbibition time of 20 seconds, microscopy analysis showed that the signal was rapidly reduced and fell below 15% over background at 23 seconds (Figure 35). Even at an imbibition time that is as fast as the substrate can support (20 seconds for Standard-17), rapid rehydration and therefore, compaction is achieved. This suggests that the rehydration rate in this context is very close to the imbibition rate and slowing down the imbibition would not result in drastically increased compaction.

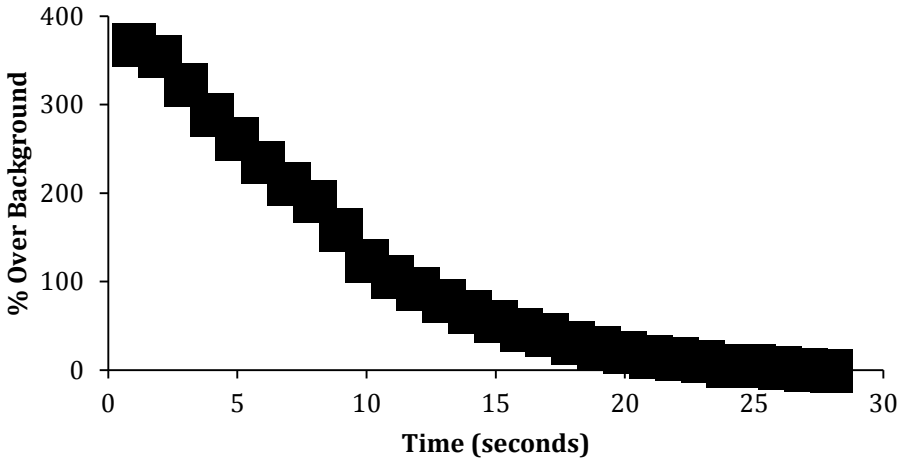

Figure 35. Fluorescence signal decrease upon rehydration of FITC-PEG dried in Standard-17 at an imbibition time of 20s. Axiovert25 inverted fluorescence microscope, 2.5x objective, 200ms exposure time, 61 HE FITC filter set.

Furthermore, when the STAmp was used to rehydrate the amplification pads instead of genomic DNA, a fairly uniform fluorescence signal is observed, suggesting that the fluorescent probe is distributed throughout the majority of the length of the pad (Figure 36). The distribution

of the probe could thereby serve as an indicator of the distribution of other components; this visualization demonstrates that the reagents are, by a few minutes after rehydration, much more evenly distributed than previously thought. The histogram analysis confirms this relative homogeneity as well as proves that none of the fluorescence signals for any ROI were saturated. The peak seen at the left-hand side of the histogram was a result of the area in which no reagents were present. As only 35 μL reaction volumes were applied to glass fiber pads with a 40 μL capacity, a non-fluorescent area corresponding to a 5 μL volume would be expected. However, this area appears to encompass approximately 25% of the pad (10μL volume), pointing to some compaction of reagents.

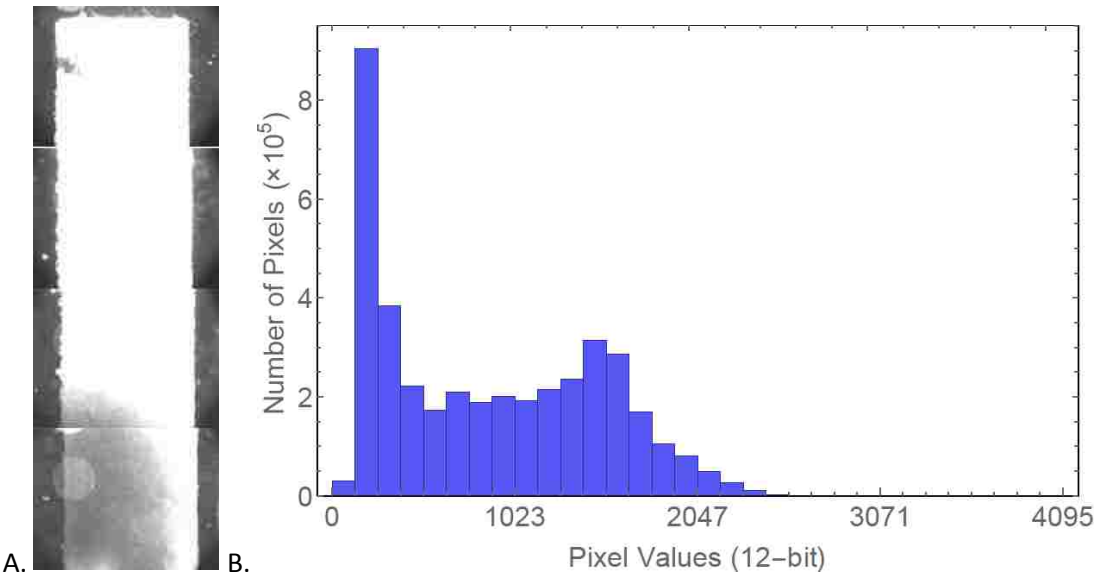

Figure 36. Rehydration and heating of iSDA reagent pad with STAmp. Image of the pad after heating at 49℃ for 30 minutes (A) and histogram distribution of intensities of ROIs (B). Higher pixel value corresponds to higher fluorescence intensity.

4.6.3 Reagent Composition

Addition of PEG. Due to inconsistencies with flow into the nitrocellulose membranes used for lateral flow detection in the MAD NAAT device, polyethylene glycol with a molecular weight of 8000g/mol (PEG-8000) was added to potentially remove the need for additional surfactants. The ability for iSDA to tolerate PEG was of concern and the fluorescence optical method had the ability to determine whether or not this addition had any effects on amplification. The amplification using pads made from the MAD NAAT standard additive formulation (consisting of 10% trehalose and 2.5% dextran) was compared with pads made with 10% trehalose and 2.5% of both the PEG-8000 and dextran.

Both the real-time curves and time to reach 15% over background were quantified in-paper over 6 runs for each condition (Figure 37). Although there is a large variability in amplicon production, a statistically significant improvement in both amplicon production and time to reach 15% over background is seen by the use of PEG. Therefore, the reagent composition that was chosen to improve lateral flow detection has the potential of improving amplification from dry reagents.

Primer Design. As mentioned previously, some of the non-target amplification products created in an iSDA reaction are due to the dimerization and polymerization of primers capable of hybridizing to one another. After further investigation, collaborators on the MAD NAAT project at General Electric designed primers that reduced the potential for base pairing overlap between primers to reduce these extraneous products. This new set of primers (primer "D") was tested for its sensitivity to reagent concentration by varying the concentration of all reagents except the probe, trehalose, dextran and PEG. The probe concentration used in this experiment was

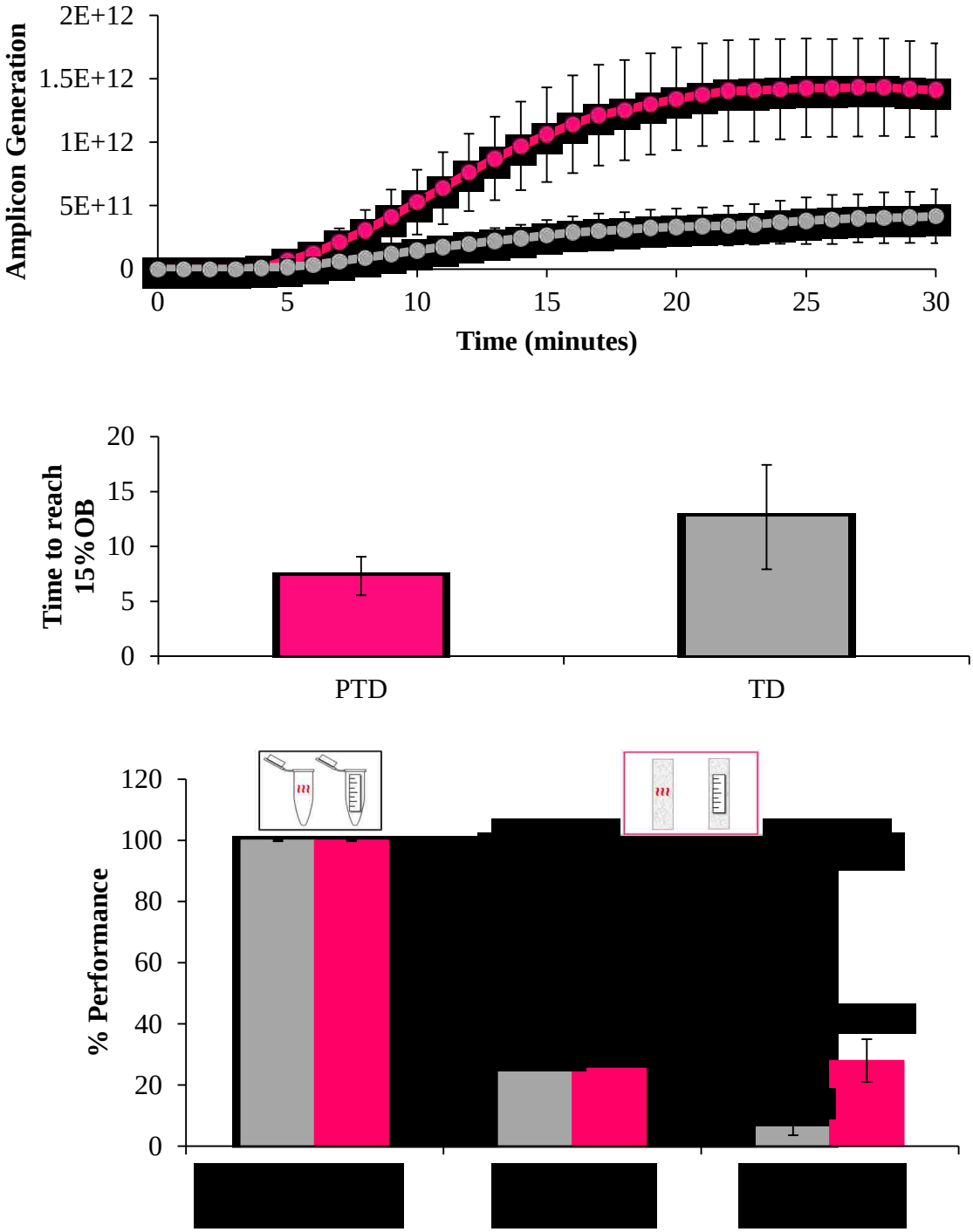

Figure 37. Effect of the addition of PEG on amplification performance at 20,000 input copies. (A) Real-time curves for T/D (gray) and P/T/D (black) for n=6. (B) Average time to reach 15% over background for each of the 6 amplification curves. (C). % Performance as compared to 2e4 fresh in-tube for iSDA reactions with PEG (black) and without (gray).

increased to 400 nM to ensure that none of the reactions were limited by the amount of probe. For this experiment, the reaction was found to no longer be as sensitive to reagent concentration. Good amplification was still observed between 0.75x and 2.0x reagent although there does appear to be some reduction in amplification performance at other reagent concentrations (Figure 38). This is a large improvement from the previous data acquired with earlier primers that required the iSDA concentration to remain between 1.0x and 1.5x for good amplification.

If the number of amplicons produced from an iSDA at 1.0x nominal reagent concentration was used to extrapolate an expected amplicon generation based only on increasing dNTP concentration, one could hypothesize that if there was no change in amplification performance based on iSDA reagent concentration the amplicon generation would be directly proportional to the dNTP concentration. This expectation is depicted by the dotted lines in Figure 38B. Furthermore, when comparing amplification reactions for the time of the fluorescence signal to reach 15% over background, this time would not change with varying reagent concentration, as noted by the dotted line in Figure 38C. However, a variation from the behavior assuming equivalency to the 1x reagent concentration is seen in both cases. Therefore, there is an effect of reagent concentration on amplicon generation, just not to the extent we had previously observed. This robustness could also be a reason for why varying imbibition rate did not seem to affect amplicon generation. It is possible the rehydration profile is changed at different imbibition rates, but most areas of the amplification region are still within the range of 0.75x-2.0x. To test this, a more thorough analysis of reagent distribution upon rehydration at various imbibition times should be obtained.

4.6.4 Improved temperature control.

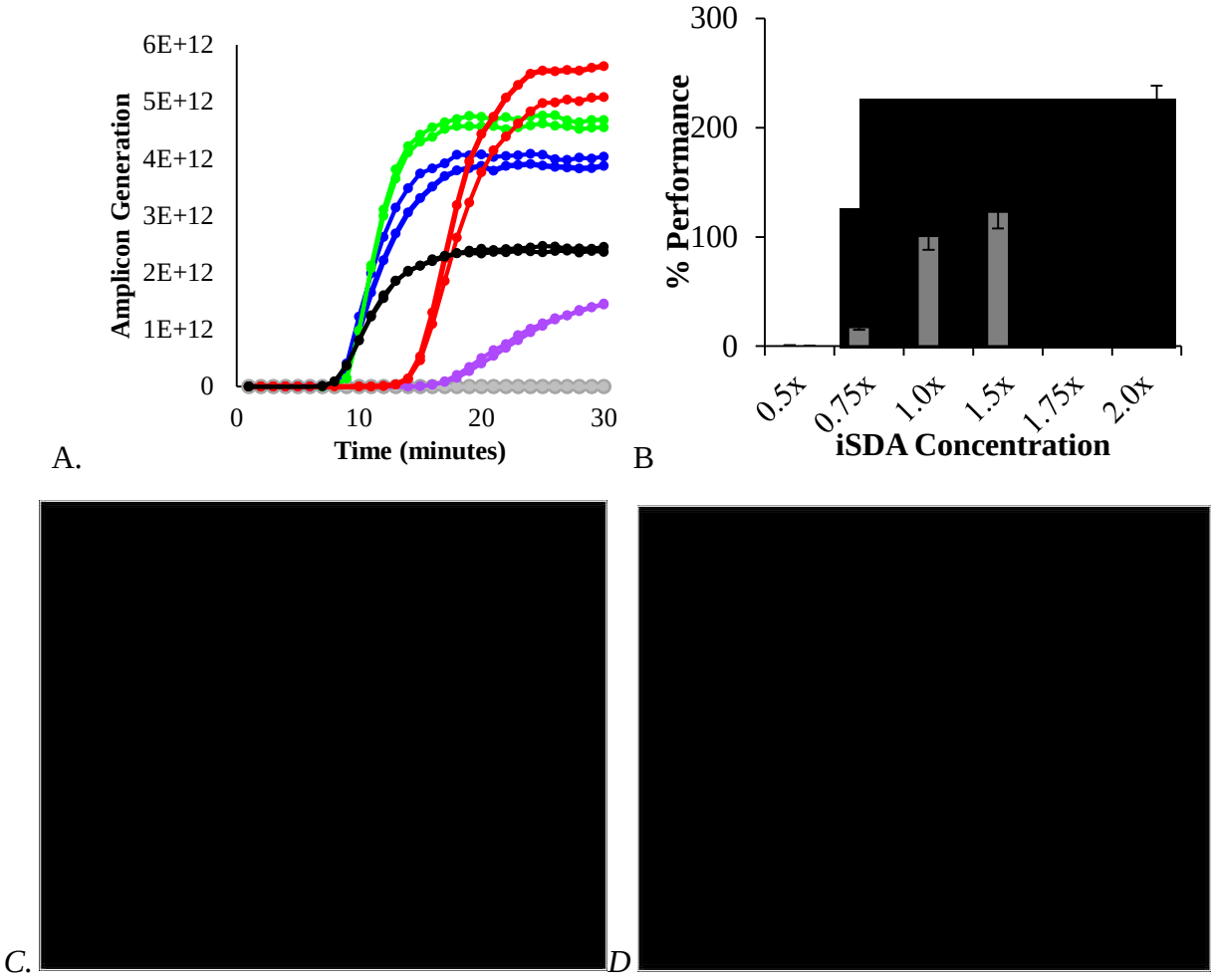

Figure 38. Amplification performance at various concentrations of iSDA reagents with primer set "D". All measurements heated and measured in-tube. Real-time curves for reactions with varying concentration of iSDA reagents (A): 0.5x (grey), 0.75x (purple), 1.0x (black), 1.5x (blue), 1.75x (green), 2.0x (red). Percent performance as compared to 1.0x concentration for old primers (grey) and new primers (black). End-point amplicon generation (C) and change in time to reach 15% OB (D). Dotted lines represent theoretical data assuming performance based on 1x.

Amplification reactions are sensitive to temperature and must operate at or close to the desired temperature for optimal performance. The temperature at the surface of the glass fiber pad was found to differ from the temperature set by the heater using a thermocouple in the

device during amplification. With this information, the temperature of the heater could be adjusted to achieve the desired temperature range of 49-51°C at the surface of the substrate. Through this monitoring, the performance of the amplification at 20,000 input copies improved (Figure 39). From previous data, the delay observed in amplification from dry reagents was thought to be a possible result of the dissolution of sugars as well as the diffusion limitations of the reagents in this two-dimensional structure. However, after improved temperature control of heating in-paper, lift off times at—or slightly before—that observed in-tube are observed. However, limit of detection (LOD) analysis performed using the STAmp suggests that the fluorescence microscope is an order of magnitude more sensitive than the Rotor-Gene.

Therefore, it is possible that this improved sensitivity is causing this apparent earlier lift-off time rather than an improved temporal performance of the amplification, although further investigation is required.

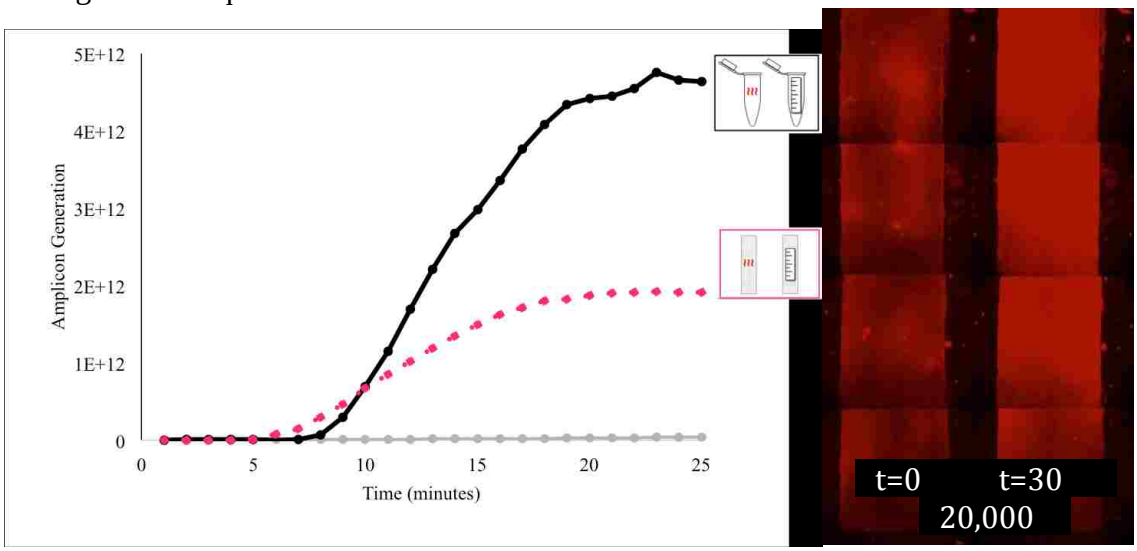

Figure 39. Amplification in-paper with improved heating control at 20,000 input copies. Real-time curve of amplification in-paper from dry reagents (pink) compared to amplification in-tube from fresh reagents at 20,000 input copies (black) (A) and corresponding image of amplification pad at t=0 and t=30 minutes (left).

4.7 LOD Analysis

With these improvements in the amplification reaction and experimental procedure, the LOD for this system was determined. Amplification pads prepared with 10% trehalose, 2.5% dextran and 2.5% PEG-8000 were run at 200, 20 and 0 input copies of DNA. Data for these reactions were compared with the data obtained at 20,000 input copies. Good amplification was observed in all scenarios where the DNA target was present, demonstrating a clinically-relevant detection level for this particular gene (Figure 40).

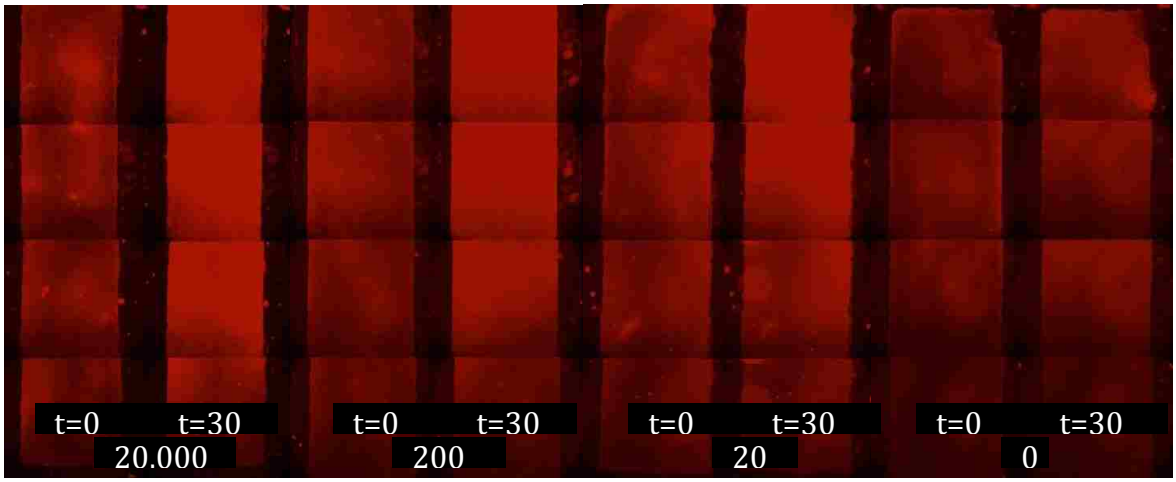

Figure 40. Images of reagent pads pre- and post-amplification for various input copy numbers. Images of the amplification pads at t=0 (left-side figures) and t=30 minutes (right side figures) for various input copy numbers.

Real-time curves and percent performance as compared to fresh in-tube reactions for these reactions are shown in Figure 41. The performance for amplification performed in-paper from dry reagents is ~50% as compared to fresh in-tube for 20,000, 200 and 20 input copies.

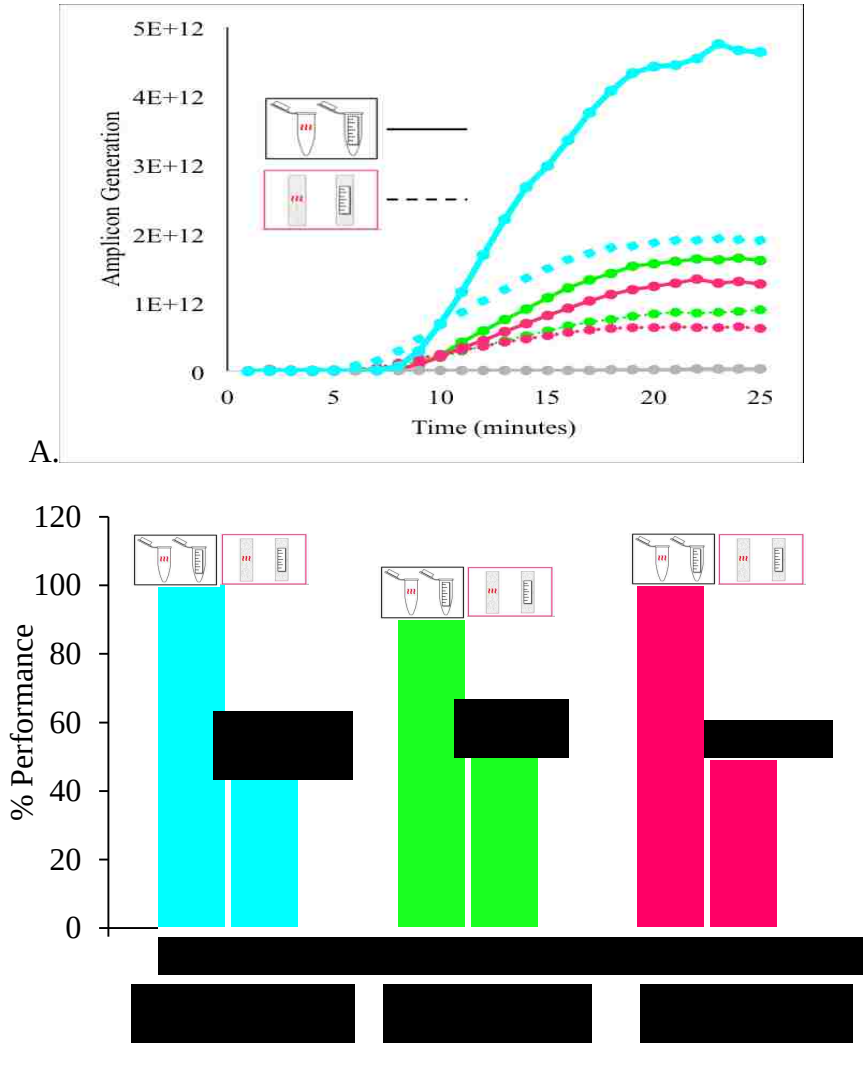

Figure 41. iSDA in-tube and in-paper at low copy number. Real-time amplification curves (A): Blue (20,000 input copies), green (200 input copies), pink (20 input copies) grey (0 input copies). Solid line: in-tube. Dashed line: in-paper. Percent performance as compared to fresh in-tube for 20,000 (blue), 200 (green) and 20 (pink) input copies.

Histogram analysis for these reactions was also assessed to analyze the second metric of importance—time for the fluorescent signal to reach 15% over background. The analysis in Figure 42 shows that at higher input copy number (20,000), the histogram is shifted farther to the left than for the other input copy numbers (200, 20). Furthermore, as you decrease the copy number a higher percentage of the amplification curves fail to reach the level of over 15% background to denote an area in which amplification occurred. This can be observed visually via the red bars in the histogram analysis in Figure 42. This optical method and quantitative evaluation tools allow for improved analysis of rehydration and amplification performance in porous substrates that can be used for optimization of POC devices.

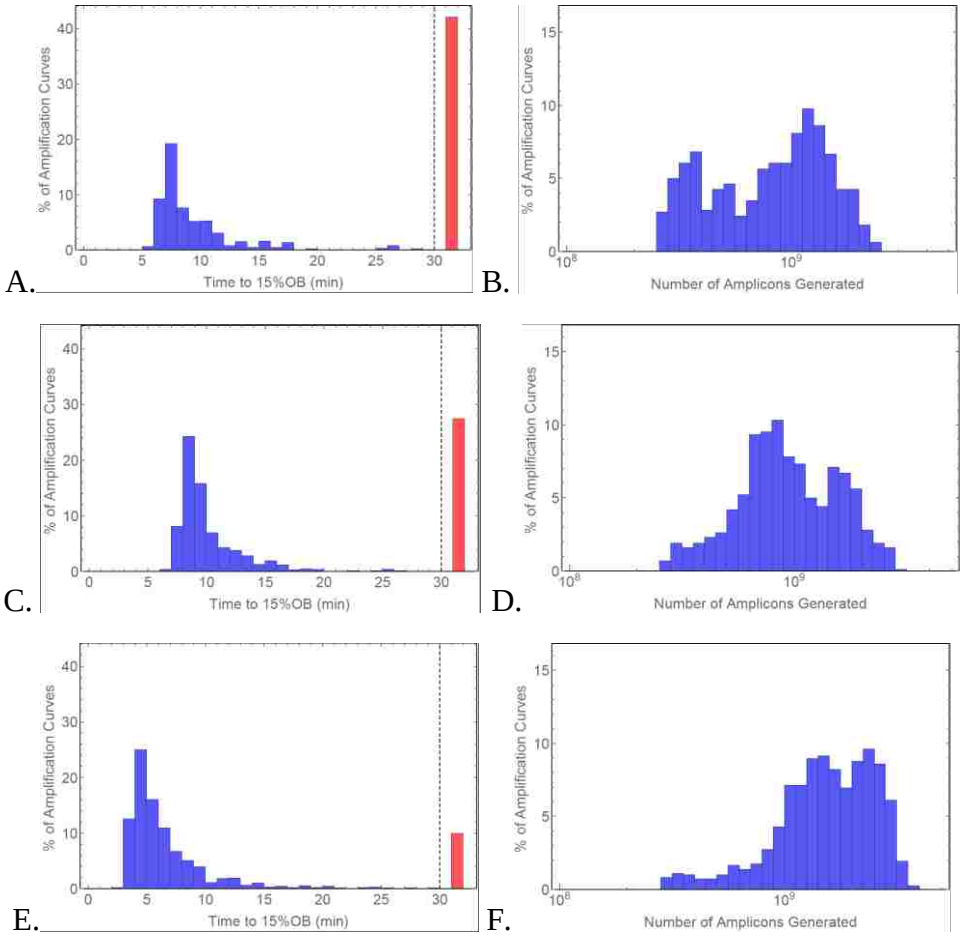

Figure 42. Histograms for 20, 200 and 20,000 input copy amplification from dry reagents . Histograms of time to reach 15% over background (left column) and amplicon generation (right column). For 20 input copies (A,B), 200 input copies (C,D) and 20,000 input copies (E,F). Red bars denote the percentage of curves whose fluorescence did not reach over 15% background.

Chapter 6. Conclusions and Future Directions

To our knowledge, this work represents the first demonstration of the visualization of real-time amplification of nucleic acids in porous media. I visualized and quantified amplification performance from both reagents added fresh to the substrate as well as reagents stored dry on the substrate. This analysis technique allows us to determine where amplification occurs and how well it performs in a device-compatible setting. The technique will enable optimization of several aspects of the current amplification assay, for some of which initial results have been shown. Using this technique, design choices in manufacturing, construction and automation of the device and assay were assessed. More specifically, the effects of the dry down process, additive composition and heating control were investigated. Initially, before any of these potential improvements were integrated, amplification from dry reagents in-paper was only 2% of that observed from fresh reagents in-tube. However, amplification performance was improved through lyophilization (6%), the addition of PEG (28%) and heating control (53%) (Figure 43).

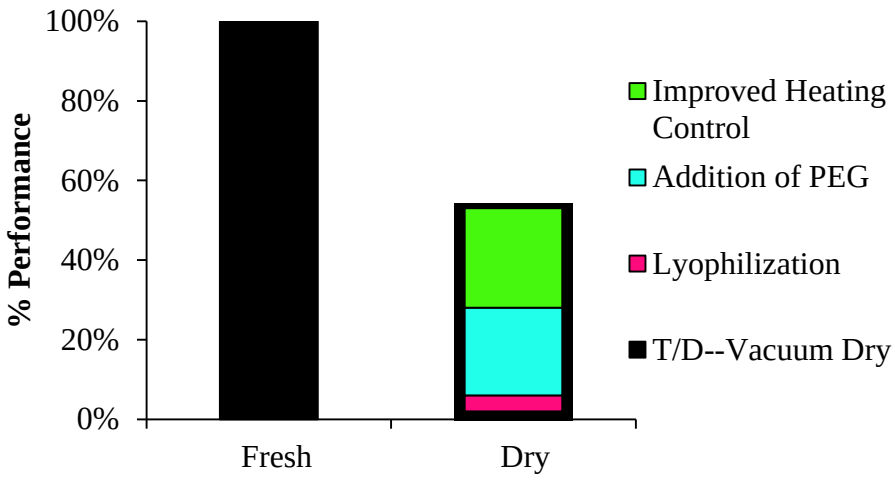

Figure 43. Summary of improvements made to amplification in-paper from dry-reagents at 20,000 input copies. Percent performance compared to fresh in-tube iSDA reaction.

Moreover, this optical technique can be used in conjunction with these improvements to the amplification assay to detect as few as 20 input copies of target gDNA while using dry reagents in porous media—under the clinical range. This tool has the ability to rapidly inform further device designs to assess impact on amplification performance in-situ. Furthermore, this method can be used to generate an improved understanding of the rehydration process under varying conditions as well as the impact of spatial effects on amplification as a whole. Both these processes are not fully understood and could benefit from further modeling and investigation.

In addition to its use as a research tool, as mentioned above, fluorescence can be used as a detection method itself. Many point-of-care assays utilize lateral flow detection for disease diagnosis. Although this method is easy to use and requires no additional equipment, it is not fully quantitative and adds additional time (~15 minutes) to the assay. While the amplification assay reaches steady state in 20 minutes, the time to reach 15% over background is typically under 10 minutes. I thus believe that a detection method based on this technique can be as sensitive, but much faster than the state-of-the-art for integration into the device. Using fluorescence allows for the quantification of diseases—necessary for some applications—and allows for detection in-situ, thereby reducing assay time. Traditionally, fluorescence detection has been bypassed for lateral flow detection because of the need for auxiliary and expensive equipment. However, there are now many demonstrations of sensitive, low cost fluorescence microscopes [55][56]. This work has the potential for integration with these low-cost optical technologies for the detection of nucleic acid amplification in-porous media for POC diagnostics for a sensitive, specific assay completed in less than 30 minutes (Figure 44).

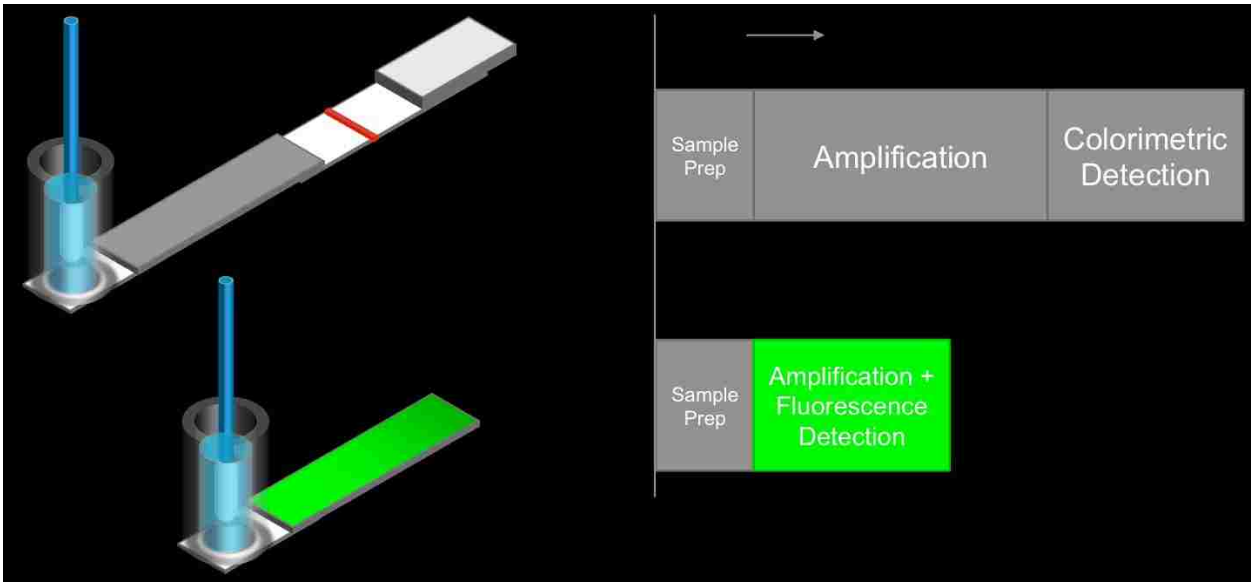

-

Figure 44. Schematic for design of a fluorescence-based MAD NAAT as compared to the standard MAD NAAT.

ACKNOWLEDGEMENTS

I would like to thank Dr. Paul Yager for his mentorship throughout my three years at the University of Washington as well as Dr. Barry Lutz for his assistance in the preparation of this thesis. I would also like to acknowledge the assistance of all members in the Yager lab, especially those in the MAD NAAT project as well as those who aided me in preparation for my defense—Dr. Paula Ladd, Dr. Erin Heiniger, Enos Kline and Josh Buser. Thanks to Sujatha Ramachandran for teaching me how to perform iSDA, to Ryan Gallagher for instruction for lyophilization, troubleshooting amplification reactions and interest in this work throughout. I would like to recognize both Dr. Carly Holstein and Dr. Lisa LaFleur for their invaluable assistance and support throughout this work. Special thanks to Samantha Byrnes for her assistance and company through many long nights in—and out of—the lab. I would like to recognize Dr. Joshua Bishop for his attempts to "manipulate me into my maximum potential", his instrumental advice and assistance with Mathematica computing. Thanks to my mentee—but often mentor—Nuttada Pranpradist for her assistance and support. One last thanks to Daniel Sedlacek for supporting me throughout this process—in both the ups and downs.

REFERENCES

[1] E. Summary, "The World Health Report HEALTH SYSTEMS FINANCING."

[2] S. Byrnes, G. Thiessen, and E. Fu, "Progress in the development of paper-based diagnostics for low-resource point-of-care settings.," *Bioanalysis*, vol. 5, no. 22, pp. 2821–36, Nov. 2013.

[3] D. Birx, M. de Souza, and J. N. Nkengasong, "Laboratory challenges in the scaling up of HIV, TB, and malaria programs: The interaction of health and laboratory systems, clinical research, and service delivery.," *Am. J. Clin. Pathol.*, vol. 131, no. 6, pp. 849–51, Jun. 2009.

[4] M. M. Lawrence Kulinsky, Zahra Noroozi, "Present Technology and Future Trends in Point-of-Care Microfluidic Diagnostics," in *Microfluidic Diagnostics*, 2012, pp. 3–23.

[5] M. Urdea, L. a Penny, S. S. Olmsted, M. Y. Giovanni, P. Kaspar, A. Shepherd, P. Wilson, C. a Dahl, S. Buchsbaum, G. Moeller, and D. C. Hay Burgess, "Requirements for high impact diagnostics in the developing world.," *Nature*, vol. 444 Suppl , pp. 73–9, Nov. 2006.

[6] O. Clerc and G. Greub, "Routine use of point-of-care tests: usefulness and application in clinical microbiology.," *Clin. Microbiol. Infect.*, vol. 16, no. 8, pp. 1054–61, Aug. 2010.

[7] J. Howick, J. W. L. Cals, C. Jones, C. P. Price, A. Plüddemann, C. Heneghan, M. Y. Berger, F. Buntinx, J. Hickner, W. Pace, T. Badrick, A. Van den Bruel, C. Laurence, H. C. van Weert, E. van Severen, A. Parrella, and M. Thompson, "Current and future use of point-of-care tests in primary care: an international survey in Australia, Belgium, The Netherlands, the UK and the USA.," *BMJ Open*, vol. 4, no. 8, p. e005611, Jan. 2014.

[8] J. H. Nichols, "Point of care testing.," *Clin. Lab. Med.*, vol. 27, no. 4, pp. 893–908, viii, Dec. 2007.

[9] C. D. Chin, V. Linder, and S. K. Sia, "Commercialization of microfluidic point-of-care diagnostic devices.," *Lab Chip*, vol. 12, no. 12, pp. 2118–34, Jun. 2012.

[10] E. Lee-Lewandrowski and K. Lewandrowski, "Perspectives on cost and outcomes for point-of-care testing.," *Clin. Lab. Med.*, vol. 29, no. 3, pp. 479–89, Sep. 2009.

[11] P. Yager, G. J. Domingo, and J. Gerdes, "Point-of-care diagnostics for global health.," *Annu. Rev. Biomed. Eng.*, vol. 10, pp. 107–44, Jan. 2008.

[12] M. R. Hartman, R. C. H. Ruiz, S. Hamada, C. Xu, K. G. Yancey, Y. Yu, W. Han, and D. Luo, "Point-of-care nucleic acid detection using nanotechnology.," *Nanoscale*, vol. 5, no. 21, pp. 10141–54, Nov. 2013.

[13] E. Keeler, M. D. Perkins, P. Small, C. Hanson, S. Reed, J. Cunningham, J. E. Aledort, L. Hillborne, M. E. Rafael, F. Girosi, and C. Dye, "Reducing the global burden of tuberculosis: the contribution of improved diagnostics.," *Nature*, vol. 444 Suppl , pp. 49–57, Nov. 2006.

[14] P. K. Drain, E. P. Hyle, F. Noubary, K. a Freedberg, D. Wilson, W. R. Bishai, W. Rodriguez, and I. V Bassett, "Diagnostic point-of-care tests in resource-limited settings.," *Lancet Infect. Dis.*, vol. 14, no. 3, pp. 239–249, Mar. 2014.

[15] A. W. Martinez, S. T. Phillips, M. J. Butte, and G. M. Whitesides, "Patterned paper as a platform for inexpensive, low-volume, portable bioassays.," *Angew. Chem. Int. Ed. Engl.*, vol. 46, no. 8, pp. 1318–20, Jan. 2007.

[16] A. K. Yetisen, M. S. Akram, and C. R. Lowe, "Paper-based microfluidic point-of-care diagnostic devices.," *Lab Chip*, vol. 13, no. 12, pp. 2210–51, Jun. 2013.

[17] P. Craw and W. Balachandran, "Isothermal nucleic acid amplification technologies for point-of-care diagnostics: a critical review.," *Lab Chip*, vol. 12, no. 14, pp. 2469–86, Jul. 2012.

[18] C.-C. Chang, C.-C. Chen, S.-C. Wei, H.-H. Lu, Y.-H. Liang, and C.-W. Lin, "Diagnostic devices for isothermal nucleic acid amplification.," *Sensors (Basel).*, vol. 12, no. 6, pp. 8319–37, Jan. 2012.

[19] P. J. Asiello and A. J. Baeumner, "Miniaturized isothermal nucleic acid amplification, a review.," *Lab Chip*, vol. 11, no. 8, pp. 1420–30, Apr. 2011.

[20] R. Saiki, D. Gelfand, S. Stoffel, S. Scharf, R. Higuchi, G. Horn, K. Mullis, and H. Erlich, "Primer-directed enzymatic amplification of DNA with a thermostable DNA polymerase," *Science (80-.).*, vol. 239, no. 4839, pp. 487–491, Jan. 1988.

[21] T. Notomi, H. Okayama, H. Masubuchi, T. Yonekawa, K. Watanabe, N. Amino, and T. Hase, "Loop-mediated isothermal amplification of DNA.," *Nucleic Acids Res.*, vol. 28, no. 12, p. E63, Jun. 2000.

[22] G. T. Walker, M. S. Fraiser, J. L. Schram, M. C. Little, J. G. Nadeau, and D. P. Malinowski, "Strand displacement amplification-an isothermal , in vitro DNA amplification technique," vol. 20, no. 7, pp. 1691–1696, 1992.

[23] A. Niemz, T. M. Ferguson, and D. S. Boyle, "Point-of-care nucleic acid testing for infectious diseases.," *Trends Biotechnol.*, vol. 29, no. 5, pp. 240–50, May 2011.

[24] G. E. Fridley, H. Q. Le, E. Fu, and P. Yager, "Controlled release of dry reagents in porous media for tunable temporal and spatial distribution upon rehydration.," *Lab Chip*, vol. 12, no. 21, pp. 4321–7, Nov. 2012.

[25] G. E. Fridley, H. Le, and P. Yager, “Highly Sensitive Immunoassay Based on Controlled Rehydration of Patterned Reagents in a 2 - Dimensional Paper Network,” *Anal. Chem.*, pp. 6447–6453, 2015.

[26] E. Garcia, J. R. Kirkham, A. V Hatch, K. R. Hawkins, and P. Yager, “Controlled microfluidic reconstitution of functional protein from an anhydrous storage depot.,” *Lab Chip*, vol. 4, no. 1, pp. 78–82, Feb. 2004.

[27] D. Y. Stevens, C. R. Petri, J. L. Osborn, P. Spicar-Mihalic, K. G. McKenzie, and P. Yager, “Enabling a microfluidic immunoassay for the developing world by integration of on-card dry reagent storage.,” *Lab Chip*, vol. 8, no. 12, pp. 2038–45, Dec. 2008.

[28] E. Fu, T. Liang, P. Spicar-Mihalic, J. Houghtaling, S. Ramachandran, and P. Yager, “Two-dimensional paper network format that enables simple multistep assays for use in low-resource settings in the context of malaria antigen detection,” *Anal. Chem.*, vol. 84, pp. 4574–4579, 2012.

[29] R. C. Wong, *Lateral Flow Immunoassay*. Totowa, NJ: Humana Press, 2009.

[30] J. Hoffmann, D. Mark, S. Lutz, R. Zengerle, and F. von Stetten, “Pre-storage of liquid reagents in glass ampoules for DNA extraction on a fully integrated lab-on-a-chip cartridge.,” *Lab Chip*, vol. 10, no. 11, pp. 1480–4, Jun. 2010.

[31] A. Ahlford, B. Kjeldsen, J. Reimers, A. Lundmark, M. Romani, A. Wolff, A.-C. Syvänen, and M. Brivio, “Dried reagents for multiplex genotyping by tag-array minisequencing to be used in microfluidic devices.,” *Analyst*, vol. 135, no. 9, pp. 2377–85, Sep. 2010.

[32] and H. H. B. Jitae Kim, Doyoung Byun, Michale G. Mauk, “A Disposable, Self-Contained PCR Chip,” *Lab Chip*, vol. 9, no. 4, pp. 606–612, 2009.

[33] Y. Jia, P.-I. Mak, C. Massey, R. P. Martins, and L. J. Wangh, “Construction of a microfluidic chip, using dried-down reagents, for LATE-PCR amplification and detection of single-stranded DNA.,” *Lab Chip*, vol. 13, no. 23, pp. 4635–41, Oct. 2013.

[34] M. Hitzbleck, L. Gervais, and E. Delamarche, “Controlled release of reagents in capillary-driven microfluidics using reagent integrators.,” *Lab Chip*, vol. 11, no. 16, pp. 2680–5, Aug. 2011.

[35] B. Lutz, T. Liang, E. Fu, S. Ramachandran, P. Kauffman, and P. Yager, “Dissolvable fluidic time delays for programming multi-step assays in instrument-free paper diagnostics.,” *Lab Chip*, vol. 13, no. 14, pp. 2840–7, Jul. 2013.

[36] P. Kozma, a Lehmann, K. Wunderlich, D. Michel, S. Schumacher, E. Ehrentreich-Förster, and F. F. Bier, “A novel handheld fluorescent microarray reader for point-of-care diagnostic.,” *Biosens. Bioelectron.*, vol. 47, pp. 415–20, Sep. 2013.

[37] E. W. Nery and L. T. Kubota, “Sensing approaches on paper-based devices: a review.,” *Anal. Bioanal. Chem.*, pp. 7573–7595, Apr. 2013.

[38] R. Pelton, “Bioactive paper provides a low-cost platform for diagnostics,” *TrAC Trends Anal. Chem.*, vol. 28, no. 8, pp. 925–942, Sep. 2009.

[39] Y. Ma, H. Li, S. Peng, and L. Wang, “Highly selective and sensitive fluorescent paper sensor for nitroaromatic explosive detection.,” *Anal. Chem.*, vol. 84, no. 19, pp. 8415–21, Oct. 2012.

[40] M. M. Ali, S. D. Aguirre, Y. Xu, C. D. M. Filipe, R. Pelton, and Y. Li, “Detection of DNA using bioactive paper strips.,” *Chem. Commun. (Camb).*, no. 43, pp. 6640–2, Nov. 2009.

[41] P. Zhao, Y. Wu, Y. Zhu, X. Yang, X. Jiang, J. Xiao, Y. Zhang, and C. Li, “Upconversion fluorescent strip sensor for rapid determination of Vibrio anguillarum.,” *Nanoscale*, vol. 6, no. 7, pp. 3804–9, Mar. 2014.

[42] P. B. Allen, S. a Arshad, B. Li, X. Chen, and A. D. Ellington, “DNA circuits as amplifiers for the detection of nucleic acids on a paperfluidic platform.,” *Lab Chip*, vol. 12, no. 16, pp. 2951–8, Aug. 2012.

[43] A. Feng Shen, Elena K. Davydova, Wenbin Du Jason E. Kreutz, Olaf Piepenburg and R. F. Ismagilov, “Digital Isothermal Quantification of Nucleic Acids via Simultaneous Chemical Initiation of Recombiase Polymerase Amplification Reactions on SlipChip,” *Anal. Chem.*, vol. 83, no. 9, pp. 3533–3540, 2012.

[44] S. a E. Marras, “Selection of fluorophore and quencher pairs for fluorescent nucleic acid hybridization probes.,” *Methods Mol. Biol.*, vol. 335, pp. 3–16, Jan. 2006.

[45] B. Juskowiak, “Nucleic acid-based fluorescent probes and their analytical potential,” *Anal. Bioanal. Chem.*, vol. 399, no. 9, pp. 3157–3176, Oct. 2010.

[46] E. a Lukhtanov, S. G. Lokhov, V. V Gorn, M. a Podyminogin, and W. Mahoney, “Novel DNA probes with low background and high hybridization-triggered fluorescence.,” *Nucleic Acids Res.*, vol. 35, no. 5, p. e30, Jan. 2007.

[47] I. V Kutyavin, I. A. Afonina, A. Mills, V. V Gorn, E. A. Lukhtanov, E. S. Belousov, M. J. Singer, D. K. Walburger, S. G. Lokhov, A. A. Gall, R. Dempcy, M. W. Reed, R. B. Meyer, and J. Hedgpeth, “3 ′ -Minor groove binder-DNA probes increase sequence specificity at PCR extension temperatures,” vol. 28, no. 2, pp. 655–661, 2000.

[48] a. Tsourkas, “Hybridization kinetics and thermodynamics of molecular beacons,” *Nucleic Acids Research*, vol. 31, no. 4. pp. 1319–1330, 15-Feb-2003.

[49] A. Penttilä and K. Lumme, “The effect of the properties of porous media on light scattering,” *J. Quant. Spectrosc. Radiat. Transf.*, vol. 110, no. 18, pp. 1993–2001, Dec. 2009.

[50] T. D. Pollard, “MB O C TECHNICAL PERSPECTIVE A Guide to Simple and Informative Binding Assays,” vol. 21, pp. 4061–4067, 2010.

[51] M. Bidinosti, D. R. Shimshek, B. Mollenhauer, D. Marcellin, T. Schweizer, G. P. Lotz, M. G. Schlossmacher, and A. Weiss, “Novel one-step immunoassays to quantify α-synuclein: applications for biomarker development and high-throughput screening.,” *J. Biol. Chem.*, vol. 287, no. 40, pp. 33691–705, Sep. 2012.

[52] H. Zhu and A. Ozcan, “Wide-field fluorescent microscopy and fluorescent imaging flow cytometry on a cell-phone.,” *J. Vis. Exp.*, no. 74, pp. 1–5, Jan. 2013.

[53] P. R. Klatser, S. Kuijper, and W. Cor, “Stabilized , Freeze-Dried PCR Mix for Detection of Mycobacteria,” vol. 36, no. 6, pp. 1798–1800, 1998.

[54] N. Grasmeijer, M. Stankovic, H. de Waard, H. W. Frijlink, and W. L. J. Hinrichs, “Unraveling protein stabilization mechanisms: vitrification and water replacement in a glass transition temperature controlled system.,” *Biochim. Biophys. Acta*, vol. 1834, no. 4, pp. 763–9, Apr. 2013.

[55] L. Novak, P. Neuzil, J. Pipper, Y. Zhang, and S. Lee, “An integrated fluorescence detection system for lab-on-a-chip applications.,” *Lab Chip*, vol. 7, no. 1, pp. 27–9, Jan. 2007.

[56] A. R. Miller, G. L. Davis, Z. M. Oden, M. R. Razavi, A. Fateh, M. Ghazanfari, F. Abdolrahimi, S. Poorazar, F. Sakhaie, R. J. Olsen, A. R. Bahrmand, M. C. Pierce, E. a Graviss, and R. Richards-Kortum, “Portable, battery-operated, low-cost, bright field and fluorescence microscope.,” *PLoS One*, vol. 5, no. 8, p. e11890, Jan. 2010.

Appendix I. Properties of Nitrocellulose

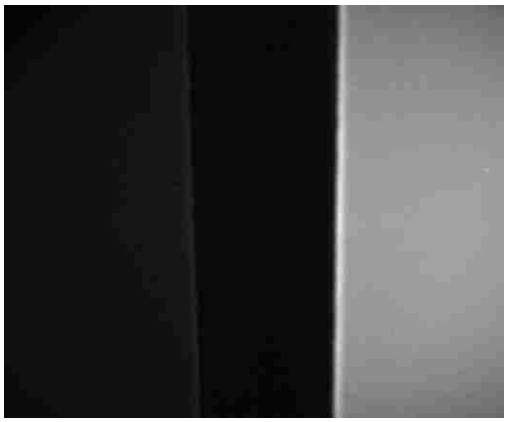

Appendix Figure 1. Background fluorescence of UBNC and MBNC. AE100 (left) and FF80 (right). Axiovert25 inverted fluorescence microscope, FITC filter set, 5x objective, 500ms exposure time.

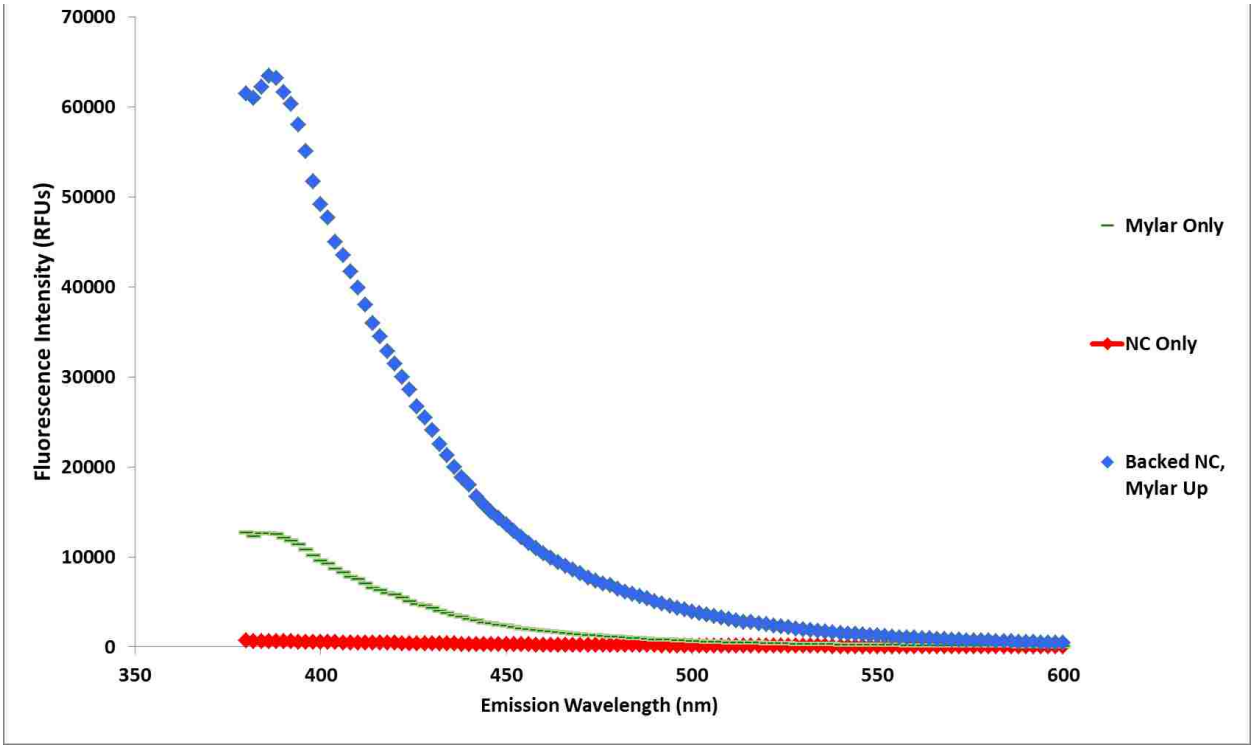

Appendix Figure 2. Emission scans on a Tecan plate reader for component parts of FF80 MBNC at excitation of 350nm.

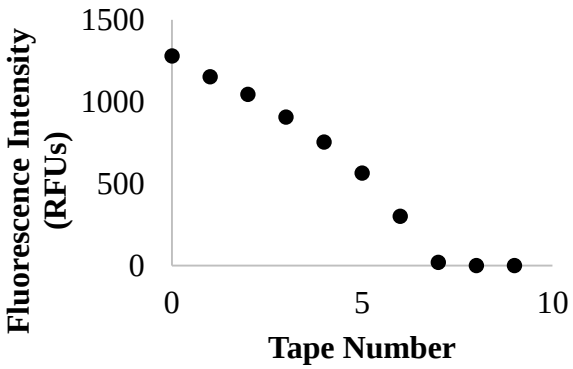

A.

B. 
C. 
D. 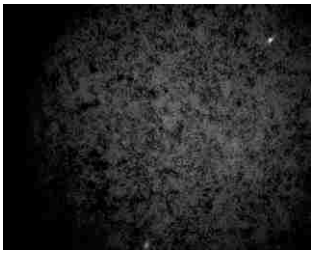

E. 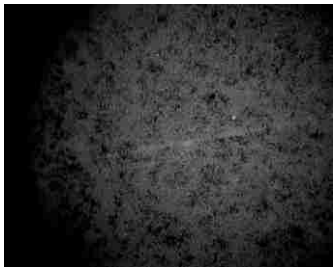
F. 

Appendix Figure 3. Removal of nitrocellulose from backed NC using Scotch tape. Fluorescence intensity of backed nitrocellulose imaged on an Axiovert25 inverted fluorescence microscope after each tape removal (A). Images of the removed nitrocellulose imaged on the tape pieces: 1st piece of tape (B), 3rd (C), 5th (D), 7th (E) and 9th (E). 1(b), 3(c), 5(d), 7(e) and 9(f).

Various substrate candidates were tested for their compatibility with iSDA. As a high throughput screening, reactions were placed onto a porous medium and placed inside a PCR tube. Fluorescence was monitored using an EvaGreen intercalating dye to observe whether any amplification could be supported whether it was target-specific or not. A fresh tube reaction in the absence of any paper was used as a control. The substrates that showed amplification were Std17, 31-ETF and AE100. Std17 was proven to be the best substrate for amplification

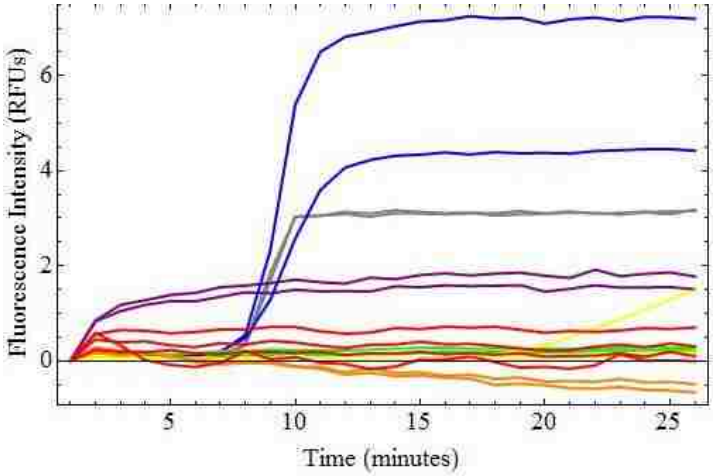

Appendix Figure 4. Real-time iSDA in-paper performed in-tube on various substrates. Control (grey), Std17 (blue), 31-ETF (purple), GF-B (green), GG-G (yellow), QMA (orange), AE100 (red). EvaGreen. 1000 copies

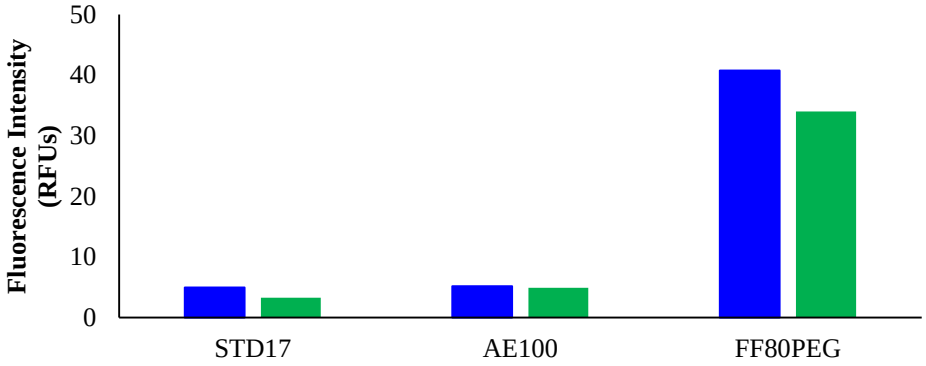

Appendix Figure 5. Fluorescence of glass fiber and nitrocellulose with two different filter sets. FITC (blue) and rhodamine (green).

Appendix II. Behavior of Fluorescent Probes in the Presence of Target

III.a. Behavior in the presence of STAmp

Pleiades probe

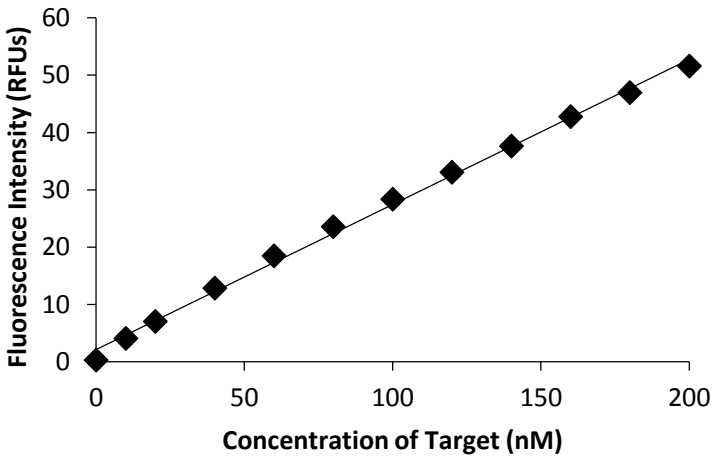

Appendix Figure 6. Standard curve for Pleiades probe. Fluorescence Intensity of P(FAM)-STAmp at 49 degrees at a probe concentration of 200 nM. Gain=10. n=3. R^2=0.997

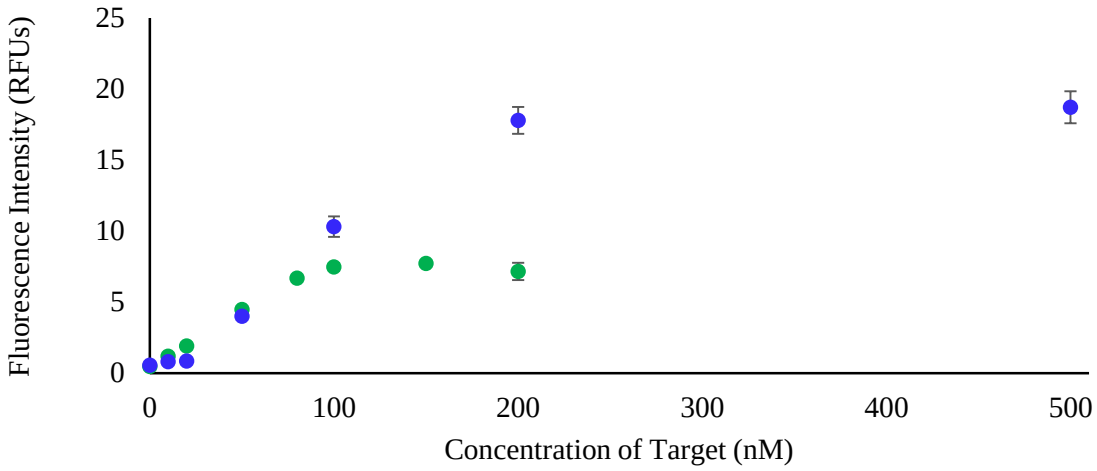

Appendix Figure 7. Pleiades-STAmp standard curve at 1x and 2x iSDA probe concentration.

Zen probe

As expected, the Zen probe did not response well to the STAmp target because it is a hydrolytic probe.

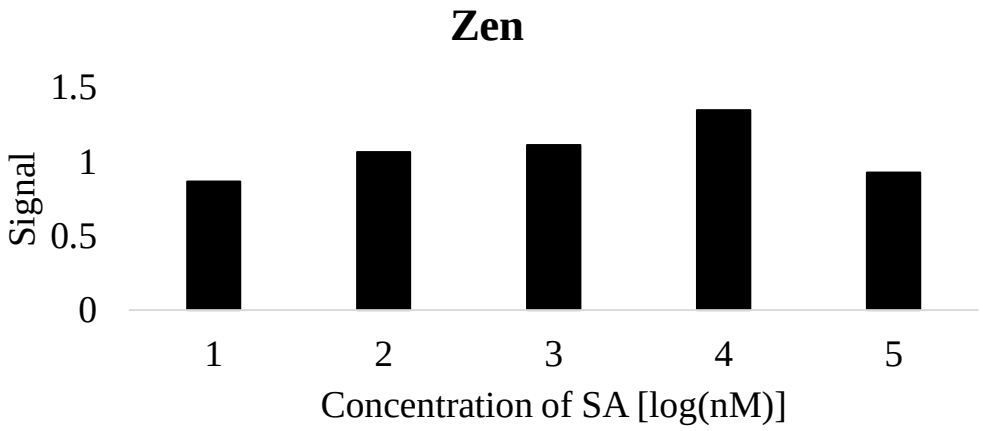

Appendix Figure 8. STAmp standard curve with Zen probe.

Although the MB probe responded to increasing inputs of STAmp at 25°C, it did not respond well at 49°C. This was due to poor design of the probe, which resulted in a melting temperature below that of the assay temperature.

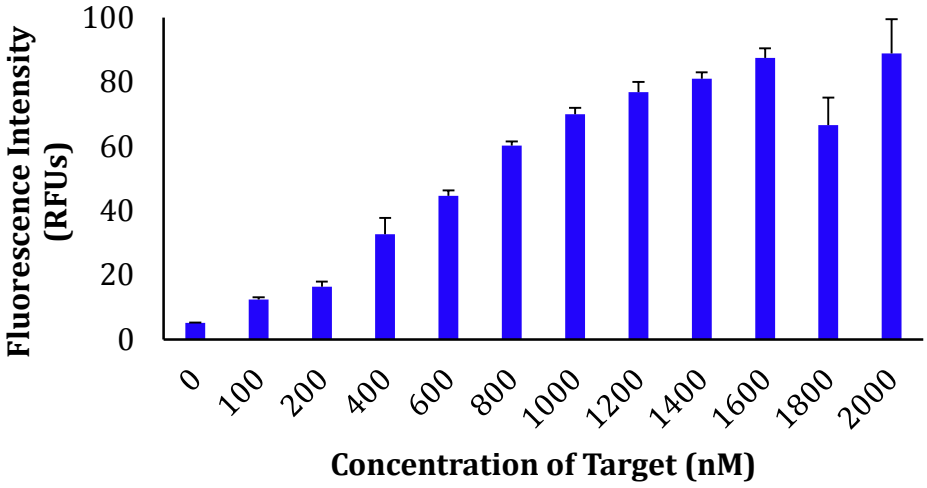

A.

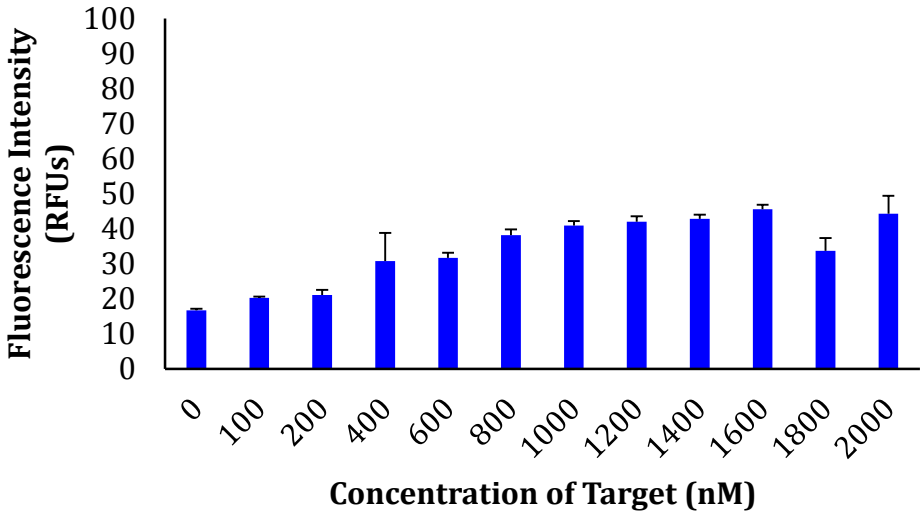

B.

Appendix Figure 9. STAmp standard curve with Molecular Beacon. STAmp standard curve with Molecular Beacon (A). Fluorescence of the MB probe in response to varying concentrations of synthetic amplicon measured at 25°C after a 3 minute incubation at 60°C (B). Subsequent fluorescence measurement at 49°C (C). Gain=10; n=3

III.b. Behavior of probe during amplification

The FAM-labeled Pleiades probe performed well in-tube. However, the MB probe exhibited oscillating behavior. The Zen probe also performed poorly, as expected.

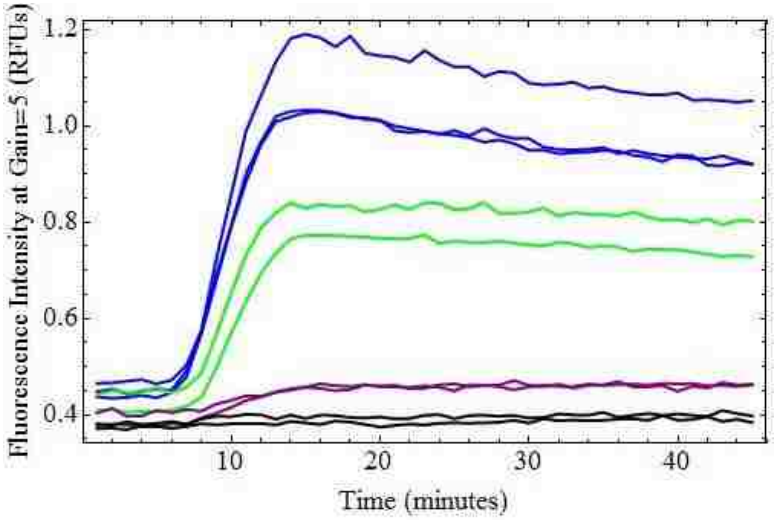

A.

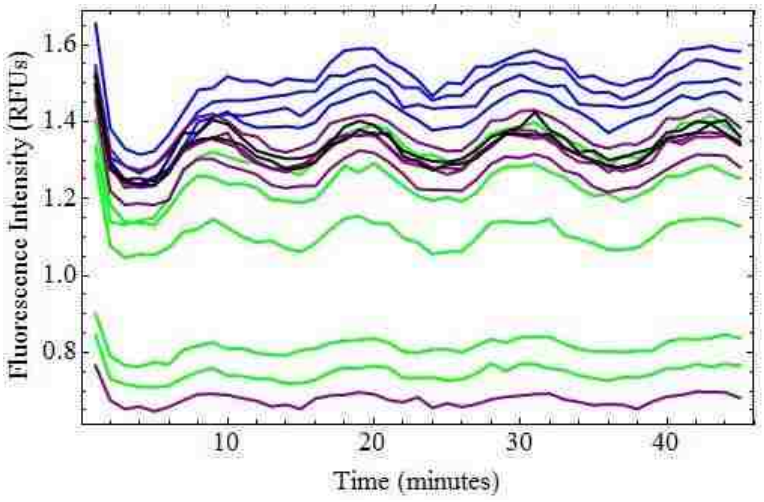

B.

C.

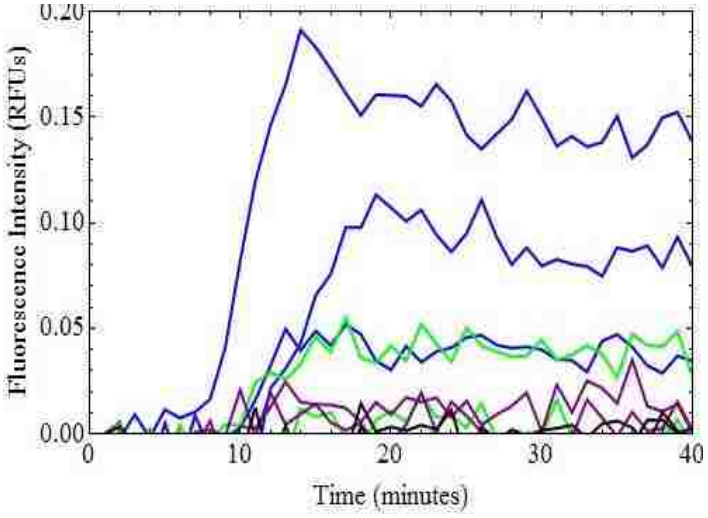

Appendix Figure 10. Real-time iSDA in-tube with various fluorescent probes. (A) Pleiades (B) MB (C) Zen. 2000 input copies (blue), 200 input copies (green), 20 input copies (purple) and 0 input copies (black).

Appendix III. Real-time amplification in-paper with additional fluorescent probes

The first probe-substrate pair considered was the FAM-labeled Pleiades probe with AE100 UBNC. However, this probe demonstrated rapid photobleaching on this substrate. This was seen in both post-amplified products (Appendix Figure 12) and attempts for real-time

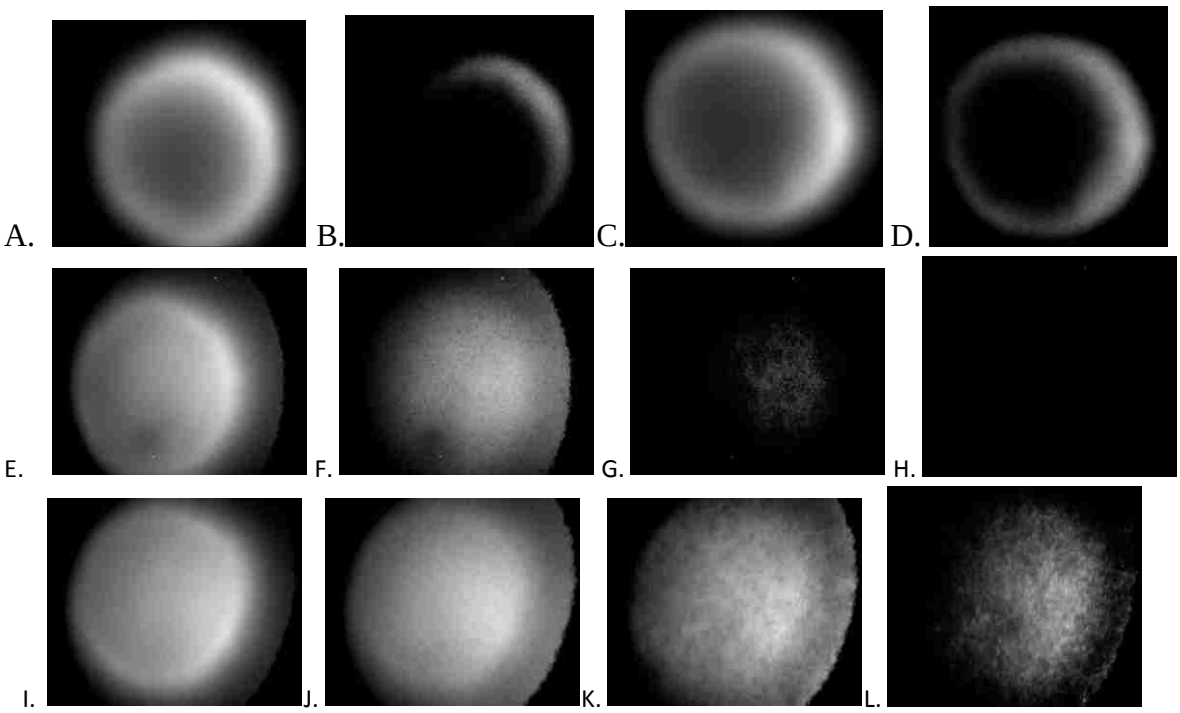

Appendix Figure 11. Images of post-amplified products. Fluorescent images of NTC with continuous illumination (A,B) and discontinuous illumination (C,D) at 2s (A,C) and 10s (B,C). Fluorescent images of post-amplified 2000 copy MRSA iSDA product with continuous illumination (E-H) and discontinuous illumination (I-L) at 0s (E, I), 60s (F,J), 120s (G,K) and 180s (H,L).

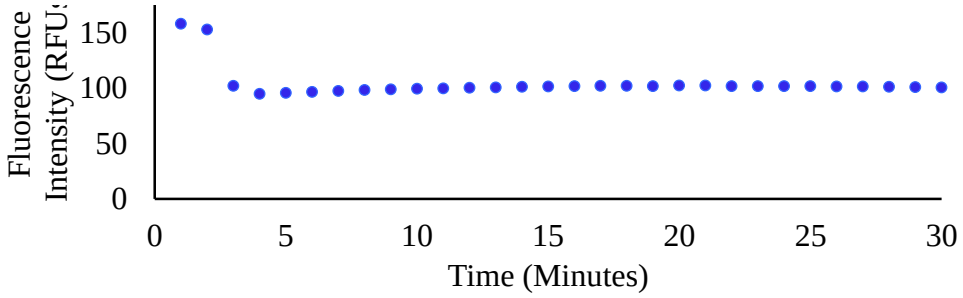

Appendix Figure 12. Real-time iSDA in-paper with FAM-labeled Pleiades probe on AE100.

The mechanism by which the FAM probe exhibits this rapid loss in fluorescent signal on porous media is not yet fully understood. However, one potential reason is that FAM labels exhibit significant decreases in their quantum yield with increasing temperature, whereas TxRed labels do not.

By utilizing a probe that was more robust, we were able to achieve the first successful visualization of real-time amplification in porous media.

a.  b.  c. 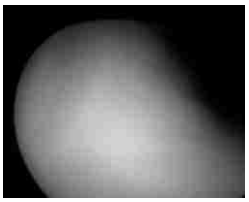 d. 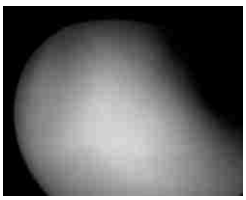

e.

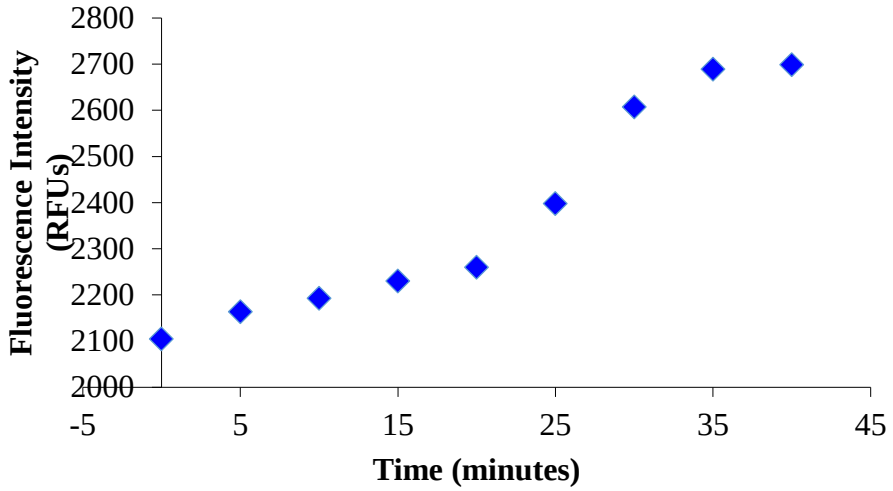

Appendix Figure 13. First demonstration of real-time amplification in-porous media. Pleiades/AE100. Change in fluorescence intensity visualized by subtracting images at t=15 minutes (a), t=20 minutes (b), t=30 minutes (c) and t=40 minutes, from an image taken at t=5 minutes. (e) Absolute fluorescence intensity of the iSDA products in a gasket for 2000 copies

All of the probes were tested for their behavior in response to amplification in-paper (Appendix Figure 14). The MB probe exhibited the same oscillating behavior as observed in-tube. Therefore, this phenomenon is not a product of the hardware. Surprisingly, the Zen probe performed well in-paper.

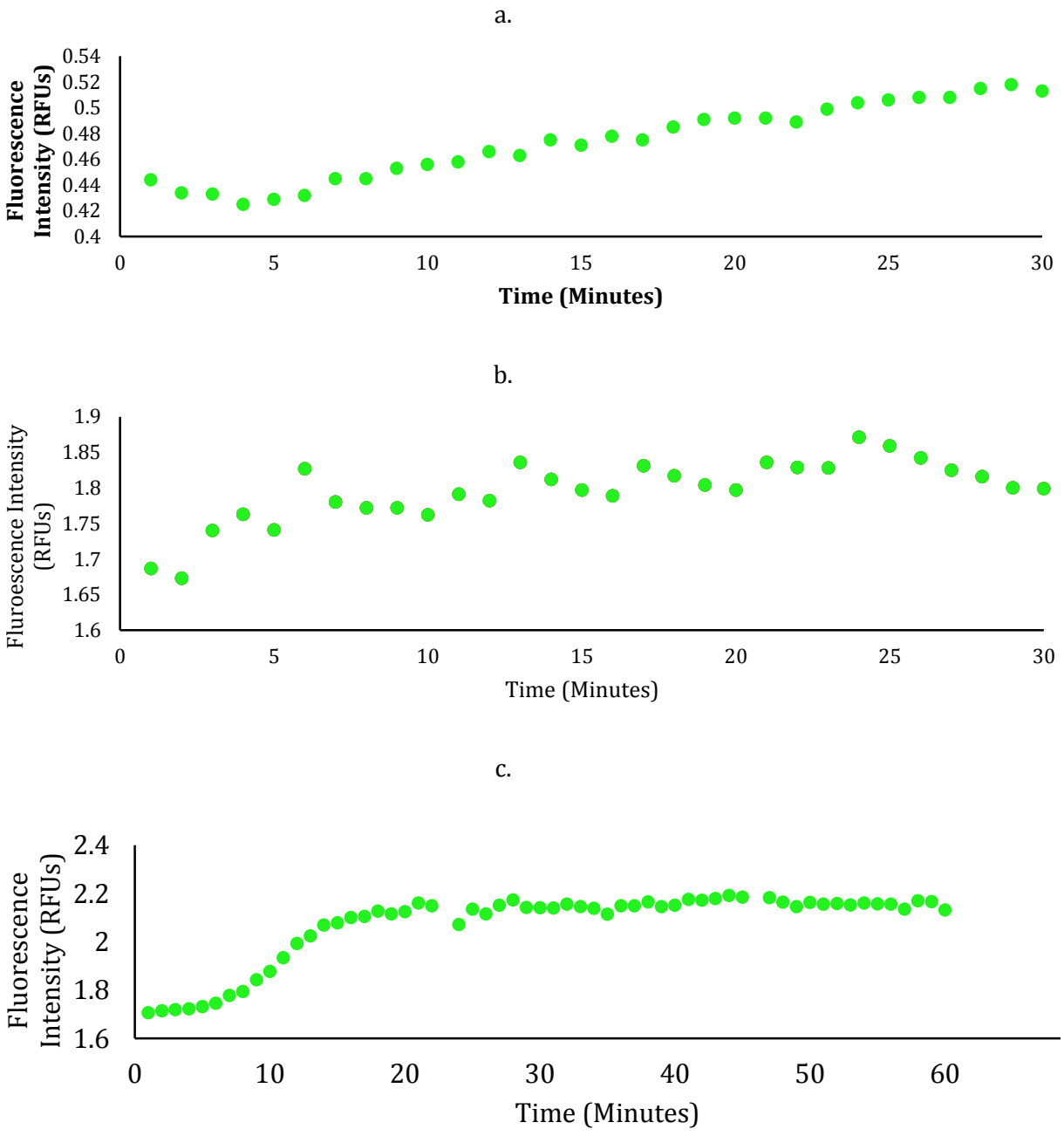

Appendix Figure 14. Real-time with various probes on glass fiber. (A) Pleiades; (B) Molecular Beacon; (C) Zen.

Appendix IV. iSDA Mechanism

To further understand the iSDA mechanism, I worked with Josh Bishop to model the chemical reaction network occurring during amplification of MRSA. Starting with the target DNA, three reaction types were considered: nicking, polymerization and hybridization. Hybridization could occur through four mechanisms: the excess primer (E1), limiting primer (L1), rear bumper primer (RB1) and front bumper primer (FB1). All possible species were drawn using an open source software program for DNA strand displacement (Visual DSD) and then organized into a flow chart (Appendix Figure 15). The reactions were then typed up into Mathematica and processed using a chemical reactions package created by Eric Klavins.

The concentration from all species in which a 7* sequence (the probe binding region) is available for binding were added up and plotted over time. In the initial model, dNTPs were considered a limiting species and were integrated into the network through each polymerization reaction, which was set to deplete the dNTPs. Under this model, many assumptions were made and the hybridization, polymerization and nicking reaction rates were estimated based on the literature and therefore, the possibility of improvement to the model still remains.

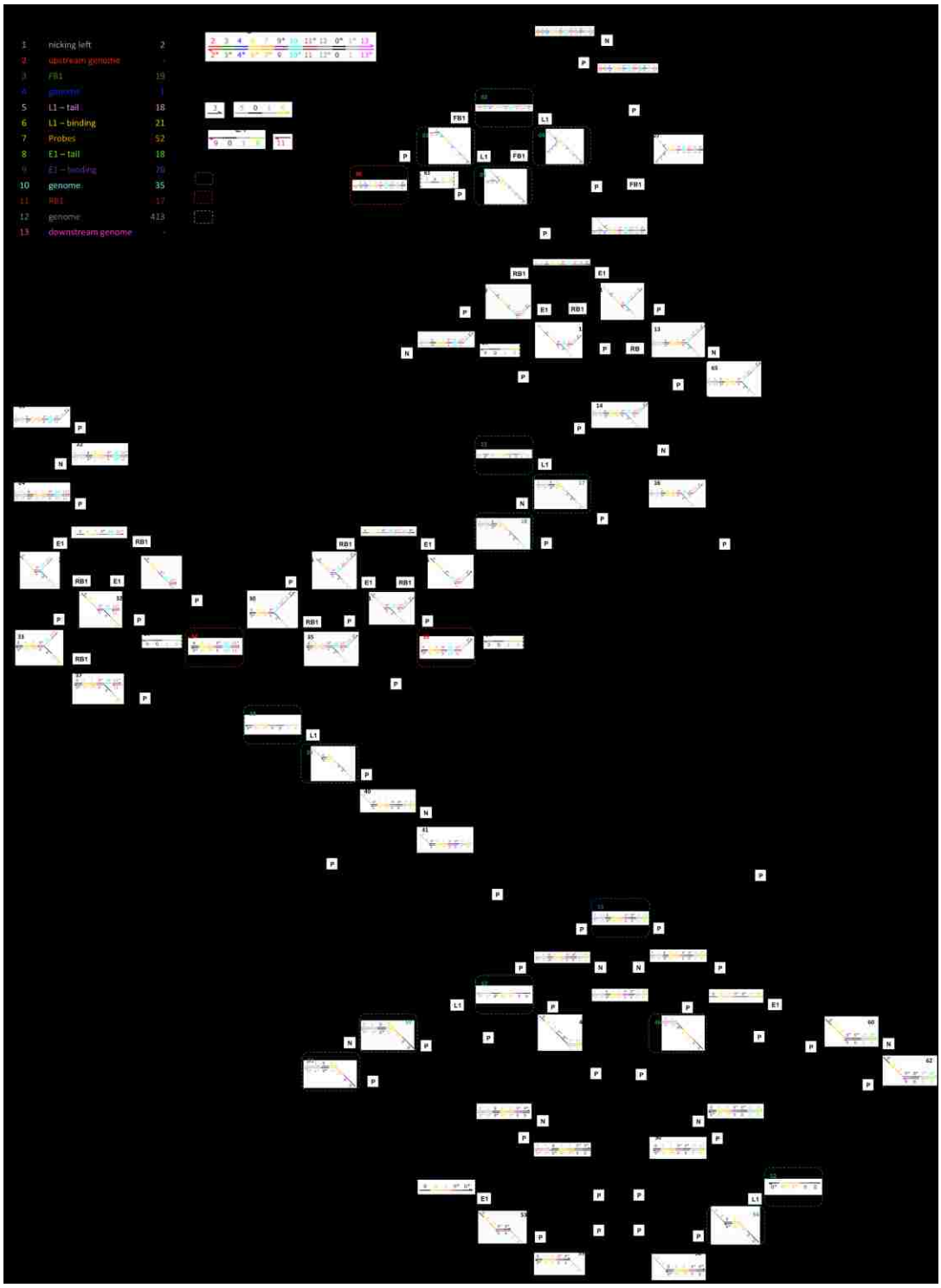

Appendix Figure 15. iSDA chemical reaction network.

Appendix V. Correction factor for measurements in-paper

The effect of additives

It was also important to check whether or not the presence of additives used in the dry down formulation for amplification had an effect on the fluorescence intensity of the system. Standard curves were performed using the reaction buffer in the presence of no additives, 2.5% PEG only and PEG+Dextran (2.5% each). Using the analysis technique, no significant change in fluorescence was observed with the addition of these components. There was a slight increase in the nominal value of fluorescence intensity with the addition of PEG. Reports from the literature (Muhammad N *et al)* postulate that the clustering of PEG molecules around the probe-target complex increase the local PEG density, thereby increasing the local refractive index surrounding the complex and increasing the fluorescence emission of the probe (higher refractive index, lower fluorescence lifetime and higher emission).

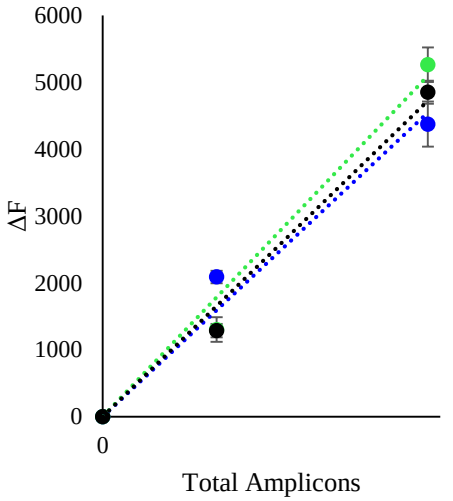

A.

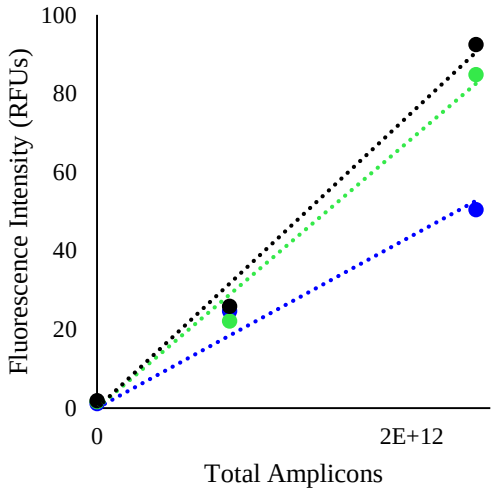

B.

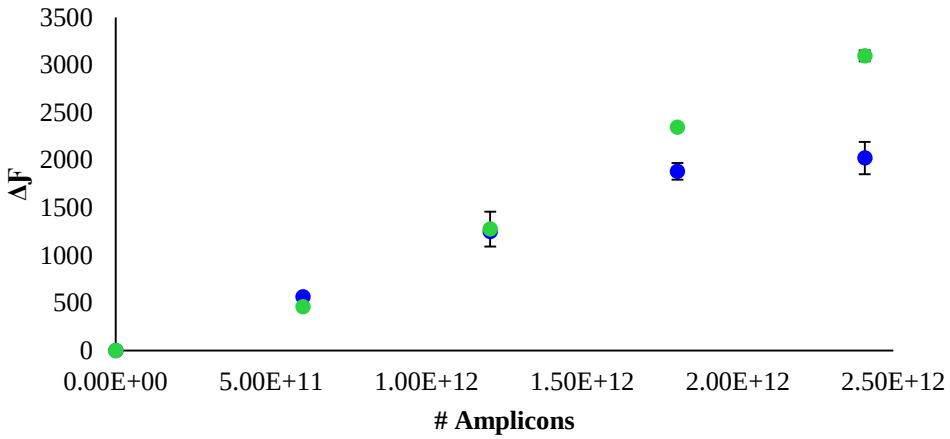

C.

Appendix Figure 16. Effect of additives on standard curve. Percent increase over background vs. amplicon number (A) and relative fluorescence intensity vs. amplicon number (B). The blue curve denotes no additives, slope=1.9E-9, , R2=.97 (A), slope=2E-11, , R2=.96 (B). PEG only is shown via the green curves: slope=2.1E-9, R2=.98 (A), slope=3E-11 , R2=.99(B). PEG+Dextran is shown via the black curves: slope=2.0E-9, R2=.99 (A), slope=4E-11, R2=.99(B). (C) With (blue) and without (green) trehalose.

Neither PEG nor dextran seemed to impact fluorescence intensity, but at higher STAmp concentrations, the addition of trehalose does. Although this behavior is unexpected, possible contamination in the trehalose solution could account for this, but further analysis is required. Since P(TxRed) has a peak emission at 615nm, this could be a potential interferent. When standard curves were compared between solutions containing 0% trehalose and solutions containing 10% trehalose, we found a 20% loss in fluorescence intensity starting at 2E12 amplicon copies and a 40% loss at 2.5E12 copies. Since 2E12 is in the range for the output at an input of 2E4 amplicon copies, this is of importance in the quantification of iSDA.

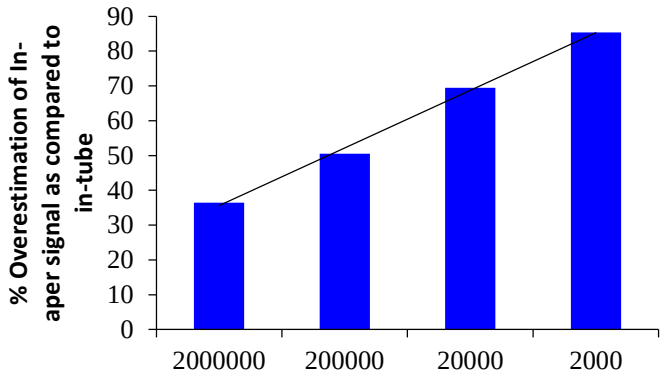

Appendix Figure 17. Percent overestimating of amplicon production in-paper as compared to in-tube. R^2=.997

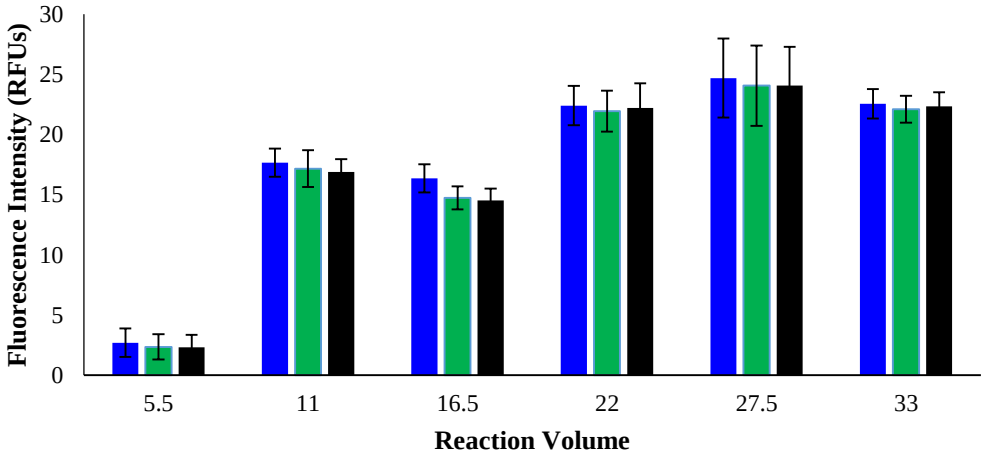

Appendix Figure 18. Fluorescence of STAmp at different volumes in-tube. Fluorescence of 80 nM STAmp in the presence of 200 nM P(TxRed) measured at different reaction volumes. Rotor-Gene software volume set at sample volumes for measurement of 5μL (blue), 11μL (green) and 33μL (black). Gain=10